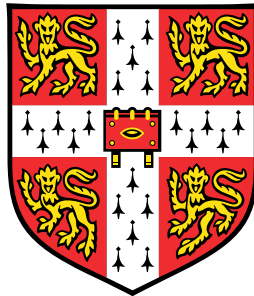


Optimal design & energy management of islanded, hybrid microgrids

For remote, isolated off-grid communities
with no external power exchange



Vineet Jagadeesan Nair

Supervisor: Dr. Ioannis Lestas

Department of Engineering
University of Cambridge

This dissertation is submitted for the degree of
Master of Philosophy in Energy Technologies

I would like to dedicate this thesis to Acha, Amma, Monu, Chinnu and Roshe . . .

Declaration

I hereby declare that except where specific reference is made to the work of others, the contents of this dissertation are original and have not been submitted in whole or in part for consideration for any other degree or qualification in this, or any other university. This dissertation is my own work and contains nothing which is the outcome of work done in collaboration with others, except as specified in the text and acknowledgements. This dissertation contains fewer than 20,543 words excluding the acknowledgment, declaration, dedication, appendices, nomenclature, bibliography, citations, footnotes, tables and equations, and has fewer than 99 figures.

Vineet Jagadeesan Nair
August 2019

Acknowledgements

I would like to sincerely thank Dr. Ioannis Lestas for supervising me during this project. His guidance, advice and expertise in the area of power systems optimization and control has been very valuable in completing this research.

I would also like to thank Dr. Stuart Scott for his support and for being a great mentor throughout this year, as well as Kate Graham for facilitating this course.

I would like to thank my family for always motivating me in my academic and professional endeavours, as well as my friends in Cambridge and beyond who provided support when I needed it the most. In particular, I would like to thank Enrique Garcia-Calvo Conde for his feedback and encouragement especially while spending numerous hours working together in the Energy MPhil centre. More broadly, I want to thank our entire ET cohort for making this a truly memorable year, both academically and otherwise.

Abstract

In this study, a multiobjective, multiperiod, global optimization for design, sizing and dispatch of an islanded, hybrid microgrid was performed using a model built in MATLAB. The system was simulated over one year for sizing and over one day for dispatch, both using hourly time steps. The model minimized lifecycle leveled costs, emissions, lost load and dumped power while maximizing penetration of clean, renewable sources in the microgrid. This found optimal capacities of the renewable, energy storage and backup generation components which provide the best combination of affordability, sustainability, reliability and efficiency.

After experimenting with several global solvers, it was determined that particle swarm optimization is most well-suited to solving the sizing optimization problem. The PV-wind microgrid using Li-ion batteries along with diesel engines was found to perform best among all the combinations considered. It was found that in spite of including additional objectives, monetary costs are the primary driver while allocating generation capacity between different renewable sources like wind versus solar PV. Furthermore, the sizing of PV, wind and battery storage depends strongly on the rating of the standby distributed generator, mainly due to reliability consideration. Generating Pareto-optimal sets revealed interesting relationships between different input variables (i.e. PV, wind and battery capacities) as well as trade-offs that arise while pursuing different objectives. Pursuing cost-minimization alone may lead to sub-optimal outcomes in terms of environmental impact, reliability and excess energy production. A sensitivity analysis was also conducted to understand the effects of various parameters like fuel price and energy storage costs on the optimal system's design and operation. Such accurate sizing programs help reduce the extent of oversizing of sub-systems during the design and planning stage, which is usually needed to achieve high reliability with distributed and decentralized energy systems like off-grid microgrids. This reduces the upfront capital investment needed to build the system, making clean electricity access affordable in the short term.

The economic-environmental dispatch produced day-ahead scheduling strategies to meet the above mentioned objectives. The system was found to be relatively robust to short-term uncertainties and disturbances in renewable generation and load, although this does cause sub-optimal performance due to increased reliance on fossil fuels. It was found that dispatching of the batteries and backup generators is most critical in minimizing impacts of such events. However, the response to longer-term disturbances still remains to be assessed.

The study also includes a comprehensive literature review of tools available for microgrid design as well as different optimization algorithms that have been used to solve microgrid sizing, dispatch and scheduling problems. Additionally, an overview is provided of various control strategies that can be used to improve robustness and resiliency of microgrids.

Contents

List of Figures	v
List of Tables	viii
Nomenclature	ix
1 Introduction	1
1.1 Motivation and problem background	1
1.1.1 Electricity access	1
1.2 Microgrids	3
1.2.1 Advantages of microgrids	4
1.2.2 Challenges with microgrids	5
2 Literature review	6
2.1 Sizing optimization	6
2.2 Overview of microgrid design tools	7
2.2.1 HOMER Pro	7
2.2.2 DER-CAM	8
2.2.3 REopt	9
2.2.4 MDT	9
2.3 Optimal dispatch	10
2.4 Survey of optimization algorithms	12
2.4.1 Genetic (GA) and evolutionary algorithms (EA)	13
2.4.2 Particle swarm optimization (PSO)	15
2.4.3 Surrogate optimization	16
2.4.4 Simulated annealing (SA)	16
2.5 Microgrid control strategies	16
2.5.1 Possible control paradigms	18
Centralized control	18
Decentralized control	19

Distributed control	19
2.5.2 Types of control methods for microgrids	20
2.6 Novelties in current study	21
3 Methodology	22
3.1 Microgrid system description	22
3.1.1 Renewable energy sources (RES)	23
Solar PV arrays	23
Wind turbines (WT)	24
Climate data	26
3.1.2 Electricity demand (load)	31
3.1.3 Backup distributed generators (DG)	32
Diesel engines (DE)	33
Micro-gas turbines (MT)	33
Converter	34
3.1.4 Battery energy storage (BS)	34
3.2 Formulation of optimization problem	35
3.2.1 Costs	35
Sizing optimization problem costs	36
Dispatch optimization problem costs	38
3.2.2 Objective functions	39
Levelized cost of electricity (LCOE)	39
Emissions	39
Deficiency of power supply probability (DPSP)	40
Relative excess or dump power generated (REPG)	41
Renewable energy penetration	41
3.2.3 Dispatch strategy	41
3.2.4 Constraints	42
3.2.5 Mathematical properties of the model	44
3.2.6 Solvers available in MATLAB	44
4 Results and discussion	46
4.1 MG planning and design optimization results	46
4.1.1 Comparison of solution algorithms	46
4.1.2 Sizing results	52
Strategy selection	52
Technology selection	54

Optimal capacities for baseline LI+DE system	55
4.1.3 Pareto optimality	59
Variation of Pareto-optimal combinations of input variables	59
Variation of different objectives on the Pareto front	64
4.1.4 Break-even distance analysis	66
4.2 Sensitivity analysis of sizing	66
4.2.1 Varying DG power rating	66
4.2.2 Varying fuel price	68
4.2.3 Varying financial factors	69
Nominal interest or discount rate	69
Inflation rate	70
4.2.4 Varying price of battery energy storage (BS)	71
4.2.5 Varying relative weights	73
Varying weight w_1 on normalized LCOE	73
Varying weight w_2 on emissions	75
Varying weight w_3 on DPSP	75
Varying weight w_4 on dump energy ratio	77
Varying weight w_5 on (1-REF)	78
4.3 Optimal economic and environmental dispatch results	78
4.4 Robustness of dispatch to uncertainty and disturbances	81
4.4.1 Intermittency and unpredictability of RES generation	81
4.4.2 Stochastic demand	84
5 Caveats of model and potential refinements	87
5.1 Alternative dispatch strategies	87
5.2 Improve computational efficiency	87
5.3 More comprehensive multiyear modelling	87
5.4 Simulation using smaller time steps	88
5.5 Demand response (DR) and Demand-side management (DSM)	88
5.6 Load and RES forecasting	89
5.7 Improved control techniques	89
6 Conclusions	91
6.1 Key takeaways	91
6.2 Future work	92
Bibliography	93

Appendix A Dispatch over longer periods	99
Appendix B Code	101

List of Figures

1.1	Share of global population with access to electricity in the year 2016 [1]	2
1.2	Selected grid extension projects and associated costs in SSA [11]	2
1.3	Comparison of grid connection charges vs monthly electricity bills [11]	3
1.4	Optimal split between different possible electrification options for sub-Saharan Africa [7].	5
2.1	Comprehensive framework of HOMER's optimization procedure [23].	8
2.2	Illustrative example of a Pareto frontier [26].	10
2.3	Flowchart illustrating an example of optimal resource scheduling in microgrids [61].	12
2.4	Genetic algorithm overview [34].	13
2.5	Pareto fronts obtained from GA or EA [37].	14
2.6	Hierarchy of control levels [52].	17
2.7	The three different levels of control methods [33].	18
3.1	Schematic illustrating key components and power flows in the hybrid microgrid.	22
3.2	WT output characteristic [19].	26
3.3	Location of proposed microgrid site in Timbila, Kenya.	27
3.4	Examples of hourly profiles of climate variables over a characteristic day.	29
3.5	Daily profiles of climate variables over the year 2018.	30
3.6	Rural African microgrid load profiles used in this study [27].	32
4.1	Plot of minimum objective value vs run time.	48
4.2	Plots describing GA optimization.	49
4.3	Convergence plot for SO.	50
4.4	Plots describing SA optimization.	51
4.5	Convergence plot for PSO.	52
4.6	Radar plot showing the values of all five objectives, when each of the four strategies is used.	53
4.7	Radar plot showing the values of all five objectives for each of the four possible technology combinations.	54

4.8	Actual dispatch during MG system operation using encoded strategy and optimal capacities for baseline LI+DE MG.	57
4.9	Variation in state-of-charge of LI BS during MG system operation using encoded strategy and optimal capacities.	58
4.10	Three rotated views of the Pareto set obtained using <code>gamultiobj</code> and optimizing with respect to n_s , n_w and $E_{b, init}$ as inputs.	60
4.11	Three rotated views of the Pareto set obtained using <code>gamultiobj</code> and optimizing with respect to $P_{PV, r, total}$, $P_{WT, r, total}$ and $E_{b, init}$ as inputs.	61
4.12	2D plots showing the variations of Pareto-optimal values of the inputs $P_{PV, r, total}$, $P_{WT, r, total}$ and $E_{b, init}$ relative to one another.	63
4.13	Almost linear relationship obtained between renewable energy fraction and normalized emissions,	64
4.14	Two-way correlations between objectives derived from Pareto-set obtained via <code>paretosearch</code>	65
4.15	Effects of varying the rated power of the backup DG.	67
4.16	Effects of varying the fuel price of diesel used in the backup engine generator. . .	69
4.17	Effects of varying the nominal interest rate.	70
4.18	Effects of varying inflation rate.	71
4.19	Price outlook for Lithium-ion battery packs [87].	72
4.20	Effects of varying the costs of BS.	73
4.21	Effects of varying the weight placed on the LCOE term in the multiobjective optimization.	74
4.22	Effects of varying the weight placed on the emissions term in the multiobjective optimization.	75
4.23	Effects of varying the weight placed on the DPSP term in the multiobjective optimization.	76
4.24	Effects of varying the weight placed on the dump or excess energy ratio in the multiobjective optimization.	77
4.25	Effects of varying the weight placed on the (1-REF) term in the multiobjective optimization.	78
4.26	Hourly power dispatch curves over one day (24 h) period on January 1, 2018. . .	80
4.27	Comparison of days with normal (baseline) and extremely low solar radiation levels. .	81
4.28	Comparison of days with normal (baseline) and extremely low wind speeds. . . .	82
4.29	Hourly power dispatch curves over one day (24 h) period under different RES output scenarios.	83
4.30	Different load profiles used in the simulation. The peakier profile was artificially generated by allowing hourly loads to vary by $\pm 30\%$ from the baseline value. The flatter profile was created by shifting hourly load values to better align with the P_{RES} curve shown, along with some additional flattening using moving averages and exponential smoothing.	84
4.31	Hourly power dispatch curves over one day period under different demand scenarios. .	86

- A.1 Optimized dispatch over a longer time period of three consecutive days. 100

List of Tables

3.1	Explanation of variables in the PV power equation.	24
3.2	Specifications of the 255 Wp PV-MLU255HC model [62].	24
3.3	Specifications of the small-scale WT system [64].	25
3.4	Geographical details of stations used to generate combined climate data [68]. . .	27
3.5	Description of MG community near Timbila, Kenya.	31
3.6	Summary statistics for annual and daily load patterns.	32
3.7	Parameters of the Li-ion and Lead-acid BS systems [74].	34
3.8	Key financial parameters used in the model.	36
3.9	Costs assumed for the RES and BS.	36
3.10	Cost assumptions for the DGs.	36
3.11	Emissions factors for both DE and MT [82].	40
3.12	Summary of prescribed load-following strategy used for sizing optimization. . .	42
3.13	Summary of MG constraints.	43
4.1	Optimization results and performance of MATLAB's global solvers. Both LCOE and emissions are reported as normalized values.	47
4.2	Strategy selection for the LI+DE microgrid.	53
4.3	Results of sizing optimization using all four strategies.	53
4.4	Results of sizing optimization using all four technology combinations.	54
4.5	Baseline LCOE and emissions for the MG running solely on a single fossil-fueled DG rated at 16 kW, calculated using the current model.	55
4.6	Sizing optimization results for baseline LI+DE system using two approaches. .	55
4.7	Default parameter values used for sensitivity analysis.	66
4.8	Summary of the dispatch results and performance with a few different possible DG and RES sizes considered. Both COE and emissions are reported as normalized values. The minimum objective value reported here was calculated as an equally weighted linear combination of <i>COE</i> , <i>emissions</i> , <i>DPSP</i> , <i>Dump</i> and $(1 - REF)$. .	78
4.9	Summary of dispatch results and performance under several scenarios representing RES uncertainty.	82
4.10	Summary of dispatch results and performance under different possible demand profiles of the MG community.	84

Nomenclature

Abbreviations

BS	Battery energy storage
CRF	Capital recovery factor
DE	Diesel engine
DER	Distributed energy resources
DG	Distributed fossil-fuel generators
DPSP	Deficiency of power supply probability
DR	Demand response
DSM	Demand-side management
EED	Economic and environmental (or emissions) dispatch
GA	Genetic algorithms
LA	Lead-acid battery
LCOE	Levelized cost of electricity
LI	Lithium-ion battery
MG	Microgrid
MIP	Mixed integer program
MPC	Model predictive control
MT	Micro turbine
NOCT	Nominal operating cell temperature
PV	Solar PV
REF	Renewable energy fraction
RES	Renewable energy sources
SDC	Shutdown costs of the DG
SOC	State-of-charge of battery

SUC Startup costs of the DG

TNPC Total net present cost

WT Wind turbines

Symbols

$E_{b, init}$ Total battery storage capacity

f Inflation or escalation rate

i Nominal interest or discount rate

IC_i Initial capital cost of component i

n_s Number of solar PV modules

n_w Number of wind turbines

$O\&M$ Operations and maintenance costs

$OM_{fix, i}$ Fixed O&M costs of component i

$OM_{var, i}$ Variable O&M costs of component i

P_i Power flow to or from

PW_i Present worth of cash flow i

r Real interest or discount rate

RC_i Replacement cost of component i

Chapter 1

Introduction

1.1 Motivation and problem background

1.1.1 Electricity access

Over 1 billion people or 13% of the world's population still lacks access to electricity, with most of these people living in Africa, India and other parts of southeast Asia. This is illustrated in fig. 1.1, showing very low electrification rates particularly in regions of sub-Saharan Africa (SSA), which hosts over 621 million people (i.e. approximately two in every three persons in Africa) who currently do not have reliable electrical power [2]. Up to 85% of the unserved population lives in remote rural villages [9], located far away from traditional 'macrogrids' that rely on centralized thermal power generation dominated by fossil fuels like coal and natural gas. Of the remaining 15% that live closer to the grid, many cannot afford to pay the exorbitant connection fees or metering and wiring costs [9].

Electricity access is also related to various other socioeconomic issues as well as the health and well-being of these populations. Improving electricity provision is highly correlated with poverty alleviation through improved living standards, increased productivity and better employment opportunities. This will also help achieve several sustainable development goals (SDGs) set by the United Nations (UN) [2].

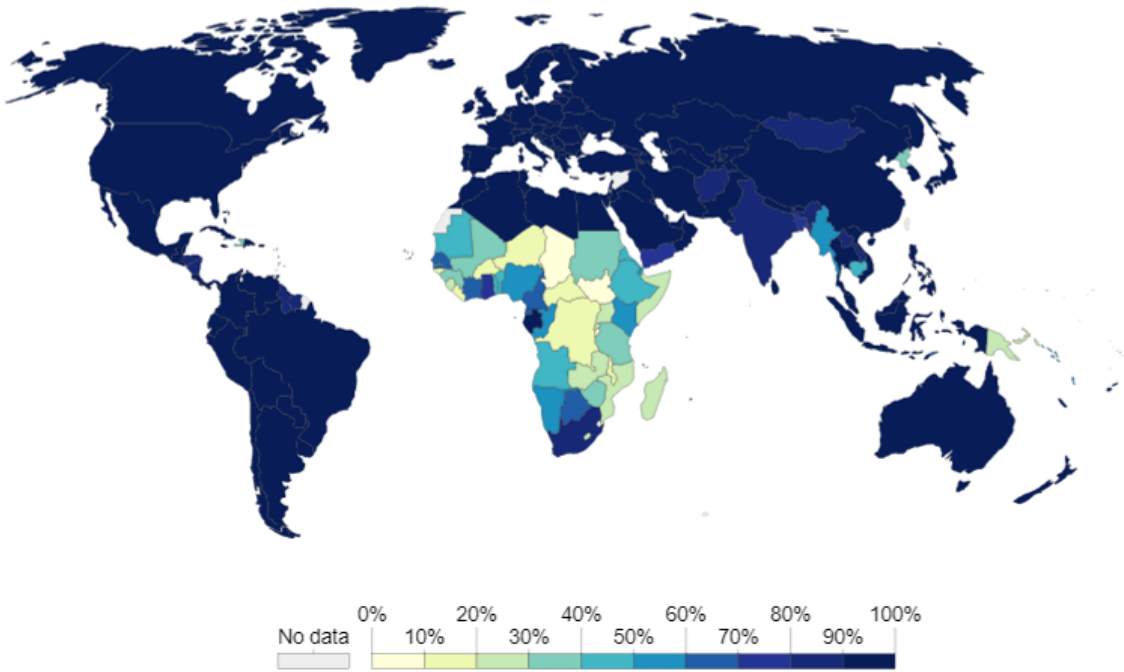


Figure 1.1: Share of global population with access to electricity in the year 2016 [1].

It is challenging to connect such isolated communities to the conventional grid due to the high costs of constructing transmission and distribution (T&D) infrastructure such as high voltage AC and DC lines. According to Power for All, grid extension projects and infrastructure upgrades in sub-Saharan Africa can cost up to \$5.5 million per MW/km as seen in table 1.2. Long planning, procurement, environmental assessment and construction phases result in budget overruns and long delays for project completion.

	Project Connection	2010	2011	2012	2013	2014	2015	2016	2017	2018	2019	2020	Unit Cost (Million USD/MW km)	Source
Kenya	Mombasa-Nairobi						Budget (USD): \$125 million Length: 482 km						0.71	[1]
	Kindaruma-Mwingi-Garissa						Budget (USD): \$8 million Length: 250 km						0.24	[2]
	Rabai-Malindi-Garsen-Lamu						Budget (USD): \$96 million Length: 329 km						1.33	[3]
Rwanda	Rusumo-Kigali-Shango						Budget (USD): \$24 million Length: 114 km						0.96	[4]
Ghana	Tumu-Han-Wa						Budget (USD): \$50 million Length: 150 km						2.07	[5]
	Kumasi-Bolgatanga						Budget (USD): \$165 million Length: 550 km						0.91	[6]
Uganda	Kawanda-Masaka						Budget (USD): \$110 million Length: 137 km						3.65	[7]
	Karuma-Kawanda						Budget (USD): \$250 million Length: 248 km						2.92	[8]
	Kawanda-Kasana						Budget (USD): \$39 million Length: 54 km						5.47	[9]

Figure 1.2: Selected grid extension projects and associated costs in SSA [11].

This implies that connection issues are extremely high across the continent, averaging around \$136¹ and can be significantly higher than monthly household incomes, as seen in graph 1.3.

¹for single phase connections

This makes such projects unprofitable even in certain urban centres and more so for sparsely populated rural areas suffering from high marginal costs and less concentrated electricity demand.

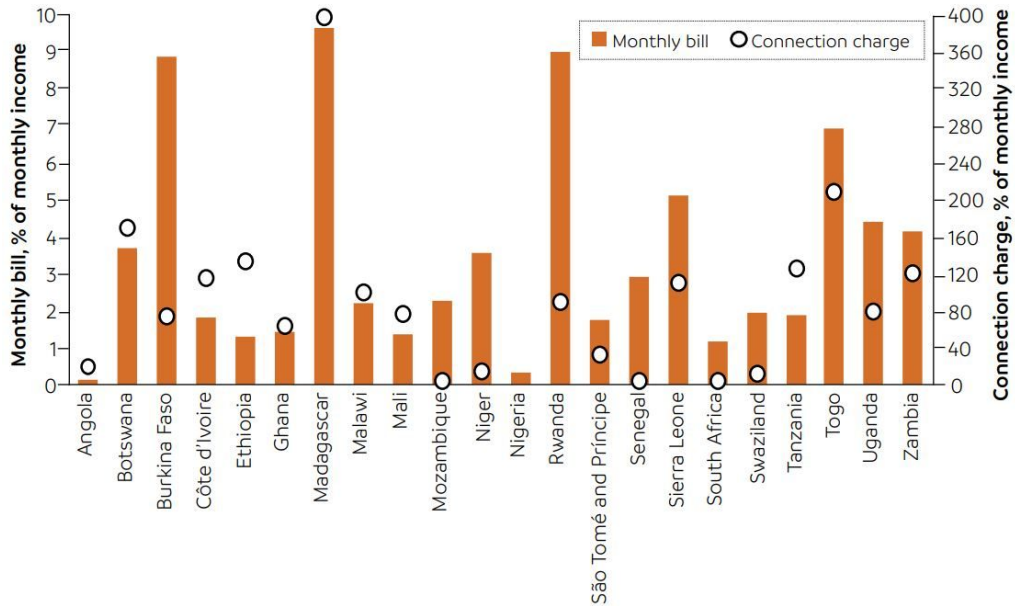


Figure 1.3: Comparison of grid connection charges vs monthly electricity bills [11].

As a result, significant segments of the global population either live without any electricity access at all or lack reliable and continuous access to power. Even when they do have access, most communities suffer from 'energy poverty' whereby they spend significant portions of their income on energy-related expenses i.e. electricity and fuel consumption. Furthermore, close to half of the global population still relies on biomass fuels like firewood or charcoal for cooking and heating, and kerosene for lighting which are expensive and have adverse impacts on human health [5]. This is especially the case in developing and less developed countries, with almost two-thirds of the world's poorest people residing in rural areas [5]. Thus, there is a need to come up with more affordable and reliable solutions for rural electrification that can be implemented rapidly in the near future.

1.2 Microgrids

Microgrids are low-voltage, localized hubs of electricity generation, storage and utilization that remain synchronous with the larger, traditional grid under normal operation, but can disconnect at the common point of coupling and operate independently if needed. Such decentralized systems have become more popular and practical due to the increased penetration of distributed generation and power production from renewable energy sources (RES) like wind, solar, geothermal, biomass and small-scale hydroelectric plants. Microgrids can operate either in:

1. *Grid-connected mode:* This allows it to exchange power with the macrogrid in both directions (under certain transmission constraints), in order to balance supply and demand. In this configuration, the microgrid operator can generate additional revenue and profits by selling excess clean power from RES back to the main grid.

2. *Islanded* mode: Here, the microgrid system is completely isolated and not connected to the larger grid network. Since no external power exchange is allowed, all power demand must be met locally and any excess generation must be curtailed by grounding to earth or using dump loads.

Due to challenges with grid extension described in section 1.1.1, this work only considers stand-alone, off-grid systems that always operate in islanded mode. This choice introduces some additional special challenges that will be discussed in greater detail in section 1.2.2.

1.2.1 Advantages of microgrids

In comparison to large-scale conventional sources such as thermal and nuclear baseload power plants used in legacy grids, microgrids have much smaller capacities but offer greater modularity and flexibility. Thus, they facilitate better integration of renewable, distributed energy resources (DERs) that are highly intermittent, variable in supply and often located far away from load centres. The unpredictability of renewables also leads to challenges and compatibility issues with the conventional grid such as poor power quality, unsteady supply voltages, undesirable harmonics and a high degree of vulnerability to disturbances like natural disasters, extreme weather, terrorism and other cyber-physical attacks. The interconnectedness and sensitivity of such centralized systems can result in cascading failures and domino effects, where a fault in one small section of the grid affects everyone else to some extent. This is evident through blackouts, brownouts and load-shedding that often occur in urban areas, especially in developing nations [12].

By reducing our reliance on fossil fuels, microgrids can help decrease greenhouse gas emissions and mitigate climate change. They will play a critical role in transitioning to a sustainable future based on clean energy sources and achieving ambitious goals such as the SDGs and Paris Climate agreement. By allowing islanded operation, they can simply disconnect from the macrogrid in case of failures or emergency to still supply local load, thus creating more resilient and secure power networks that are robust to disturbances.

Well designed, controllable microgrids can also enable grid optimization by relieving congestion and providing various ancillary services to the main grid as needed, for e.g. load shifting, frequency or voltage control and peak shaving. Moving generation sites closer to demand will help reduce transmission and distribution (T&D) losses while allowing for T&D investment deferral. Furthermore, microgrids are one of the only realistic options to meet the need for low-cost, locally available energy supply in other remote, resource-constrained locations apart from rural areas as well, such as islands, military bases, harsh environments like the Arctic. Overall, microgrids promise to democratize cost-effective electricity access globally, with the International Energy Agency (IEA) estimating that about 70% of rural areas that currently lack access will be connected using mini-grid, microgrid or off-grid solutions [4] as depicted in fig. 1.4. This means ≈ 140 million rural Africans could get access to electricity through the creation of 100,000 mini-grids by 2040 [6].

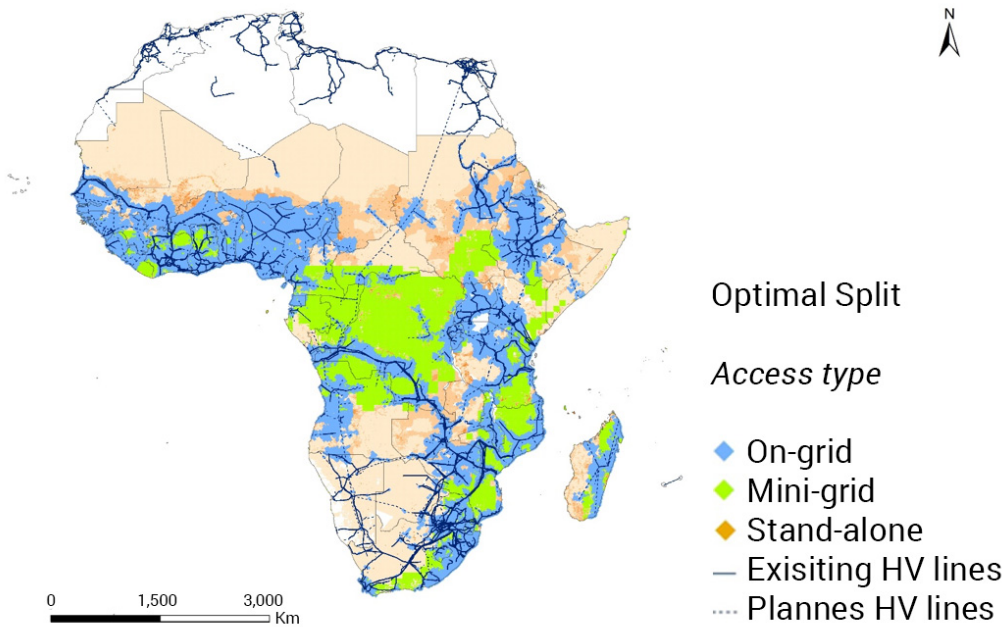


Figure 1.4: Optimal split between different possible electrification options for sub-Saharan Africa [7].

1.2.2 Challenges with microgrids

Despite the numerous merits of microgrids, they still face some serious practical challenges that hinder widespread implementation. Owing to their smaller size, they lack the averaging effects that help balance supply and demand across different locations and nodes in larger networks. This can lead to stability issues as well as unmet load in case of excess demand or insufficient RES generation due to unfavorable weather conditions e.g. extended periods of wind lulls, cloudy or rainy days. Load fluctuations occurring in microgrids can be more extreme due to their smaller capacities. Larger, conventional power systems have transmission spanning across multiple regions with distinct weather patterns load profiles, which helps smooth out variations over time. In addition to highly stochastic demand, microgrids must balance this with the unpredictability and intermittency of renewables. In order to accommodate for the worst-case scenarios, both RES and storage capacity often need to be oversized which raises project costs.

These issues are further intensified in the case of isolated microgrids since these do not have the main grid (e.g. backup peaker plants and interconnectors) as a safety net to fall back on. They also lack large fossil-fueled synchronous generators that offer high inertia and oppose sudden changes in grid frequency or voltage. Thus, decisions need to be made over faster timescales in order to rectify supply-demand mismatches in both real and reactive power to ensure frequency regulation and voltage stability, respectively [13].

This study focuses only on power balancing at slower time-scales on the order of months, days and hours. Frequency and voltage stability are not considered here since these require faster control actions and responsiveness on the order of minutes and seconds. These are primarily achieved through the design of appropriate switches and other power electronics equipment, not through the optimization and control methods which are the topic of the current project.

Chapter 2

Literature review

There is already a large body of existing research in the field of microgrid design and operation. Past studies range from optimal selection and sizing of generation and storage technologies, to optimizing the energy management and dispatch of these components in real time.

2.1 Sizing optimization

Once the most suitable technology types are selected based on a combination of economic, technical and socio-political factors, the next step is to decide the optimal sizes of these subsystems. For RES such as wind turbines (WT) and solar photovoltaic panels (PV), this involves setting the power ratings of each individual unit as well as the total number of units needed (e.g. no. of turbines, total surface area of PV array). For energy storage technologies like batteries and pumped hydro schemes, this would mean fixing their rated powers as well as total energy capacity. Finally, for standby diesel engines or gas turbines, their total rated power is the primary decision variable.

Most studies consider *hybrid* microgrid designs for standalone power systems i.e. integrated systems combining two or more renewable sources as primary generation with conventional distributed generators (DG) based on fossil fuels, as secondary, backup systems to meet reliability requirements [17] [20]. A techno-economic, multi-objective optimization is performed to minimize pre-determined objectives including economic costs [18], pollutant emissions (to reduce negative environmental impacts) and other performance metrics for power quality, system reliability and efficiency [19]. These reflect various goals of the community that the microgrid serves. A more detailed description of individual cost terms will be provided in chapter 3.

Past studies have shed interesting insights into tradeoffs that occur during MG design. For instance, it has been shown that PV/WT systems that use both diesel generators and batteries are more economically viable than those using either only batteries or diesel engines alone [17]. The same study also found that system configurations with much lower number of wind turbines relative to solar PV modules have the lowest energy costs and net equivalent CO_2 emissions. This resulted from the strong solar potential in the region considered in Algeria [17] which is also likely to be the case for the location of Timbila, Kenya chosen here. This is an example of how location-specific the planning and design process is owing to the regional characteristics of climatic conditions, availability of wind and solar energy as well as electricity demand profiles. The sizing results also vary depending on the choice of objectives and financial parameter values (like interest, discount and inflation rates) used in the analysis since capital costs tend to be significant for renewables and storage while running fuel costs are the major expense for backup

generation. Furthermore, different objectives often compete with one another since more reliable, cleaner systems often imply higher project costs. It has also been found that in order to attain the same reliability as the usual grid, *off-grid* systems can be up to ten times more expensive than *on-grid* solutions using solar PV with batteries [24].

Overall mathematical models for hybrid microgrids are constructed by combining fundamental models for individual sub-systems. Well-established, proven models already exist for each of the wind, solar, diesel, gas and battery bank systems included in this study [20]. In particular, studies have found that the sizing of energy storage and backup generators often plays the crucial role in determining system performance. For example, the efficiency of microgrid operation depends strongly on the battery scheduling due to the key role it plays in peak load shifting and stabilizing fluctuations¹ [21]. Most studies that formulate their own optimization models choose to simulate the problem over a 1-year period (i.e. 8760 h), resulting in excellent convergence to feasible optimum solutions [22]. However, it is possible to simulate over longer periods using existing commercial software as well.

2.2 Overview of microgrid design tools

2.2.1 HOMER Pro

HOMER (Hybrid Optimization of Multiple Energy Resources)² Pro is a tool originally developed by the National Renewable Energy Laboratory (NREL) and now distributed by the commercial entity HOMER Energy. Based on literature surveyed, this is the most widely used commercial tool for microgrid design optimization in both academia and industry today. It is currently the global standard for optimizing microgrid design in all sectors, from village power and island utilities to grid-connected campuses and military bases³.

HOMER is a simulation model that simulates a viable system for *all* possible combinations of technologies being considered. It uses a proprietary, derivative-free optimization algorithm that uses brute force permutations and exhaustive search [24] to minimize the total net present costs (TNPC) of the system⁴. It requires six types of inputs - meteorological or climate data, load profiles, equipment characteristics, search space specifications, economic and technical data [23]. Optimal sizes of components are then determined in three stages of simulation, optimization and sensitivity analysis as shown in fig. 2.1, using time-steps ranging from 1 minute to 1 hour which capture intra-day variability. The simulation and optimization occur simultaneously while the sensitivity analysis determines the effects of uncertainty in non-deterministic parameters (such as fuel cost, wind speed, solar radiation, component costs) on the results in terms of the best (lowest NPC), feasible system plans.

¹in both demand and RES supply

²also known as Hybrid Optimization Model for Electric Renewables

³<https://www.homerenergy.com/products/pro/index.html>

⁴defined as present value of sum total of costs minus revenues

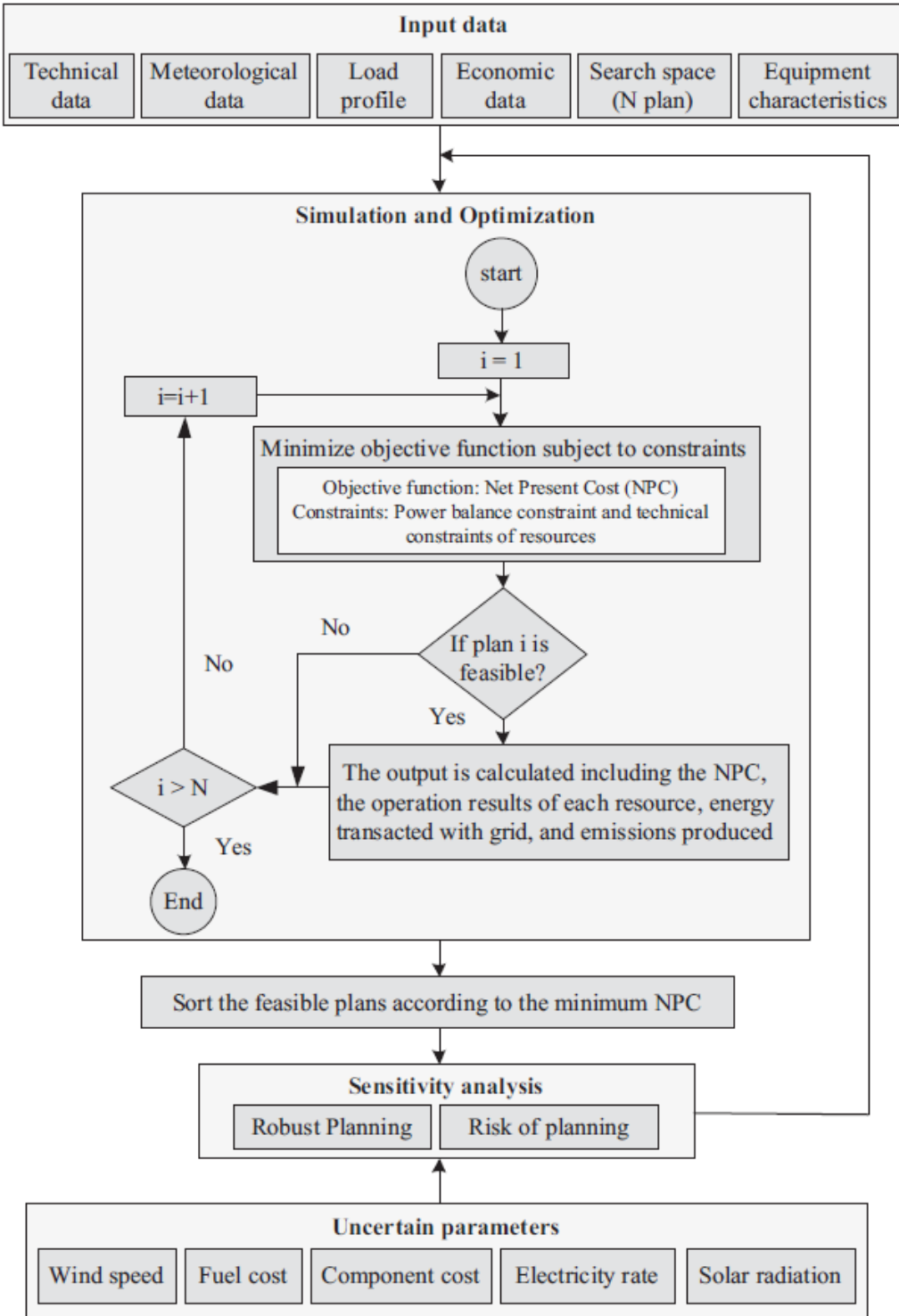


Figure 2.1: Comprehensive framework of HOMER's optimization procedure [23].

2.2.2 DER-CAM

The Distributed Energy Resources Customer Adoption Model (DER-CAM) is a decision-support tool developed by Lawrence Berkeley National Laboratory (LBNL) that is capable of optimizing *both* design *and* dispatch for DER investments used in either buildings or hybrid, multi-energy microgrids⁵. Compared to HOMER, it offers more flexibility in terms of modifying the objective

⁵<https://building-microgrid.lbl.gov/projects/der-cam>

function and allowing for multi-objective optimizations. Unlike HOMER which is a simulation model based on heuristics and non linear formulations, it uses a mixed integer linear program (MILP) to find global optima quickly [25] with key inputs required being similar to HOMER. Rather than using a full time series, it models loads and solar irradiance as characteristic day types to capture seasonal variations [24]. Its outputs include optimal selection and capacity of DERs, their relative placement at nodes and dispatch schedules to meet economic, resiliency and reliability targets. In addition to monetary costs, it also considers carbon emissions and environmental criteria in its optimization - providing a breakdown of both costs and emissions associated with various end-use loads among its outputs. It assumes no deterioration in output or efficiency over each component's lifetime and constraints on start-up, shut-down and ramp rates are excluded by default [25].

2.2.3 REopt

REopt is an MILP-based techno-economic decision support model from NREL to optimize decentralized energy systems for a variety of applications⁶ including both grid-connected and off-grid microgrids, using hourly or sub-hourly simulation time steps. It recommends the optimal mix, sizes and operating strategies of renewables, conventional thermal generation and storage to maximize economic performance and cost savings while connected to the grid, and increase survivability and days of autonomy during outages in islanded mode [26].

The full software is not publicly available and the accessible, rudimentary version⁷ is not very comprehensive since it offers only a small subset of free features. However, supporting NREL datasets obtained from REopt cost models were used here to estimate load profiles and explore variations in Levelized costs of electricity (LCOE) specific to rural Africa [27].

From the sample results obtained by NREL comparing LCOE for multiple system configurations, it can be concluded that diesel-only systems are the cheapest option but may not meet other design objectives. Although the PV+battery system is more expensive, the inclusion of a diesel backup makes the combined system even cheaper than the diesel-only option. This indicates that hybrid designs incorporating RES and storage along with fossil-fuels are likely to be optimal and most cost-effective for isolated microgrids.

2.2.4 MDT

The Microgrid Design Toolkit (MDT) is a software developed by Sandia National Laboratories that uses both MILP and genetic algorithms⁸. Rather than using time steps, it is a discrete event simulation (examples of events could include changes in load, fuel outage, equipment failures etc.) [26]. In addition to its sizing capability, MDT also helps to identify and characterize the trade-space of alternative microgrid design decisions in the early, preliminary stages. It optimizes both technology and performance management according to user-defined criteria to output a set of efficient trade-off design options as a Pareto optimal frontier shown in fig. 2.2.

⁶<https://reopt.nrel.gov/>

⁷REopt Lite web tool

⁸<https://www.sandia.gov/CSR/tools/mdt.html>

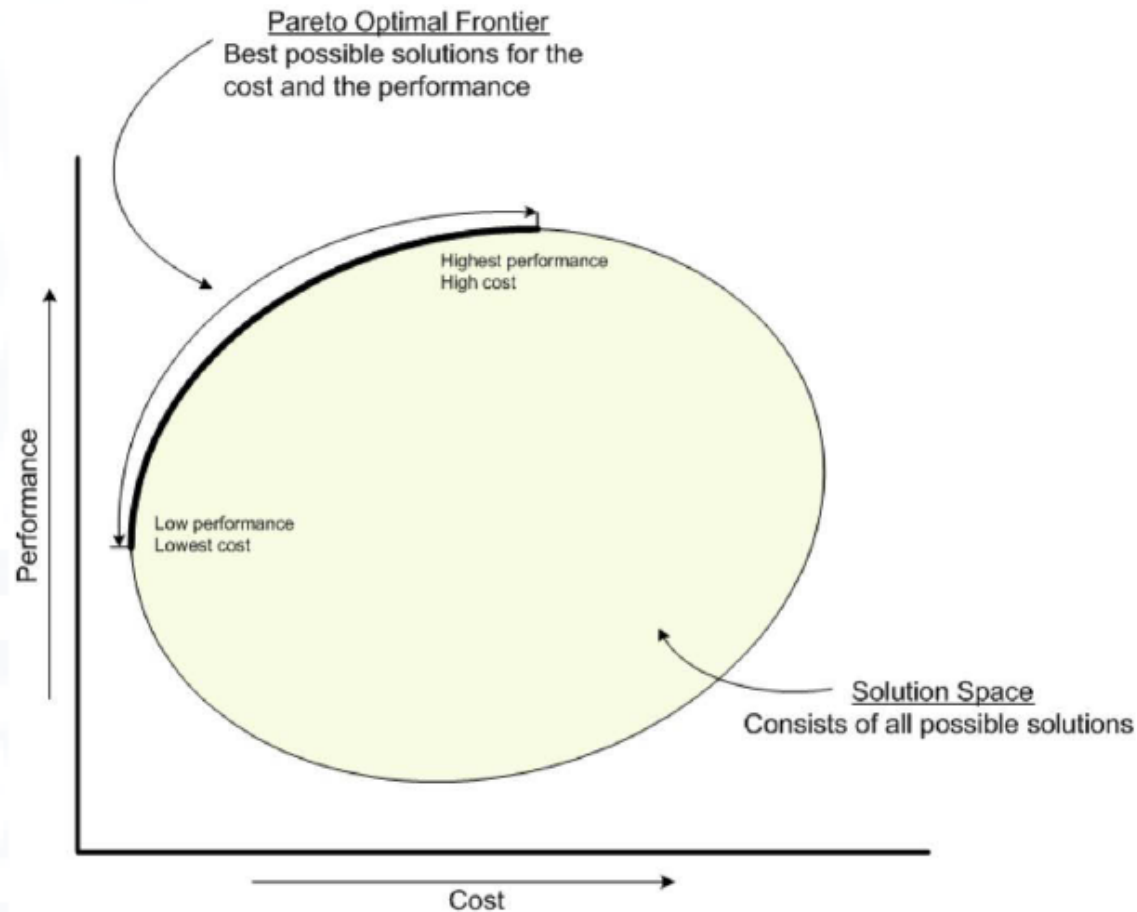


Figure 2.2: Illustrative example of a Pareto frontier [26].

2.3 Optimal dispatch

This area of research studies methods for both:

- Unit commitment: Decisions regarding the production scheduling of different power generation units to meet forecasted future energy demand at minimum cost. This determines which dispatchable units (including both generators and storage devices) are online and producing energy versus being offline at any given time instant [28].
- Unit dispatch: These are production decisions that set exactly how much power each online unit is generating in a specific time interval.

Whereas single-objective optimizations generally minimize purely economic costs, multiobjective problem formulations are becoming increasingly more common. These simultaneously optimize with respect to several objectives such as emissions, cost, power loss and heat [29]. However, conventional optimization methods are not well-suited to such combined emissions-economic dispatch problem since they are generally nonlinear, non-smooth and non-convex with severe equality and inequality constraints [29]. There is also the issue of convergence to local minima that may not be globally optimal solutions. Furthermore, these mixed integer programming problems generally involve both discrete as well as continuous, multi-index decisions variables and constraints with high dimensionality. This precludes the use of popular

solver packages like CVX⁹ which only work for disciplined convex programs, and have led to the development of metaheuristic based optimization approaches. Instead of enforcing hard constraints, some studies use soft constraints with large violation penalties to introduce slackness and ensure feasibility of the optimization problem [30].

Some focus areas of past microgrid operations research include mechanisms for seamless, automatic islanding and reconnection to the grid when necessary to improve reliability and robustness [15]. Passive primary and secondary control strategies have also been explored to regulate both grid supply frequency and voltage, respectively. Furthermore, unlike larger grid networks, microgrids require a third, higher level of control for micro-economic optimization [15]. Modelling and optimization in microgrids can also borrow insights, tools and methods from related applications including electric vehicles as controllable loads, feature-dependent power generation (e.g. solar PV) which depends on environmental factors often outside the designer's control, controllable generation (feature-independent feeds) and existing models for energy storage systems [16]. Some studies have also used popular programming tools like MATLAB Simulink to create and simulate simplified, dynamic models of small-scale microgrids.

In addition to geographical and spatial factors, temporal variations are critical, including both long (seasonal, monthly etc.) and short-term (daily, hourly etc.) patterns in load and RES supply. In particular, these determine the optimal cycling strategies for the battery and operational time of the backup DG, which in turn affect fuel consumption and operating costs [18]. Optimal configuration and operation of microgrids have been shown to improve power quality, reliability, security, sustainability and decrease electricity costs to consumers [29].

In case of islanded and isolated microgrids lacking macrogrid support, literature indicates that incentive-based demand response (DR) programs [35] and/or model predictive control [30] are essential to reject forecasting errors and noise in RES generation and load, improve optimality of both supply and demand and thus reduce costs. In terms of DR implementation and demand side management (DSM), it has been shown using game-theoretic approaches that globally optimal aggregate demand profiles can be achieved by incentivizing individual agents to locally minimize costs, through price signals [36].

Finally, several recent simulations have also focused on using *integrated design and operation optimization*, a combined approach where both system sizing and dispatch are optimized simultaneously in a single stage rather than sequentially in two distinct steps [45]. An example of the process flow for optimal dispatch and scheduling is shown in fig. 2.3.

⁹<http://cvxr.com/cvx/>

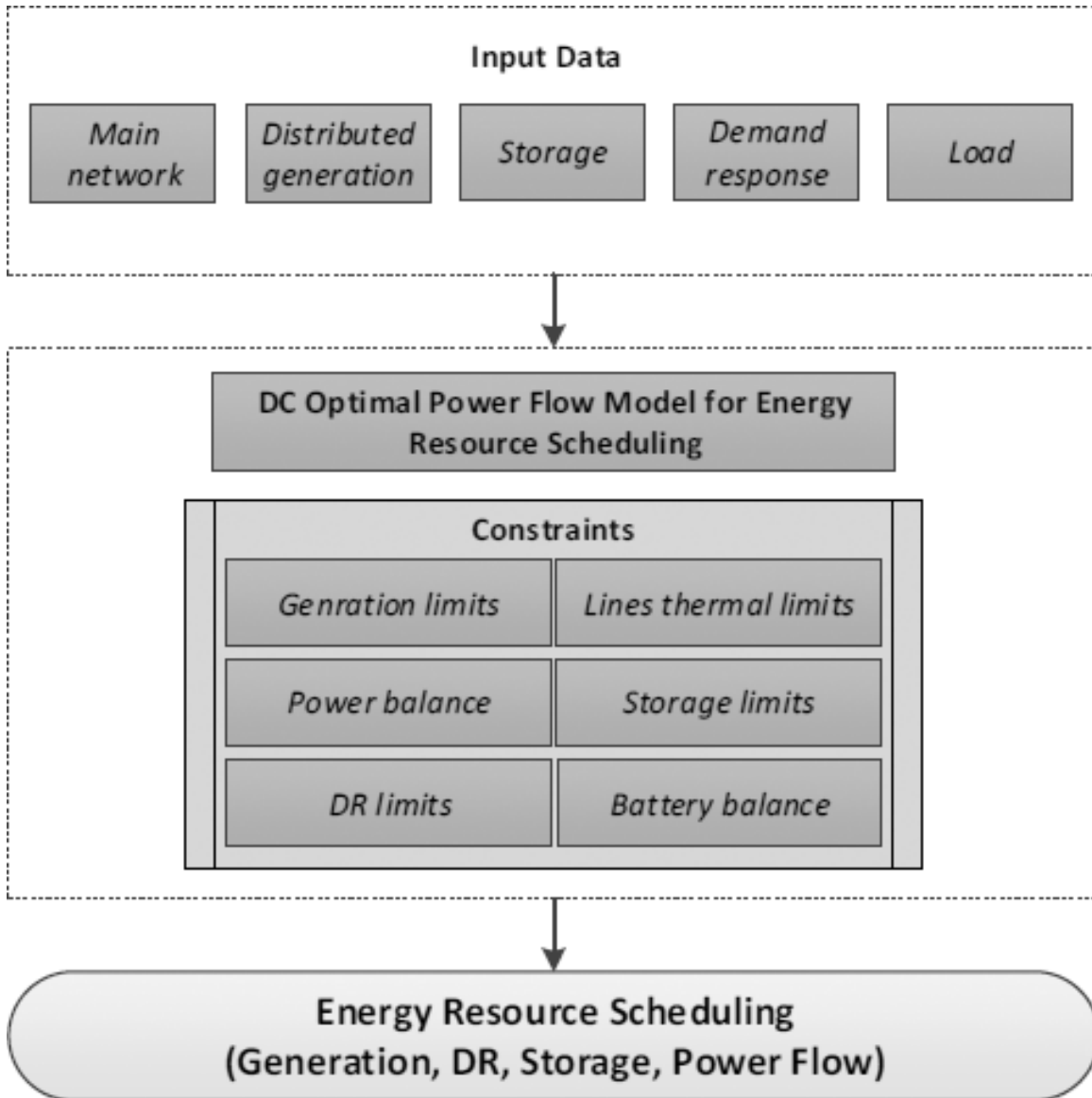


Figure 2.3: Flowchart illustrating an example of optimal resource scheduling in microgrids [61].

2.4 Survey of optimization algorithms

In addition to using available tools like HOMER Pro and DER-CAM, many studies have built their own optimization models by formulating sizing and dispatch problems usually as non-linear mixed integer minimization programs. Relaxations and variable transformations could also be used to convert these to mixed integer linear programs while certain assumptions and functions could be modified to potentially also convexify the problem. Linearized formulations are more computationally tractable and efficient than quadratic programs. Thus, quadratic functions like the fuel costs of DGs are often approximated to linear expressions like the maximum over affine functions as done in [31]. Some of the most common global optimization techniques used to solve such problems are described in more detail in the following subsections. These artificial intelligent search techniques usually prove to be more effective than classical methods like linear programming when the dispatch problem becomes more complex [39]. In addition, other methods like Lyapunov optimization [29] and discrete Fourier transforms [40] have also been used in the literature.

2.4.1 Genetic (GA) and evolutionary algorithms (EA)

These are a class of optimization algorithms capable of solving smooth or non-smooth optimization problems with any type of constraints including integer constraints. It is a stochastic, population-based method which randomly searches the space of candidate solutions by *selection*, *mutation* and *crossover* among population members. It imitates the biological process of evolution by natural selection and represents individual members as potential solutions to a complex optimization problem [34]. The solution population of chromosomes is first initialized as a vector or array of bits or character strings. The algorithm seeks to minimizes the fitness value since it measures deviations from predefined objectives and constraints. It can be formulated as a weighted sum of the cost (objective function value), penalties on constraint violations and the parity degree¹⁰ as per eq. (2.1), where W_{Pen} and W_{Par} are variable weighting factors while $R_{Cost/Pen}$ and $R_{Cost/Par}$ are ratios of mean values used to normalize the three criteria to be comparable. The parity term shows diversity and improves the survival probability of individuals that differ from the group, thus decreasing the likelihood of quickly converging to, and getting stuck at local optima [34].

$$F = Cost + W_{Pen} \cdot R_{Cost/Pen} \cdot Penalty + W_{Par} \cdot R_{Cost/Par} \cdot Parity \quad (2.1)$$

In accordance with Charles Darwin's theory of 'survival of the fittest', the fitness of each chromosome is assessed at each iteration and the best or minimizing solution is selected [29]. These solutions then repeatedly undergo processes of slight modification and recombination with one another to retain properties that better adapt them to their environment than competitors, for several generations until a preset stop criterion (generation number) is met [34]. This process flow is summarized in fig. 2.4 where P and Q are real and reactive power values respectively, for unit commitment and economic dispatch.

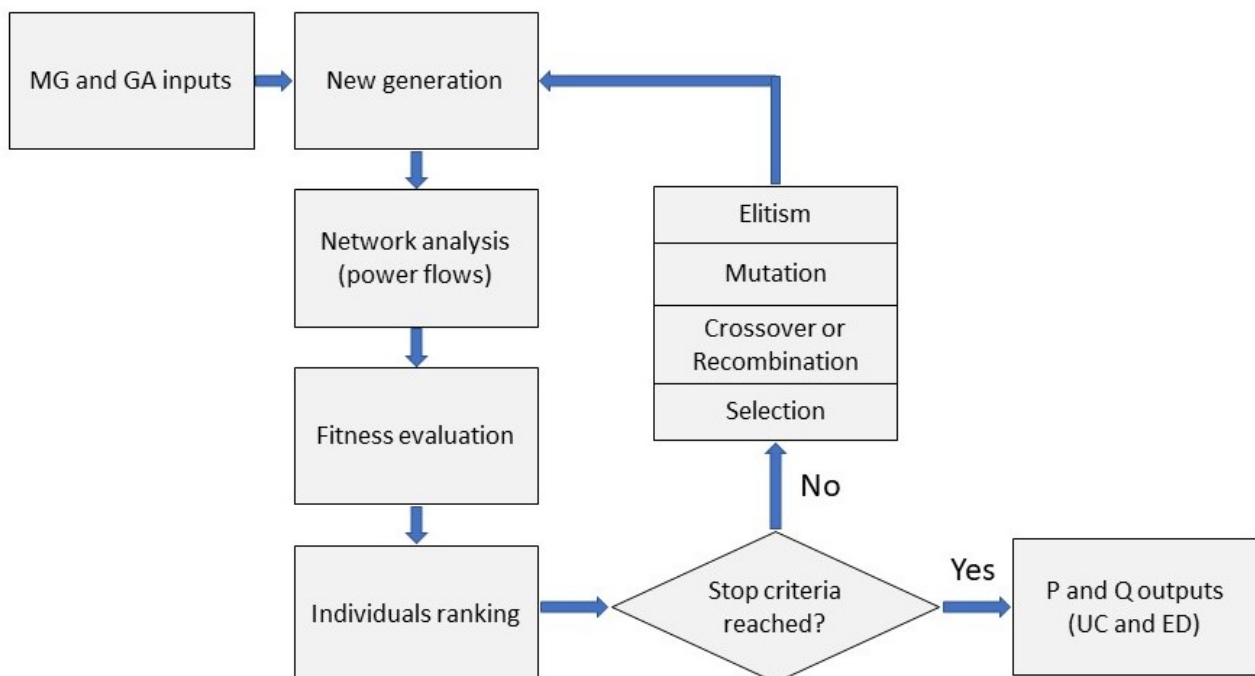


Figure 2.4: Genetic algorithm overview [34].

¹⁰this is a measure of similarity among individuals or possible solutions

Similar to genetic algorithms, evolutionary programming also relies on Darwinian principles of evolution and adaptation. Whereas GA attempts to simulate micro-level processes like chromosomes, evolutionary algorithms seek to mimic macro-processes such as phenotype variations and inheritance [29]. Since these methods use a population of solutions in their search, multiple well-distributed, non-dominated solutions can be found in a single run while requiring little information about the domain or search space for a given problem [39]. *Differential evolution* is a variant of evolutionary algorithms that differs in the solution selection step due to their use of non-domination sorting and ranking selection procedures [39]. These have proven to be effective in solving environmental/economic dispatch (EED) problems [42].

One approach for multiobjective optimization is to combine the different individual objective functions into a single composite using weights that sum up to unity. Another more general method is to identify a whole solution set that's Pareto optimal. This is the set of all non-dominated feasible solutions which cannot be improved further relative to any objective without worsening performance on at least one other objective, as shown in fig. 2.5. Genetic and evolutionary methods prove to be useful to generate such sets and help designers clearly visualize tradeoffs amongst pursuing various objectives like cost-effectiveness, efficiency, and reliability [37].

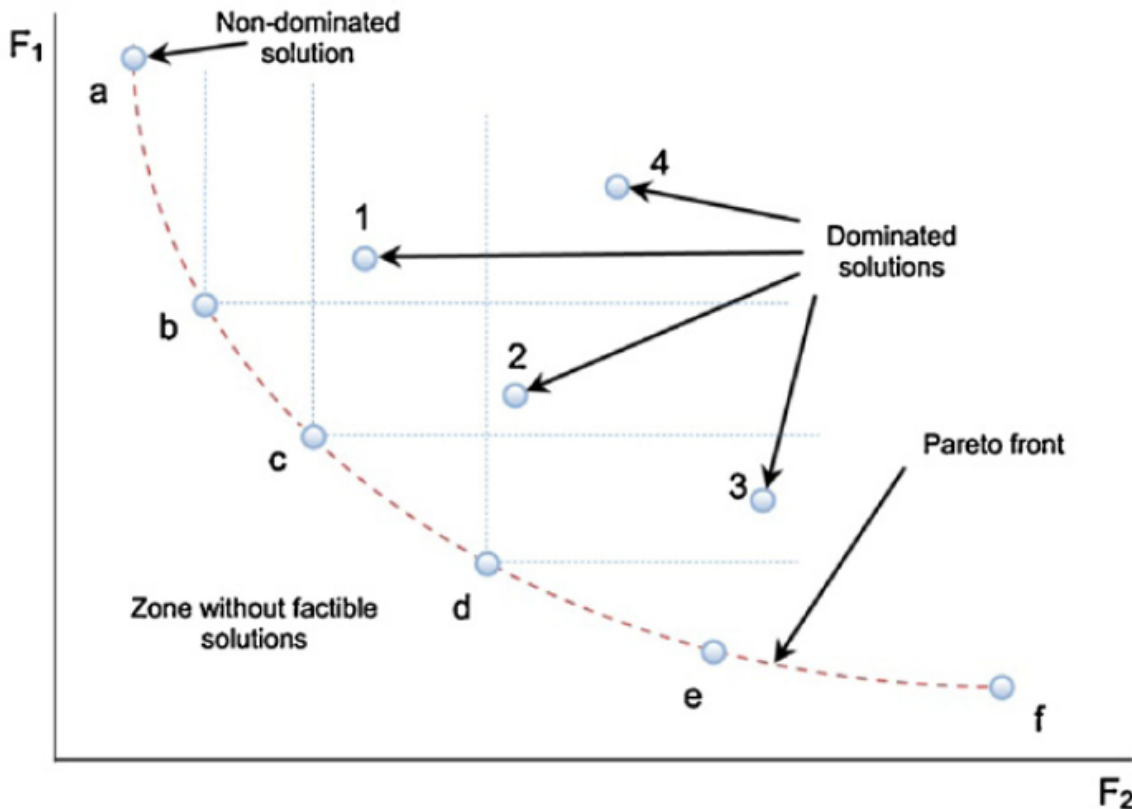


Figure 2.5: Pareto fronts obtained from GA or EA [37].

The main disadvantage with these methods is that complexity rises significantly with the number of problem parameters which also increases the programming and solving difficulty [38]. Exploration of new solution spaces is limited with traditional GA and adaptability is low due to the crossover and mutation operations being preset according to experience. In order to resolve such issues, some studies have developed modified versions such as improved adaptive genetic algorithms which avoid phenomena like premature, local convergence and arrive at global optima in a faster, more stable manner [41].

2.4.2 Particle swarm optimization (PSO)

Particle swarm optimization is another biologically inspired algorithm that attempts to mimic dynamics of group behaviour and swarm intelligence in order to converge to the optimal solution. It is an iterative, agent-based, distributed problem-solving method that simulates the social interactions of a swarm of individuals moving together in search of food inside a specific region [38], as seen in animal societies and insect colonies [29]. It employs a population of particles representing potential solutions to thoroughly explore the hyperspace of feasible solution [46]. In comparison to others, the PSO algorithm is often easier to implement owing to its relative simplicity, fewer parameter settings and strong optimization ability. However, it may get stuck at local optima and has trouble satisfying equality constraints in the initialization and updating processes of the particle swarm [43]. Additionally, GA is more efficient in cases where there are more than three components to the solution. Improved and enhanced multiobjective PSO algorithms have been successfully used to accurately size battery systems for microgrids and solve a variety of EED problems efficiently. This includes highly complex and even non-convex large-scale examples such as optimal power flow (OPF) [46], resulting in quick convergence to high quality solutions with relatively low computational cost [29].

The conventional PSO algorithm randomly initializes a particle community with positions $[x_{i1}, x_{i2}, \dots, x_{id}]$ and speeds $[v_{i1}, v_{i2}, \dots, v_{id}]$ where $i = 1, 2, \dots, n$ and n is the population size while d is the dimension of the search space describing each parameter or coordinate of the solution. Each particle's position is determined by two best values, (1) the best fitness value (minimal objective function) that the individual particle itself has achieved so far ($pbest$) and (2) the global best value obtained by the optimizer for the entire population so far ($gbest$). In addition to positions tracking the values of input variables, each particle also has a velocity moving it towards the individual and global bests in terms of fitness [44], to find the best among all feasible solutions within the predefined space (set by the initial population). The procedure can be summarized as:

1. Evaluate fitness of each particle or potential solution
2. Update both $pbest$ and $gbest$
3. Update velocity and position of each particle in the population using [43]:

$$x_{i,d}^{k+1} = x_{i,d}^k + v_{i,d}^k \quad (2.2)$$

$$v_{i,d}^k = \omega \cdot v_{i,d}^k + c_1 \cdot rand_1^k \cdot (pbest_{i,d}^k - x_{i,d}^k) + c_2 \cdot rand_2^k \cdot (gbest_{i,d}^k - x_{i,d}^k) \quad (2.3)$$

The velocity is calculated as a random weighted integer as in eq. (2.2) where $v_{i,d}^k$ is the speed and $x_{i,d}^k$ is the position along dimension d of particle i in iteration k , ω is the inertia weight factor, c_1 and c_2 are learning factors, $pbest_{i,d}^k$ and $gbest_{i,d}^k$, respectively, are the local and global best values of coordinate d in iteration k , and $rand_1^k$ and $rand_2^k$ are random numbers uniformly distributed in $(0,1)$ [43]. The algorithm keeps updating each particle's location and speed until some predefined termination condition such as the maximum number of iterations or a target fitness value is met, at which point the optimal group value $gbest$ provides the desired solution.

Similar to PSO, there are several other swarm-intelligence based approaches such as ant or bee colony optimization, bacterial foraging algorithms and group search optimizers [29]. These are just a small subset of the larger, more general group of bio-inspired algorithms to solve complex, multiobjective optimization problems.

2.4.3 Surrogate optimization

This algorithm is useful while working with expensive, time-consuming objective functions that entail a great deal of computational complexity and effort. It uses a surrogate function that approximates the actual objective function but takes less time to evaluate. The algorithm chooses quasirandom points within the bounds on input variables and then constructs the surrogate by interpolating upon the true objective using a radial basis function interpolator [47]. Thus, the best point minimizing the surrogate can be taken as a reasonable approximation for the minimizer of the objective. The method tries to balance two competing goals: (1) Complete exploration of search space for a global minimum and (2) Increase speed by arriving at a good solution using as few objective function evaluations as possible. This works best when the objective is smooth and continuous, and has been proven to arrive at globally optimal solutions on bounded domains even though the convergence is not fast [47]. However, smoothness is not strictly required to use this technique. Such an approach can greatly speed up computational times for complex component sizing and economic dispatch problems with non-linear cost functions and a large number of variables and constraints. There is usually no stopping criterion that can accurately recognize when the solver is near a global optimum. Instead the program terminates upon reaching a prescribed number of iterations, function evaluations or time duration and outputs the 'best' solution found within that preset computational budget¹¹.

2.4.4 Simulated annealing (SA)

This is a stochastic search technique modelled after the annealing process in metals that are molten at high temperatures and then allowed to cool and freeze into crystalline structures with minimum energy, with temperature control being the crucial element. A randomly chosen current state is perturbed to a new state at a fixed temperature T with ΔE being the energy gap between the two states. If $\Delta E < 0$, the new state is accepted as the updated current state and if $\Delta E \geq 0$, the new state is accepted with probability:

$$Pr(\text{acceptance}) = \exp\left(\frac{-\Delta E}{k_B T}\right) \quad (2.4)$$

where k_B is the Boltzmann's constant. These perturbations are repeated until the system reaches thermal equilibrium with its environment at temperature T , following which the sequence can be repeated by slightly decrementing the temperature set point. Such an approach can be extended to hybrid microgrid optimization problems where system energy E is replaced by the objective cost function, temperature T corresponds to the control parameter and eq. (2.4) describes the acceptance probability of a particular solution (i.e. system configuration or dispatch strategy) [38]. However, SA is less commonly used for sizing and dispatch of hybrid energy systems compared to popular tools like GA, EA and PSO. Certain past studies have concluded that SA can be faster to converge, but are less efficient than other metaheuristic methods like tabu-search algorithms for optimal sizing problems aimed at minimizing LCOE [50].

2.5 Microgrid control strategies

After completing (1) initial design to choose and size the generation and storage technologies and (2) devising the optimal strategy to schedule and dispatch these components, the next

¹¹<https://uk.mathworks.com/help/gads/surrogate-optimization.html>

major area of research focuses on the real-time, active control of such microgrid systems. Closed loop systems are likely to be superior to open-loop model-based approaches in practical implementation, due to their ability to better predict future system behavior, compute control signals and corrective actions needed to deal with both demand and supply variations [48]. In particular, control is essential to accommodate the high degree of uncertainty in RES power generation due to their intermittency and unpredictable fluctuations.

This becomes even more critical with increased penetration of localized, distributed and decentralized power generation especially in the case of islanded and off-grid systems, where there are special concerns regarding low power quality, safety and overload issues [49]. Furthermore, there is added complexity due to bidirectional flows of both power and information. Thus, some form of feedback control is necessary to improve the robustness of the system and minimize the impact of forecasting errors¹², uncertainties and external disturbances. Examples of disturbances include extreme weather (like wind lulls) affecting wind or solar power output, natural disasters, sudden spikes in demand (particularly due to heating or cooling loads) etc.

Conventional microgrid control structures can be hierarchically differentiated into three levels as shown in fig. 2.6.

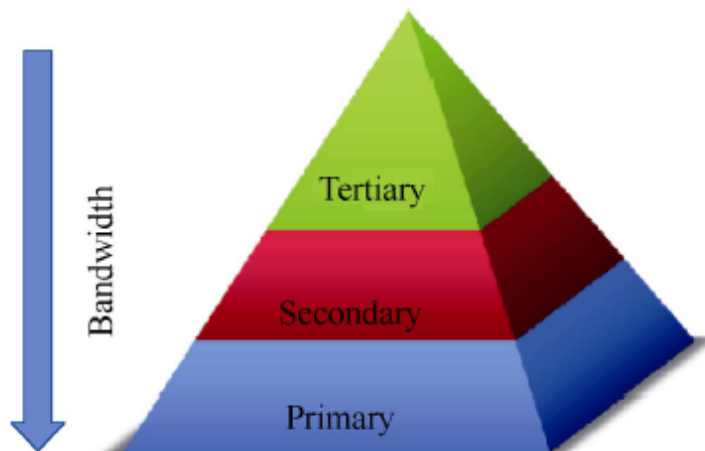


Figure 2.6: Hierarchy of control levels [52].

Primary control is responsible for regulating voltage, frequency and power of individual converters. Secondary control regulates power quality and mitigates voltage or frequency deviations, imbalances and undesirable harmonics. In practice, this translates to maintaining grid frequency around a certain target value and stabilizing supply frequency by regulating real and reactive power flows in real-time, respectively. Finally, the tertiary control handles power exchanges with the external macrogrid and/or other adjacent microgrids [52]. It could also include higher-level tasks like system-wide techno-economic optimization during the design stage and efficiency improvements while making day-to-day dispatch and operational decisions [15].

¹²in load and RES availability

2.5.1 Possible control paradigms

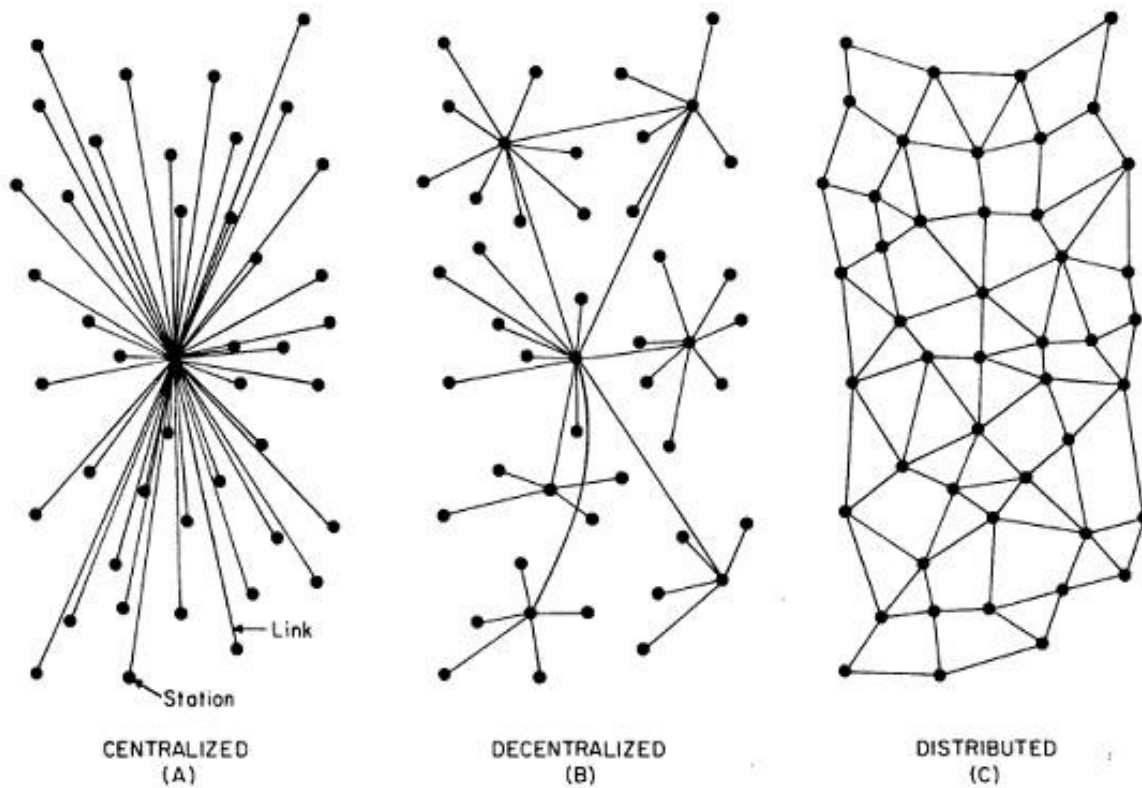


Figure 2.7: The three different levels of control methods [33].

As shown in fig. 2.7, there are broadly three types of control strategies possible in large scale, cyber-physical systems applications like microgrids: Centralized, decentralized and distributed control. These also relate to other electricity distribution networks like macrogrids as well as information exchange networks.

Centralized control

This is the most mature and well-researched of the three methods and has been commonly used to control and economically dispatch generators in electrical power systems [51]. Data is collected from all over the system and processed together in a single controller in order to make decisions which will be directly sent as control signals to each individual agent through supervisory, control, and data acquisition (SCADA). SCADA is an advanced automation control system which centrally manages the control, gathering and monitoring of a power system's operation [53]. Such schemes have a simple conceptual and theoretical framework and have been studied for decades, resulting in the development of a large number of controllers particularly for linear systems [54].

However, these are challenging to implement in reality due to the high level of connectivity and two-way communication links needed, especially as the number of agents increases. Real-time transmission of measurements and computation of control variables may not be feasible if the network is deployed over a large physical area. Thus, these systems may not be cost-effective or computationally tractable and complexity scales poorly with network size. Model-based, offline synthesis may also be difficult to achieve for larger systems with many inputs, states and outputs. Finally, such an approach may be unappealing for socioeconomic and political

reasons as well, especially since all agents are required to share their private information with the central controller [54].

Nevertheless, centralized controllers are a good starting point for smaller microgrids with limited number of agents¹³ and relatively simple network topology. After designing an effective centralized scheme, the microgrid operator could explore ways to transition this to a distributed scheme to account for increasing size and complexity.

Decentralized control

This is a schematic where each agent, node or subsystem (e.g. DG, consumer or BS unit) has its own controller, allowing them to make decisions and apply control actions based only on local measurements like voltage or frequency [49]. This avoids the need for global information over the entire system and allows individual agents to protect their privacy since they no longer exchange their information with a central unit or with other nodes [55]. This can also speed up processes by computing control variables in parallel and allows for easier real-time communication since sensors, controllers and actuators within a given subsystem will be located closer to one another [54].

However, the lack of communication between controllers at different nodes limits attainable performance and cannot guarantee *global* optimality or stability [49]. Nevertheless, both centralized and decentralized methods have been demonstrated to improve transient stability in small-scale power systems like microgrids [56]. Decentralized systems can also be more stable than centralized alternatives having similar configurations, if some nodes get disconnected due to faults or failure, other agents in the system can still keep functioning using local information.

Distributed control

This is a consensus-based approach where individual agents or nodes use both locally measured parameters at their node as well as information shared by their nearest neighbours. In contrast to decentralized control with no information sharing, adjacent agents here share their private information with each other through two-way communication channels. This enables global optimization while still allowing efficient, parallel computation. Furthermore, it allows the designer to tune the trade-off between system performance versus communication burden among controllers and modify network design accordingly [54], while still allowing agents to retain some control over their privacy.

Thus, distributed control is a compromise which offers some of the best properties of both centralized and decentralized control, making it an increasingly popular tool for microgrids. In particular, this approach is well-suited to handle the varying nature of the microgrid and is not greatly impacted by structural changes expected in smart grids in the near future, due to local information sharing. This enables to satisfy both the *peer-to-peer* and *plug-and-play* requirements. The 1st condition ensures reliability, implying that there is no single component which is absolutely critical to microgrid operation and the system can function even in case of failure of individual generators or storage devices. The 2nd, plug-and-play characteristic means that an additional, new unit can be installed at any point in the electrical system without having to reconfigure the network or controller [57]. This allows the microgrid¹⁴ to easily extend and grow as more producers and customers get connected [49], making it an appropriate solution for remote rural electrification.

¹³i.e. producers, consumers and prosumers

¹⁴or any decentralized power grid, in general

Distributed approaches also intuitively lend themselves well to real-time DR and demand-side management (DSM) algorithms that engage both users and generators [58], as well as systems involving dynamic, flexible DGs and smart, responsive loads [59, 60], owing to their scalable nature, fast response and model independence. However, they still face challenges in designing the right communication and control network topology, upgrading existing infrastructure to facilitate bidirectional flows and achieving convergence through consensus among local agents quickly [49].

2.5.2 Types of control methods for microgrids

Model predictive control (MPC) is by far the most common method used in the literature for optimal microgrid operation. This makes the originally static optimization problem dynamic by repeatedly optimizing over a receding, finite time horizon and solving an open-loop optimal control problem at each sampling instant using the current state as the initial state. Only the 1st control action of the resulting sequence is applied to the plant, after which the process is repeated using the new state [95]. The controller therefore uses the current state as a basis for estimating future state variables, by coupling inputs and outputs to be dependent on one another in the observer. Linear MPC generally solves either a quadratic (QP) or linear program (LP) at each iteration or control interval i.e. either a quadratic or linear cost function (objective) subject to linear constraints. Thus, MPC differs from traditional controllers like PI and PID since it solves the optimal control problem 'online' for the *current* state of the system instead of offline control law synthesis (i.e. a uniform precomputed feedback policy that applies to all states) [95]. This gives it a unique, predictive ability valuable for MG control as it can anticipate future events like RES supply fluctuations or demand changes and take actions needed to damp their effects, while satisfying time-varying request and operation constraints [31]. This allows it to achieve better performance over relatively long periods during which disturbances could occur.

Variants of predictive control implemented in literature include formulations using mixed-integer linear as well as nonlinear programs since MG modeling requires both discrete¹⁵ and continuous¹⁶ decision variables [32, 31]. Such feedback mechanisms have been successful in compensating for uncertainty in RES outputs and time-varying loads. Robust linear and nonlinear economic MPC (E-MPC) methods have been developed to optimize setpoints for microgrid dispatch that minimize operational cost [30] and/or maximize profits from selling power back to the main grid [96]. Finite horizon objectives in MPC comprise of stage, terminal and penalty costs, with E-MPC using economic costs as the stage cost function. Closed loop discrete linear MPC has been applied to a photovoltaic–wind–diesel–battery system similar to that considered here [48]. In addition to load and RES uncertainty, predictive control has also been used to deal with uncertainty arising from variations in model parameters of generators [97]. Another interesting example is the use of adaptive, switched MPC where switching constraints are used instead of switched state-space models to model shifting between modes like battery charging and discharging [98].

¹⁵e.g. ON/OFF states of DGs

¹⁶e.g. battery SOC and charge/discharge rates

2.6 Novelties in current study

Although a great deal of work has been conducted in microgrid optimization and control, there still remain several key areas and open research questions that are worth exploring. Most studies surveyed in the literature have focused heavily on grid-connected systems capable of exchanging power with the macrogrid network under ordinary operation and are only islanded in special circumstances. Thus, past research has largely overlooked the optimal design and operation of off-grid microgrids that are completely isolated, in spite of the special stability, reliability and security issues they present for planning, energy management and control.

A few studies have considered systems with constrained external power exchange e.g. by placing hourly bounds on energy transfers with the macrogrid [30] and even islanded ones but have not analyzed their long-term performance under a variety of scenarios, as well as their responses to potential disturbances over extended periods of time. Such analyses are essential to accurately assess the reliability and robustness of off-grid systems. Furthermore, the limited number of studies on islanded microgrids so far have mainly focused on the sizing, design optimization and planning stages but relatively less work has been conducted on devising the best day-to-day and hourly operating plans for such systems.

Chapter 3

Methodology

3.1 Microgrid system description

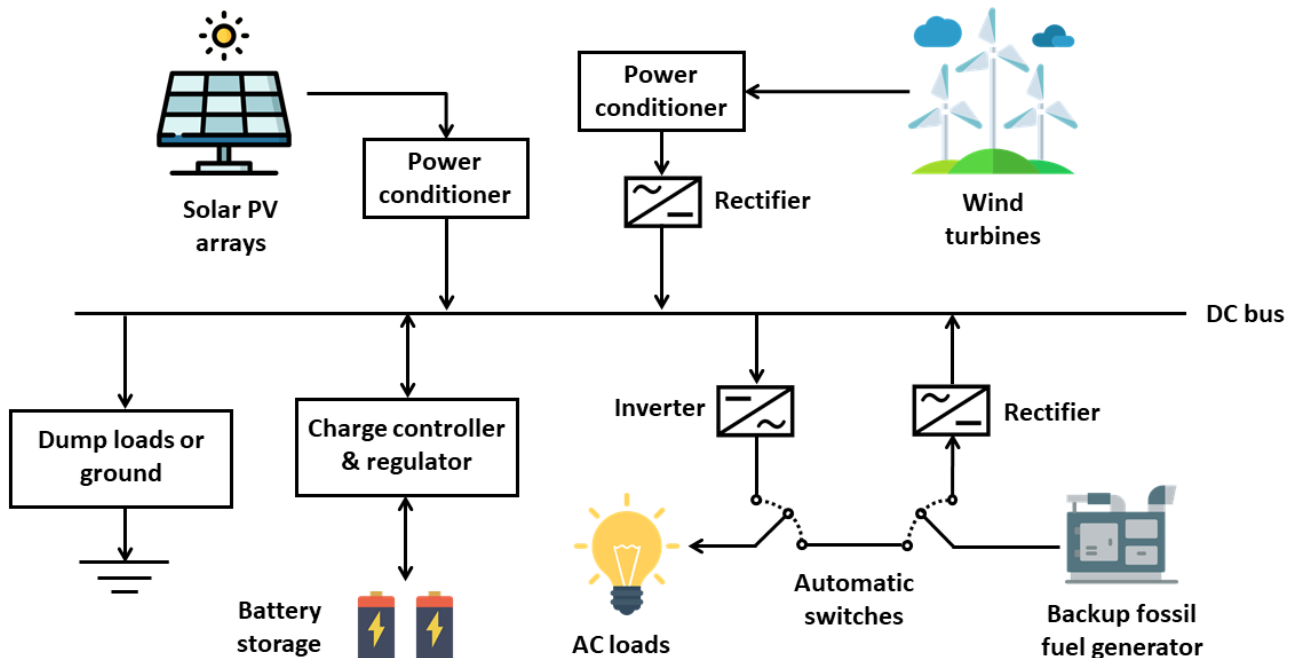


Figure 3.1: Schematic illustrating key components and power flows in the hybrid microgrid.

The microgrid consists of the following key components as shown in fig. 3.1:

- Decentralized renewable power generation sources (RES) that are non-controllable, non-deterministic devices
 - Solar photovoltaic arrays (PV)
 - Wind turbine generators (WT)
- Standby, fossil fuel distributed generators (DG) for backup which are controllable, deterministic units
 - Diesel engines (DE)

- Micro turbines (MT)
- Battery energy storage (BS)
 - Lithium ion (Li^+) batteries (LI)
 - Lead-acid batteries (LA)
- Charge controllers that regulate the state of charge (SOC) as well as charging and discharging processes of the batteries
- Power conditioners which regulate and improve the quality of power delivered from the RES generators to the DC bus
- Bidirectional power converters that can function either as an inverter (DC-to-AC conversion) or rectifier (AC-to-DC conversion) depending on the system requirement

The modelling of each of these systems is described in greater detail in the following subsections. This is a hybrid microgrid since it consists of both conventional and renewable generation sources. It is an isolated system in islanded mode serving a remote, rural community implying that there are no connections or power transfers with any larger, external macrogrid. Thus, the MG can neither sell excess power to, nor purchase power from, the main grid.

3.1.1 Renewable energy sources (RES)

The renewable power generation sector today is heavily dependent on (1) biomass ¹ which often has adverse implications for vegetation and biodiversity despite being carbon-neutral, and (2) large hydroelectric schemes which negatively affect local ecosystems and displace communities. Furthermore, bioenergy is land-intensive, leads to deforestation and often competes with crop cultivation for food purposes, while most of the geographical sites well-suited to hydropower have already been developed. This is especially true in east African countries like Kenya and Tanzania which are the focus of this study. Furthermore, there have recently been recurring droughts in the region which affect the head², flow rate and thus the amount of hydropower available [86]. Thus, these two major sources were excluded from this study. Wind turbines and solar photovoltaics were the only two renewables considered.

Solar PV arrays

The hourly DC power output [W] of the PV generator is calculated using [18]:

$$P_{PV} = n_s \eta_{PV} A_c I_{PV} \quad (3.1)$$

where the variables are described in table 3.1:

¹such as firewood, charcoal etc.

²level of water in reservoirs

Symbol	Description
n_s	Total number of PV modules used in the MG
$\eta_{PV} [\%]$	Power conversion efficiency of each module
$A_c [m^2]$	Collector area of each PV array
$I_{PV} [kW/m^2]$	Hourly solar irradiation incident on the array i.e. the global horizontal irradiance (GHI)

Table 3.1: Explanation of variables in the PV power equation.

PV module efficiency varies as a function of incident radiation I_{PV} , ambient outside air temperature T_a and test parameters of the solar cell which are measured at nominal operating cell temperature (NOCT) and standard test conditions [18]:

$$\eta_{PV} = \eta_r \eta_{pc} \cdot \left(1 - 0.9\beta \left(\frac{I_{PV}}{I_{PV,NOCT}} \right) (T_{c,NOCT} - T_{a,NOCT}) - \beta(T_a - T_r) \right) \quad (3.2)$$

where η_r is the PV efficiency measured at reference cell temperature T_r and standard test conditions. β is the temperature coefficient of cell efficiency which tracks degradation in cell performance with rising temperature. $I_{PV,NOCT}$ is the average solar radiation incident on the array per hour at NOCT while $T_{c,NOCT}$ and $T_{a,NOCT}$ are the cell and ambient external temperatures at NOCT test conditions, respectively. Maximum power point tracking (MPPT) via the power conditioner is also used to extract maximum possible power from the system. The power conditioning efficiency $\eta_{pc} = 1$ since it's assumed that a perfect MPPT controller is used [63].

In this system, Mitsubishi Electric photovoltaic modules were used with characteristic parameters shown in table 3.2. These use monocrystalline Silicon cells with a power rating of 255 W each.

Parameter	Value
$\eta_r [\%]$	15.4
$T_r [{}^\circ C]$	25
$I_{PV,NOCT} [kW/m^2]$	0.8
$T_{c,NOCT} [{}^\circ C]$	45.7
$T_{a,NOCT} [{}^\circ C]$	20
$\beta [\%/{}^\circ C]$	0.0045
$P_{PV,r} [kw]$	0.255
$A_c [m^2]$	1.4602

Table 3.2: Specifications of the 255 Wp PV-MLU255HC model [62].

Wind turbines (WT)

A small scale on-shore horizontal-axis wind turbine system from Raum energy rated at 3.5 kW each was considered. This is a 5-blades downwind system. A low power rating was chosen due to the relatively lower energy requirements of the rural microgrid community as well as the lower installation ³ and permitting fees associated with such compact systems. This results in lower upfront investment and initial capital costs. The technical specifications are listed in table 3.3.

³civil engineering, construction, land requirements and supporting infrastructure

The power output of the WT depends on several factors including the wind speed pattern at the particular location, air density ρ_{air} , swept area A_{swept} and the efficiency η_w with which the rotor converts the kinetic energy of wind to electrical energy [48]:

$$P_{WT} = n_w \frac{1}{2} \eta_w \rho_{air} C_p A_{swept} v_{hub}^3 \quad (3.3)$$

where n_w is the total number of wind turbines and v_{hub} is the wind speed at the rotor hub (at height h_{hub}) and can be estimated using [48]:

$$v_{hub}(t) = v_{ref}(t) \left(\frac{h_{hub}}{h_{ref}} \right)^\beta \quad (3.4)$$

where v_{ref} is the hourly wind speed measured at reference height h_{ref} close to ground level and β is the power law exponent or roughness coefficient which ranges from less than 0.1 for flat land, water or ice to more than $\frac{1}{4}$ for heavily forested regions [19]. A value of $\frac{1}{7}$ (0.14) was used in this study which is appropriate for wind farm installations on flat surfaces like open-terrain grasslands (such as those found in Kenya and Tanzania) away from tall trees and buildings (as is the case with rural areas) [66].

For this work, a variable speed permanent magnet generator was used due to its capability to maintain the system at its optimal designed tip-speed ratio (λ) that maximizes the power coefficient C_p , generator conversion efficiency and thus also the power output produced η_w [65].

Parameter	Value
h_{hub} [m]	14.5
h_{ref} [m]	1
$P_{WT, r}$ [kW]	3.5
A_r [m^2]	12.6
v_c [m/s]	2.8
v_r [m/s]	11
v_f [m/s]	22

Table 3.3: Specifications of the small-scale WT system [64].

However, η_w and C_p were not readily available from the manufacturer's data sheet and neither was their variation with wind speed given for this specific model. Thus an empirical model was used to calculate power output based on $P_{WT, r, total}$ ($= n_w \cdot P_{WT, r}$) and v_{hub} by dividing the WT power output curve into three characteristic regions as shown in fig. 3.2 [67]:

$$P_{WT}(v_{hub}) = \begin{cases} n_w \cdot P_{WT, r} \cdot (A + B \cdot v_{hub} + C \cdot v_{hub}^2) & \text{if } v_c \leq v_{hub} \leq v_r \\ n_w \cdot P_{WT, r} & \text{if } v_r \leq v_{hub} \leq v_f \\ 0 & \text{otherwise} \end{cases}$$

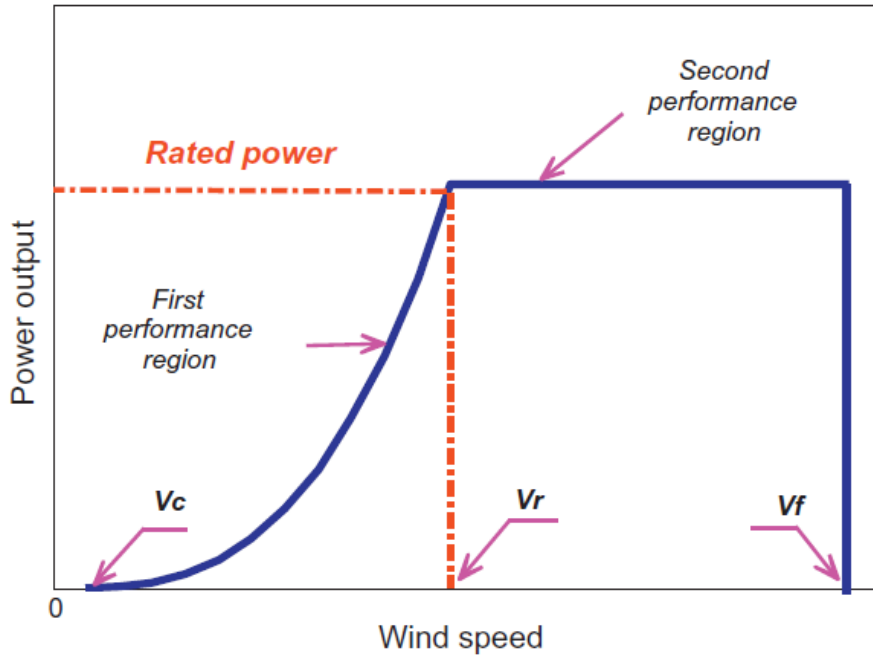


Figure 3.2: WT output characteristic [19].

where v_c , v_r and v_f are the cut-in (start-up), rated and cut-out (failure) wind speeds, respectively. The constants A , B and C can be computed using [67]:

$$A = \frac{1}{v_c^2 - v_r^2} \left(v_c(v_c + v_r) - 4v_c v_r \left(\frac{(v_c + v_r)}{2v_r} \right)^3 \right) \quad (3.5)$$

$$B = \frac{1}{v_c^2 - v_r^2} \left(4(v_c + v_r) \left(\frac{(v_c + v_r)}{2v_r} \right)^3 - 3(v_c + v_r) \right) \quad (3.6)$$

$$C = \frac{1}{v_c^2 - v_r^2} \left(2 - 4 \left(\frac{(v_c + v_r)}{2v_r} \right)^3 \right) \quad (3.7)$$

Climate data

In order to estimate solar and wind power generation, historical temperature, wind speed and solar irradiance data were obtained at an hourly resolution for an entire year (2018) from ground-based weather stations which tend to be more accurate than satellite measurements, on average. These hourly averaged values were made available by the Trans-African HydroMeteorological Observatory (TAHMO), a public benefit organisation that maintains a vast network of weather stations across Africa [68].



Figure 3.3: Location of proposed microgrid site in Timbila, Kenya.

The microgrid was designed for a rural village near Timbila in southern Kenya close to the Tanzanian border as shown in fig. 3.3. This location was chosen due to required weather and load data being available more easily. However, several of the wind speed values were missing in the TAHMO datasets⁴. These values were approximated by averaging the wind speed from four other neighbouring TAHMO stations located close to Timbila, specified in table 3.4.

Location	Lat (°N)	Lon (°E)	Elevation (m)
Timbila High School, Kenya	-3.39	37.72	743
Imurtott Primary School, Kenya	-2.88	37.39	1853
South Eastern Kenya University - Mtiti Adei Campus	-2.66	38.11	854
Our Lady of Perpetuah Girls Sec- ondary School, Kenya	-3.50	38.59	1158
Bangalala, Tanzania	-4.23	37.85	877

Table 3.4: Geographical details of stations used to generate combined climate data [68].

It was also found that the wind speeds measured by the TAHMO stations were consistently lower than actual, real-time values for Timbila reported online [69]. The TAHMO values averaged only ≈ 0.86 m/s even though the actual values from weather forecasts averaged ≈ 3.19 m/s. This indicates some systematic error in the TAHMO wind speed measurements⁵. However,

⁴due to various reasons like the anemometer malfunctioning or the station being taken offline temporarily for repairs

⁵this could be due to some form of calibration, bias or offset error

the temporal variation in the TAHMO data agrees with actual observed wind speed patterns on an hourly, daily and annual basis. Thus, the TAHMO wind speed values were scaled by a correction factor of ≈ 3.70 ($= \frac{3.19}{0.86}$) so that the new scaled annual average is close to 3.19 m/s.

Sample hourly profiles of solar irradiance, wind speed and ambient air temperature are shown in fig. 3.4 for TAHMO data recorded on January 1, 2018. In addition, daily averaged profiles of solar irradiance, total solar radiation, wind speed and temperature are shown in fig. 3.5.

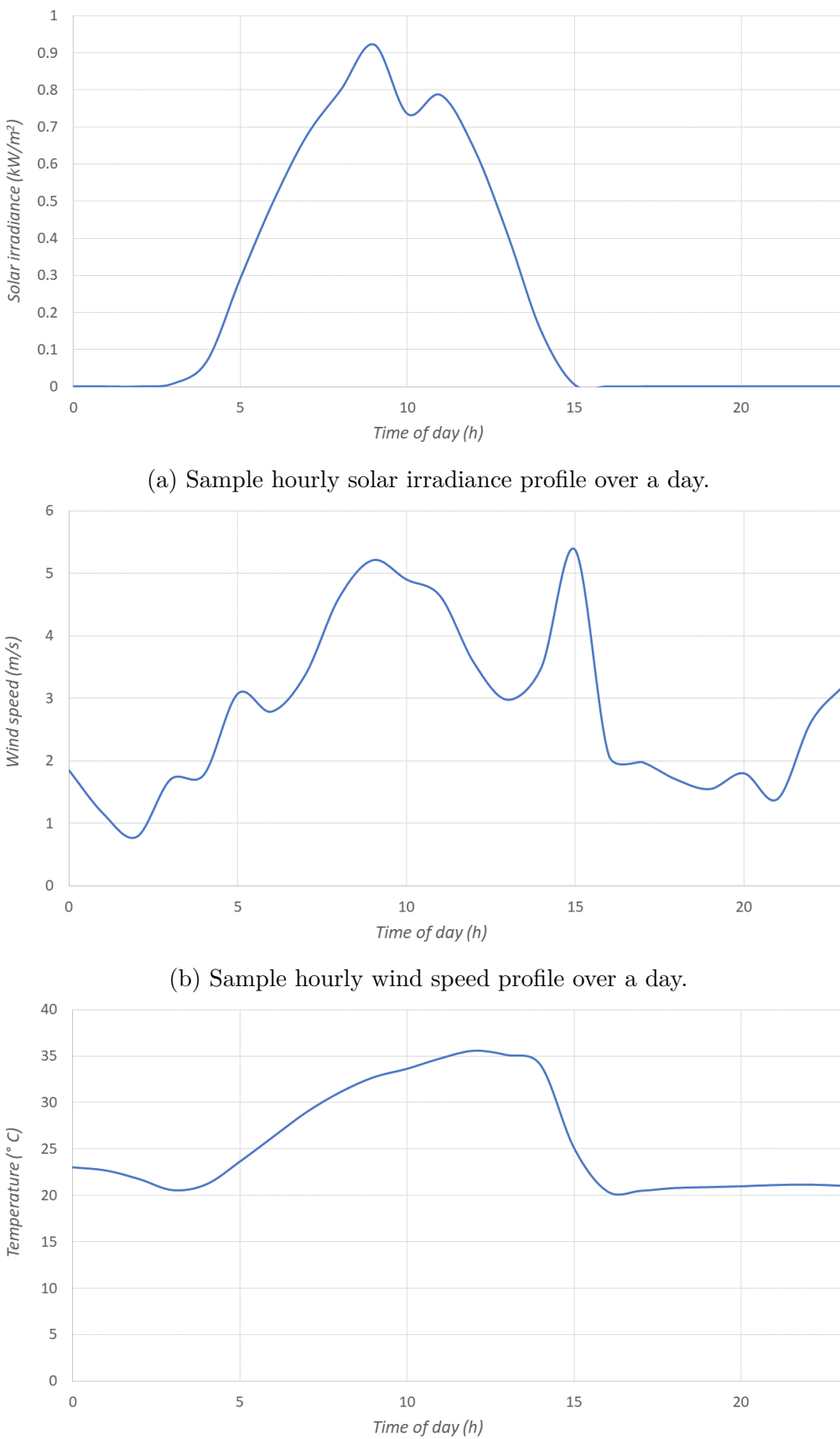


Figure 3.4: Examples of hourly profiles of climate variables over a characteristic day.

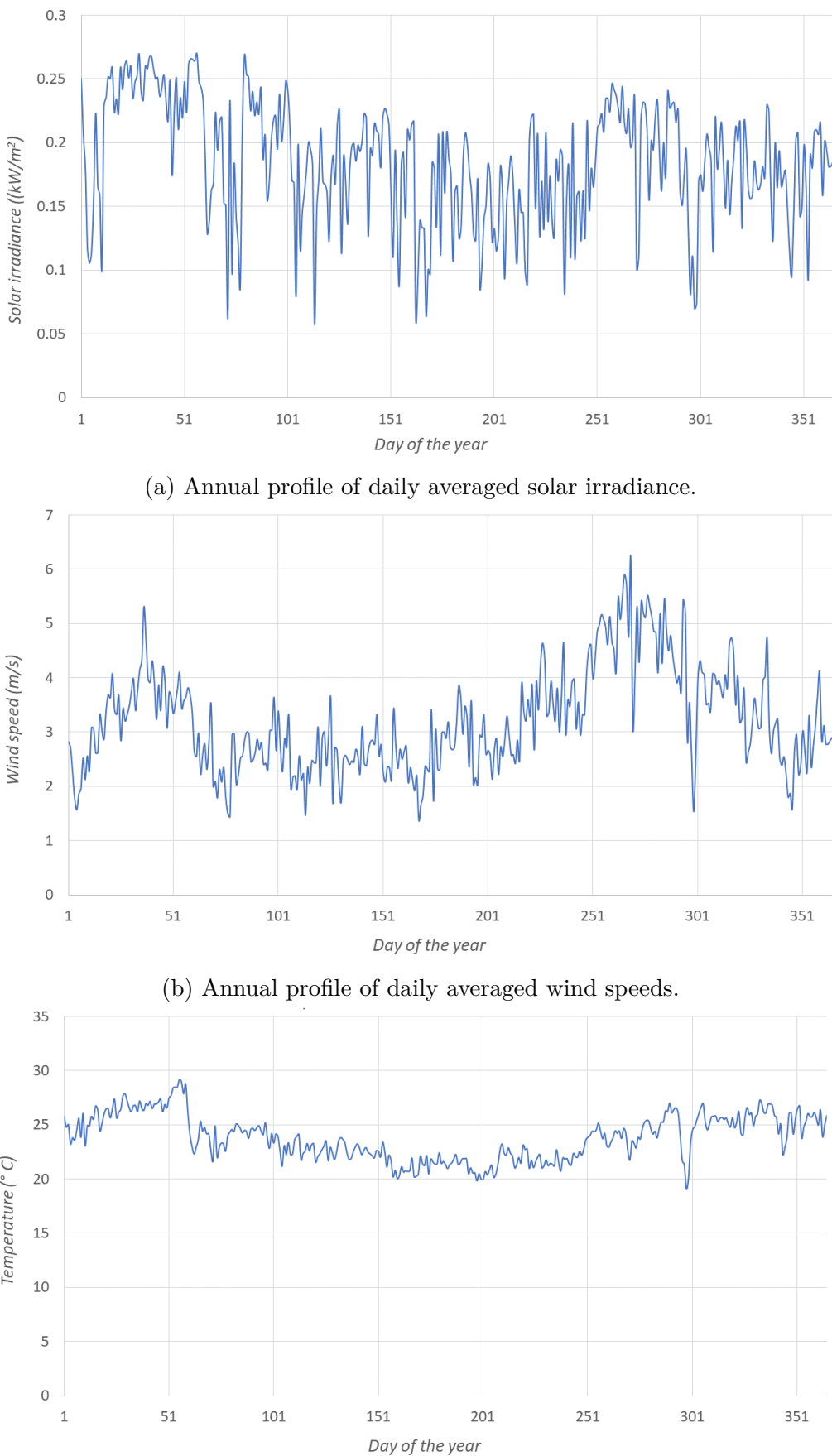


Figure 3.5: Daily profiles of climate variables over the year 2018.

3.1.2 Electricity demand (load)

Characteristic rural African load profiles were obtained using NREL's ReOpt tool [27]. The assumptions made regarding the MG community (small, remote village) are listed in table 3.5. For simplicity, it was assumed that there is no significant variation in load profiles between weekdays and weekends or from season to season. These assumptions are reasonable given the tropical climate in Timbila⁶ with similar weather conditions all year round, and the relatively low penetration of commercial entities and businesses in the largely residential village. Household, commercial and combined demand profiles are shown for one characteristic day (24 h period) in fig. 3.6. Since the sizing optimization was conducted over a horizon of one year, the daily profile was used to artificially generate an annual load profile giving hourly power demands for all 365 days of the year. This was done by setting the profile for January 1, 2018 to that shown in fig. 3.6 and then allowing hourly demand in subsequent days to randomly vary by $\pm 20\%$. By introducing random variability in day-to-day (instead of hour-to-hour) fluctuations, the load curves in other days still maintain a similar shape or pattern. Key summary statistics for the resulting daily load profile are listed in table 3.6.

Parameter	Value
Number of households	100
% of high income households	33%
% of medium income households	33%
% of low income households	33%
Number of water pumping operations	6
Number of milling operations	4
Number of small shops	10
Number of schools	1
Number of clinics	3
Number of street lights	30

Table 3.5: Description of MG community near Timbila, Kenya.

⁶located just a few degrees south of the equator

Parameter	Value
Average kWh/day	203
Total kWh/year	74,251
Maximum kW/day	12.52
Minimum kW/day	3.21
Average kW/day	8.48

Table 3.6: Summary statistics for annual and daily load patterns.

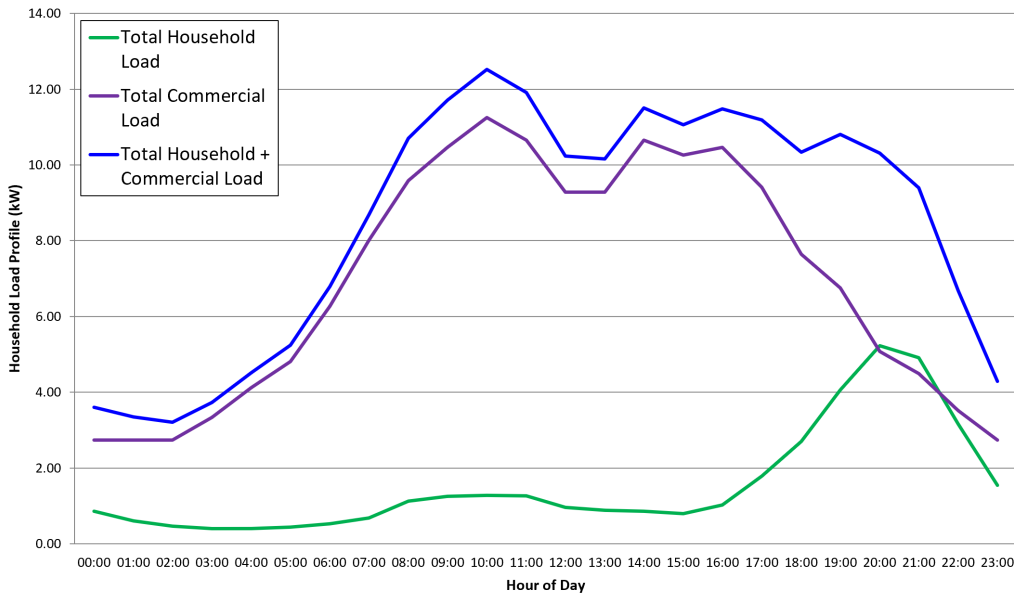


Figure 3.6: Rural African microgrid load profiles used in this study [27].

3.1.3 Backup distributed generators (DG)

In order to ensure system reliability, standby distributed generators using conventional fossil fuels must provide backup power. These are only called upon to satisfy excess demand that cannot be met by renewables and battery storage. This is essential in cases of sudden jumps in demand or insufficient supply from renewable sources due to inclement weather, natural disasters etc.

Similar to the wind turbines, variable speed control was used for the fossil-fueled distributed generators as well due to its lower fuel consumption compared to constant speed operation. Such control allows the engine or turbine to operate at lower speeds to meet low power demand levels and vice versa, thus maximizing the operational efficiency of the DG [65].

In order to simplify the problem, it was assumed that the system uses only one DG rather than having to individually dispatch multiple units. The sizing of the diesel generator or micro turbine was not considered as a variable in the optimization problem. Instead, the rated power of the DG was set to meet the microgrid community's peak demand for electric power [71]:

$$P_{DG, r} = P_{load, peak} \cdot (1 + SF) \quad (3.8)$$

where SF is a safety factor that determines the extent to which the DE or MT is oversized. This excess backup power is considered as spinning or operating reserves since it is the extra capacity obtained by increasing the rotational speed of the synchronous generator.

Diesel engines (DE)

These are traditional reciprocating, internal combustion engines based on compression ignition that diesel as their fuel. These offer several advantages including their dispatchable nature (unlike RES), quick startup and load-following ability but also have demerits such as high fuel costs, pollutant emissions including greenhouse gases and particulates and noise generation [15]. Based on a peak load of 12.52 kW, the maximum power rating of the DE was set to 16 kW, thus oversizing by $\approx 28\%$ ($SF \approx 0.278$). According to [38], the lower limit on the DE's power output can be estimated as:

$$P_{DE, min} = 0.3 \cdot P_{DE, r} = 4.8 \text{ [kW]} \quad (3.9)$$

The hourly volumetric fuel consumption of the DE can be calculated using the following linear law depending on the power output level $P(t)_{DE, gen}$ [in L/h] needed by the load [17]:

$$Fuel_{DE}(t) = \alpha_{DE} P(t)_{DE, gen} + \beta_{DE} P(t)_{DE, r} \quad (3.10)$$

where α_{DE} [L/kWh] and β_{DE} [L/kWh] are fuel consumption curve coefficients supplied by the manufacturer, assumed to be 0.246 and 0.08145 respectively [17]. The hourly fuel costs of the DE can be calculated assuming a unit price of \$ 3.20 per US liquid gallon of diesel⁷:

$$C_{fuel, DE}(t) = 3.20 \cdot \frac{Fuel_{DE}(t)}{3.78541} \quad (3.11)$$

Micro-gas turbines (MT)

Another option for the backup DG is a microturbine, which can run on a diverse range of gaseous and liquid fuels. These offer similar advantages to DEs with additional benefits of being compatible with combined heat and power (CHP) applications. For CHP purposes, natural gas is the most common fuel. Furthermore, these have lower greenhouse gas emissions than DEs and much less than larger, centralized natural gas plants, especially for NO_x and CO_2 exhausts [43]. However, microturbines are more expensive upfront with higher initial capital costs and often higher fuel costs as well when compared to diesel. They are also not nearly as prevalent across the African continent as diesel gensets currently are.

Microturbines tend to be larger on average than diesel engines, generally ranging from 30 to 330 kW. However, for direct comparison with the diesel alternative, the same size was chosen for the MT as well, with $P_{MT, r} = P_{MT, max} = 16 \text{ kW}$ and $P_{MT, min} = 4.8 \text{ kW}$. According to [73], the fuel consumption of a 61 kW MT is 0.84 MMBtu per hour of operation at its fully rated power. Extrapolating from this, the hourly fuel consumption of the MT [in MMBtu/h] can be approximated using the output level P_{MT} :

$$Fuel_{MT}(t) = \frac{0.84}{61} \cdot P_{MT}(t) \quad (3.12)$$

⁷1 US gal = 3.78541 L

The hourly fuel consumption cost of the MT can then be computed assuming a unit price of $C_{NG} = \$2.19/MMBtu$ for natural gas [83].

$$C_{fuel, MT}(t) = 2.19 \cdot Fuel_{MT}(t) \quad (3.13)$$

Converter

A bidirectional converter was used that is capable of acting as both an inverter and rectifier, with a power rating equal to the peak load (12.52 kW). The efficiencies of both AC-DC and DC-AC conversion were assumed to be equal i.e. $\eta_{inv} = \eta_{rec} = 90\%$ [76] and the lifetime was assumed to be 20 y [45]. The capital cost of the converter was taken to be $IC_{conv} = \$2800$ [85].

3.1.4 Battery energy storage (BS)

Two options for electrochemical energy storage are considered: Lithium-ion (Li^+) and Lead-acid batteries. Although these two differ in their parameters, the same discrete time model was used to describe their charging and discharging processes [48]:

$$SOC(t+1) = (1 - \delta)SOC(t) - \frac{1000 \cdot P_{BS} \Delta t \eta_{overall}}{E_C} \quad (3.14)$$

where P_{BS} [kW] is the DC power dispatched either to or from the battery in each time step Δt and δ is the hourly self-discharge rate (%/h). A positive P_{BS} value indicates that the battery is being discharged while a negative P_{BS} implies charging. SOC is its state of charge which indicates the remaining available battery capacity as a percentage of its current maximum energy capacity E_C .

$$SOC = \frac{E_{releasable}}{E_C} \quad (3.15)$$

Since it is difficult to measure both charging and discharging efficiencies separately, an overall round-trip Coulombic efficiency $\eta_{overall}$ for the battery is used, which applies to both stages. Key properties of both batteries are listed in table 3.7:

Parameter	Li-ion (LI)	Pb-acid (LA)
SOC_{min}	10%	50%
SOC_{max}	90%	90%
δ [%/month]	7.5	5
$\eta_{overall}$	90%	75
Lifetime [in y]	15	5
Lifetime t_{BS} [in cycles]	5475	1400
$P_{BS, r}$ [kW]	3.68	0.42
Capacity fading Δ_E [%/cycle]	0.0055	0.0214

Table 3.7: Parameters of the Li-ion and Lead-acid BS systems [74].

The battery's state of charge must remain within the upper and lower limits SOC_{max} and SOC_{min} respectively, throughout its operation. In the simulation, the BS was assumed to be fully charged at the start ($t = 0$) i.e. $SOC = SOC_{max} = 90\%$ for both the LI and LA systems. The lower limit is determined by the maximum level until which the battery can be safely

discharged, known as the depth of discharge DoD i.e. $E_{b, min} = (1 - DoD) \cdot E_C$. The maximum capacity of the battery E_C is initially equal to the original rated capacity $E_{b, init}$ but then gradually degrades linearly with increased cycling in a process known as capacity fading.

$$E_C = E_{b, init} \cdot (1 - n_{cycles} \cdot \Delta_E) \quad (3.16)$$

where n_{cycles} is the cumulative number of charge-discharge cycles so far, a variable that's updated at each iteration in the dispatch algorithm. Since the system is simulated over a horizon of one year, this gives the total number of cycles per year. Capacity fading values for both Li-ion and Pb-acid were calculated assuming that the battery is replaced once E_C has reduced to 70% of its original rated value from table 3.7. Some of the Li-ion parameters were updated using the latest values for the Tesla Powerwall [75], assuming that the battery can be fully cycled daily for five years beyond the specified 10-year warranty period [74].

Table 3.7 clearly shows tradeoffs in terms of relative advantages and disadvantages of the two options. Lead-acid batteries have lower lifetimes (requiring more frequent replacement) and lower round-trip efficiencies than Li-ion. Li-ion also allows deeper discharge enabling the battery capacity to be utilized more fully, while the much higher peak power allows for faster discharge to meet more of the demand. However, it has a slightly higher self-discharge mainly owing to the parasitic protection circuit and is currently more expensive, requiring greater initial investment than Lead-acid. However, the slower capacity fading means it needs to be replaced less often, this could make it the more economical depending on the manner in which the battery is dispatched and how often it's cycled during operation.

3.2 Formulation of optimization problem

A discrete-time, iterative optimization is performed:

1. **Design and sizing optimization:** Over a time horizon of 1 year (8760 h) using time steps of 1 h each ($\Delta t = 1 h$). Three variable inputs in this problem are the number of solar PV modules n_s , number of wind turbines (n_w) and initial rated battery capacity ($E_{b, init}$). The sizing is done to minimize several objectives including levelized lifecycle costs, emissions, dump energy and lost load.
2. **Day-ahead dispatch optimization:** This is an economic and environmental/emissions dispatch (EED) over a time horizon of 1 day (24 h) using hourly time steps. This is conducted by taking as given the optimal sizes and capacities outputted by the design/sizing optimization above and then optimizing with respect to $P_{DG}(t)$ and $P_{BS}(t)$ as variable inputs. Thus, it optimizes the scheduling and operation of dispatchable units (DG and BS) while renewable power output P_{RES} is decided by climatic conditions and thus non-dispatchable.

3.2.1 Costs

Since this problem involves a multi-period optimization over the entire lifecycle of the project ($t_{sys} = 25y$), it is necessary to discount all cash flows to the present. Table 3.8 lists the assumptions made for this discounting.

Parameter	Symbol	Value
Nominal interest or discount rate (%)	i	9 [91]
Inflation or escalation rate (%)	f	5.7 [90]
System lifetime (y)	t_{sys}	25
PV lifetime	t_s	25
WT lifetime	t_w	20

Table 3.8: Key financial parameters used in the model.

Sizing optimization problem costs

The initial capital (IC) investment for the RES sources (PV and WT) and backup DGs are calculated using installed cost values per unit of rated power, while the upfront expenditure for the batteries is calculated using the cost per unit of rated energy capacity. Replacement costs (RC) are estimated to be a smaller fraction of IC since it excludes one-time fees like permitting and installation. RES sources and batteries were assumed to only have fixed annual operation and maintenance (O&M) costs calculated as a fraction of one-time capital costs, while the converter was assumed to have zero O&M costs. However, the DGs have running costs in addition to fixed O&M, for fuel consumption, variable O&M (depending on its number of operational hours) as well as startup SUC (to bring the DG online) and shutdown SDC (to turn off the DG) costs. These are summarized in table 3.9 and table 3.10.

Parameter	PV	WT	Li-ion	Pb-acid
IC_{kW} [\$/kW]	1210	1500	-	-
IC_{kWh} [\$/kWh]	-	-	300	255
RC [% of IC]	-	-	90	90
OM_{fix} [% of IC /y]	1	3	1	1

Table 3.9: Costs assumed for the RES and BS.

Parameter	DE [45]	MT [73]
IC_{kW} [\$/kW]	781.25	3320
RC	88	90
OM_{fix} [% of IC /y]	2	2
OM_{var}	0.24 [\$/h]	0.013 [\$/kWh]
SUC [\$]	0.45	0.45
SDC [\$]	0.23	0.23
Lifetime t_{DG} [h]	15000	40000

Table 3.10: Cost assumptions for the DGs.

The capital costs for WT and PV were assumed to be globally weighted averages of installed capital costs⁸ [77] while the fixed O&M costs were taken from [19] and the battery values from

⁸The assumed initial investment costs for WT and PV are likely to be slight underestimates since these average values also consider much larger, utility scale projects (of the order of MW) which tend to have lower installed costs than small-scale installations like those in MG, due to economies of scale.

[78]. Replacement was considered only for components with the shortest lifetimes i.e. the BS and backup DGs. Since the converter and WT have much longer lifetimes close to the overall project lifetime, these were not included in the replacement costs.

Discrete vector variables $\overrightarrow{DG_{ON}}(t)$ ⁹ were created to keep track of the operational state (ON/OFF) of the DG in each time interval t , in order to calculate the total startup, shutdown and variable O&M costs. $DG_{ON}(t) = 0$ implies that the DG is switched off while $DG_{ON}(t) = 1$ indicates that it has been brought online. Another discrete variable $BS_{cycled}(t)$ records whether the battery has already been cycled before ($= 1$) or not ($= 0$) in the current iteration, to avoid being self-discharged twice within the same time step during dispatch. The total initial capital (or installed) costs are:

$$IC_{total} = IC_{PV} + IC_{WT} + IC_{BS} + IC_{DG} + IC_{conv} \quad (3.17)$$

$$= IC_{PV, kW} \cdot P_{PV, r, total} + IC_{WT, kW} \cdot P_{WT, r, total} \quad (3.18)$$

$$+ IC_{BS, kWh} \cdot E_{b, init} + IC_{DG, kW} \cdot P_{DG, r, total} + IC_{conv} \quad (3.19)$$

$$= IC_{PV, kW} \cdot n_s \cdot P_{PV, r} + IC_{WT, kW} \cdot n_w \cdot P_{WT, r} \quad (3.20)$$

$$+ IC_{BS, kWh} \cdot E_{b, init} + IC_{DG, kW} \cdot P_{DG, r, total} + IC_{conv} \quad (3.21)$$

The total annual recurring costs are:

$$C_{rec} = OM_{fix, PV} + OM_{fix, WT} + OM_{fix, BS} + OM_{fix, DG} \quad (3.22)$$

$$+ OM_{var, DG, annual} + C_{fuel, DG, annual} + SUC_{DG, annual} + SDC_{DG, annual} \quad (3.23)$$

$$(3.24)$$

where

$$OM_{var, DG, annual} = \sum_{t=1}^{t=8760} DG_{ON}(t) \cdot OM_{var, DG} \quad (3.25)$$

$$C_{fuel, DG, annual} = \sum_{t=1}^{t=8760} C_{fuel, DG}(t). \quad (3.26)$$

and $SUC_{DG, annual}$ and $SDC_{DG, annual}$ are incremented by SUC_{DG} and SDC_{DG} respectively, whenever there is a change in the operational state of the DG (i.e. if $DG_{ON}(t) \neq DG_{ON}(t-1)$).

The recurring costs incurred above in the 1st year of operation are assumed to remain the same in all years of the MG operation henceforth. Thus the present worth (PW) of these recurring costs can be calculated using [79, 80]:

$$PW_{C_{rec}} = C_{rec} \frac{\left(\frac{1+f}{1+i}\right) \left(\left(\frac{1+f}{1+i}\right)^{t_{sys}} - 1\right)}{\left(\frac{1+f}{1+i}\right) - 1} \quad (3.27)$$

The total non-recurring costs are due to periodic replacement of the DG and BS:

$$C_{non-rec} = RC_{DG} + RC_{BS} \quad (3.28)$$

These can also be converted to PW using [79, 80]:

$$PW_{C_{non-rec}} = C_{non-rec} \frac{\left(\frac{1+f}{1+i_{adj}}\right) \left(\left(\frac{1+f}{1+i_{adj}}\right)^{t_{sys}} - 1\right)}{\left(\frac{1+f}{1+i_{adj}}\right) - 1} \quad (3.29)$$

⁹i.e. $\overrightarrow{DE_{ON}}(t)$ and $\overrightarrow{MT_{ON}}(t)$

where i_{adj} is an adjusted interest rate computed as:

$$i_{adj} = \frac{(1+i)^L}{(1+f)^{L-1}} - 1 \quad (3.30)$$

where L is the time period of replacement¹⁰. Assuming that the system is operated in a similar manner to its first year throughout its subsequent operation, the replacement period of the DG and BS can be determined using the variables n_{cycles} and DG_{ON} . The number of years between successive BS replacements is given by:

$$L_{BS} = \frac{t_{BS}}{n_{cycles}} \quad (3.31)$$

Furthermore, if an hourly simulation time-step is used (i.e. $\Delta t = 1 h$), then DG_{ON} gives the total number of operational hours of the DG each year and the years between its replacement is:

$$L_{DG} = \frac{t_{DG}}{\sum_{t=1}^{t=8760} DG_{ON}} \quad (3.32)$$

The total net present cost (TNPC) can then be obtained by summing up all the lifecycle costs of the system over its lifetime and then discounting back to a common base (the present) [19]:

$$TNPC [\$] = IC_{total} + PW_{C_{non-rec}} + PW_{C_{rec}} \quad (3.33)$$

Subsequently, the total annualized cost (TAC) can be calculated as:

$$TAC = TNPC \cdot CRF \quad (3.34)$$

where CRF is the capital recovery factor and is used to calculate the present value of an annuity¹¹ [66]:

$$CRF = \frac{r(1+r)^{t_{sys}}}{(1+r)^{t_{sys}} - 1} \quad (3.35)$$

where r is the real interest rate, given by¹²:

$$r = \frac{i-f}{1+f} \quad (3.36)$$

Dispatch optimization problem costs

The cost calculations for day-ahead dispatch are similar to those for sizing, except that it only considers the running operational costs like daily O&M and fuel costs incurred over a 24 h period, excluding initial capital and replacement costs. Thus, there is no need for discounting in this case and total daily costs can be readily calculated as:

$$C_{daily} = C_{fuel, DG, daily} + OM_{var, DG, daily} + SUC_{DG, daily} + SDC_{DG, daily} \quad (3.37)$$

$$+ \frac{OM_{fix, PV} + OM_{fix, WT} + OM_{fix, BS} + OM_{fix, DG}}{365} \quad (3.38)$$

¹⁰i.e. the number of years between two consecutive payments of the non-recurring cost

¹¹a series of annual cash flows

¹²the formula for real discount or interest rate was borrowed from https://www.homerenergy.com/products/pro/docs/3.11/real_discount_rate.html

where

$$OM_{var, DG, daily} = \sum_{t=1}^{t=24} DG_{ON}(t) \cdot OM_{var, DG} \quad (3.39)$$

$$C_{fuel, DG, daily} = \sum_{t=1}^{t=24} C_{fuel, DG}(t). \quad (3.40)$$

3.2.2 Objective functions

While optimizing the design, sizing and dispatch of the MG, there are several objectives that need to be pursued simultaneously and sometimes, these may even compete or be in conflict with one another. Thus, it is necessary to perform a multiobjective, multiperiod, constrained and bounded optimization in order to obtain a holistic and comprehensive solution while also being able to clearly visualize tradeoffs between the various goals. Five distinct objectives are considered in the current optimization problem:

Levelized cost of electricity (LCOE)

LCOE [\$/kWh] is the ratio of total annual costs to the total annual electrical load served:

$$LCOE = \frac{TAC}{\sum_{t=1}^{t=8760} E_{load}(t)} \quad (3.41)$$

$$= \frac{TAC}{\sum_{t=1}^{t=8760} P_{load}(t) \cdot \Delta t} \quad (3.42)$$

$$= \frac{TAC}{\sum_{t=1}^{t=8760} P_{load}(t)} \quad (3.43)$$

where $\sum_{t=1}^{t=8760} E_{load}(t)$ is the total electrical energy [in kWh] consumed by the load in a year (8760 h) assuming that an hourly time step ($\Delta t = 1$ h) is used. Designers seek to minimize *LCOE* during sizing optimization in order to ensure affordable electricity access.

For dispatch optimization, the daily cost of electricity (COE) [\$/kWh] is minimized instead, given by:

$$COE = \frac{C_{daily}}{\sum_{t=1}^{t=24} P_{load}(t) \cdot \Delta t} \quad (3.44)$$

$$= \frac{C_{daily}}{\sum_{t=1}^{t=24} P_{load}(t)} \quad (3.45)$$

Emissions

In order to mitigate negative environmental impacts of the MG, it is necessary to minimize emissions of harmful airborne pollutants¹³ from the backup DGs. The emissions factors arising from the use of diesel in the DE and natural gas in the MT are listed in table 3.11. The total emissions *Em* [in kg] can be obtained by summing up these factors and multiplying it by the total energy derived from fossil sources: $\sum_{t=1}^{t=T} P_{DG}(t) \cdot \Delta t$ where T = either 24 h or 8760 h, for dispatch and sizing optimization respectively.

¹³including particulate matter (PM), volatile organic compounds (VOC) and greenhouse gases (GHG)

Parameter	DE	MT
$CO_2 [kg/kWh]$	0.649 [41]	0.631 [73]
$CO [g/kWh]$	4.063	2.851
$NO_x [g/kWh]$	18.857	20.884
$SO_2 [g/kWh]$	0.074	0.003
$VOC [g/kWh]$	1.502	0.604
$PM [g/kWh]$	1.338	0.047
$PM2.5 [g/kWh]$	1.338	0.047
$PM10 [g/kWh]$	1.338	0.047

Table 3.11: Emissions factors for both DE and MT [82].

In order to normalize both $LCOE$ and emissions so that they always lie between 0 and 1 (like the other three objectives), these values are divided by the equivalent LCOE and emissions from a hypothetical, base-case scenario where the same MG community is run solely on a single backup DG (either a DE or MT chosen accordingly) of sufficient rated power (i.e. $P_{DG, r} = P_{load, peak} \cdot (1 + SF)$, where $SF \geq 0$). Here the DG is run continuously throughout the study period to meet the entirety of the load. Startup and shutdown costs are incurred only once each at the beginning and end of the time horizon, respectively. There is also no need for a converter since the DG's AC output can directly supply loads. Thus, the costs for the base case (used to calculate $LCOE_{base}$) are comprised of:

$$\begin{aligned} IC_{base} &= IC_{DG} \\ C_{rec, base} &= OM_{fix, DG} + OM_{var, DG, annual} \\ &\quad + C_{fuel, DG, annual} + SUC_{DG} + SDC_{DG} \\ C_{non-rec, base} &= RC_{DG} \\ C_{daily, base} &= C_{fuel, DG, daily} + OM_{var, DG, daily} \\ &\quad + SUC_{DG} + SDC_{DG} + \frac{OM_{fix, DG}}{365} \end{aligned}$$

where $OM_{var, DG, annual}$ and $C_{fuel, DG, annual}$ are calculated assuming the DG is run for 8760 h to meet the entire annual load. Similarly, $C_{fuel, DG, daily}$ and $OM_{var, DG, daily}$ are calculated assuming the DG is run for 24 h to meet the entire daily load. The base emissions Em_{base} are also calculated assuming that the DG meets all the power demand, on a daily and annual basis.

Deficiency of power supply probability (DPSP)

DPSP is the ratio between the total unmet or deficit load that's not satisfied by the MG¹⁴ and the sum total of load demand in the same study period [81]:

$$DPSP = \frac{\sum_{t=1}^{T=24} P_{lost}(t)}{\sum_{t=1}^{T=24} P_{load}(t)} \quad (3.46)$$

where $T = 8760 h$ for sizing and $T = 24 h$ for dispatch. Thus, $0 \leq DPSP \leq 1$ and a value of 1 implies that the load will never be satisfied while a value of 0 means that load will always be satisfied. DPSP must be minimized in order to maximize the system's reliability.

¹⁴i.e. consumption that's either curtailed, interrupted or disrupted

Relative excess or dump power generated (REPG)

This is the ratio between excess power (DC) generated by the system (over the total demand) that is sent to dump loads or grounded to earth, and the total power (DC) generated [63]:

$$REPG = Dump = \frac{\sum_{t=1}^{t=T} P_{dump}(t)}{\sum_{t=1}^{t=T} P_{gen}(t)} \quad (3.47)$$

$$= \frac{\sum_{t=1}^{t=T} P_{RES}(t) + P_{DG}(t) \cdot \eta_{rec} + P_{BS}(t) - \frac{P_{load}}{\eta_{inv}}}{\sum_{t=1}^{t=T} P_{RES}(t) + P_{DG}(t) \cdot \eta_{rec}} \quad (3.48)$$

where eq. (3.48) arises from power balance in the system. *REPG* is a measure of the system's efficiency. Thus, it is desirable to minimize this ($0 \leq REPG \leq 1$) in order to reduce wastage of energy and keep the RES curtailment as low as possible.

Renewable energy penetration

The renewable energy fraction (REF) measures the proportion of total power generation coming from clean, renewable sources:

$$REF = \frac{\sum_{t=1}^{t=T} P_{RES}(t)}{\sum_{t=1}^{t=T} P_{gen}(t)} \quad (3.49)$$

$$= \frac{\sum_{t=1}^{t=T} P_{PV}(t) + P_{WT}(t) \cdot \eta_{rec}}{\sum_{t=1}^{t=T} P_{RES}(t) + P_{DG}(t) \cdot \eta_{rec}} \quad (3.50)$$

where T is either 8760 h or 24 h for sizing and dispatch, respectively. In order to improve sustainability of the MG and reduce dependence on fossil fuels, it is essential to maximize *REF* ($0 \leq REF \leq 1$) or equivalently minimize $1 - REF$.

3.2.3 Dispatch strategy

For the sizing and design optimization, a priority order for scheduling the generation and storage units was encoded directly into the objective function. The load-following dispatch strategy assumed is described in table 3.12:

Scenario	Action
1	Use RES power output to meet all load.
2	If generation RES (PV and WT) exceeds power demand, use it to charge the storage devices (BS).
3	If the excess RES supply exceeds the capacity and safe operating limits of the battery (i.e. $SOC = SOC_{max}$), then send the remaining excess power generated to dump loads or ground.
4	If RES generation is insufficient to meet demand, then discharge the BS.
5	If batteries are fully discharged up to their lower limit or DoD (i.e. $SOC = SOC_{min}$) and there's still some unsatisfied load, then dispatch the backup DG until either all the demand has been met or it has been ramped up to its maximum (rated) power, whichever occurs first.
6	There is a lower limit on the power output at which the DG can be operated when online. If the remaining excess load in step 5 above is less than this value ($P_{DG, min}$), then the extra DG output is inverted from AC to DC and then either used to charge the BS or dumped, depending on the SOC of the BS (i.e. go to step 3).
7	At this point, if there is still some unmet demand, then this is recorded as lost load and contributes to DPSP. An alternative option is to use some form of incentive-based demand response (DR) or demand-side management (DSM) and thus encourage consumers to either shift or voluntarily curtail their loads, instead of resorting to load-shedding. This possibility will be discussed in more detail in section 5.5.

Table 3.12: Summary of prescribed load-following strategy used for sizing optimization.

3.2.4 Constraints

The main constraints in this problem are listed in table 3.13:

Constraint	Description
Power limits of the DG	Whenever the DG is online (i.e. when $P_{DG}(t) > 0$), its power output must lie between the rated minimum and maximum powers specified.
Positivity constraints	The power output of the DG must be non-negative at all times.
Ramp rate limits on the DG	This determines how quickly it can be ramped up to, or ramped down from the rated power. However, NERC (North American Electric Reliability Corporation) disturbance control standards specify that regulating and supplemental reserves must be able to reach their full name-plate capacity within 10-20 minutes [84]. Thus, it did not make sense to try and enforce this constraint in the current model since an hourly time step is used.
Power limits on the BS	Both the charging (-ve) and discharging (+ve) powers of the BS must not exceed its maximum power rating.
Safe battery operation	Upper and lower limits on the <i>SOC</i> of the BS.
Reliability requirement	Upper limit on the DPSP for the MG to be reliable and ensure power balance.

Table 3.13: Summary of MG constraints.

Thus, the multiobjective, weighted and constrained sizing optimization problem can be written as:

$$\min_{n_s, n_w, E_b, \text{init}} w_1 \cdot \frac{LCOE}{LCOE_{base}} + w_2 \cdot \frac{Em}{Em_{base}} + w_3 \cdot DPSP + w_4 \cdot REPG + w_5 \cdot (1 - REF) \quad (3.51)$$

where all the weights sum up to unity i.e. $w_1 + w_2 + w_3 + w_4 + w_5 = 1$ and is subject to the following non-negativity constraints on the inputs:

$$n_s, n_w, E_b, \text{init} \geq 0 \quad (3.52)$$

All the remaining constraints are directly coded into the MATLAB program that calculates the objective function through the prescribed dispatch strategy detailed in section 3.2.3. Thus, these are already enforced implicitly.

Similarly, the optimization problem for day-ahead dispatch can be written as:

$$\min_{P_{DG}, P_{BS}} w_1 \cdot \frac{COE}{COE_{base}} + w_2 \cdot \frac{Em}{Em_{base}} + w_3 \cdot REPG + w_4 \cdot (1 - REF) \quad (3.53)$$

subject to the following constraints:

$$\vec{0}_{1 \times 24} \leq \overrightarrow{P_{DG}}(t) \leq P_{DG,r} \cdot \vec{1}_{1 \times 24} \quad (3.54)$$

$$P_{DG,min} \cdot \mathbb{1}\{P_{DG}(t) > 0\} \leq P_{DG}(t) \leq P_{DG,r} \quad (3.55)$$

$$SOC_{min} \cdot \vec{1}_{1 \times 25} \leq \overrightarrow{SOC}(t) \leq SOC_{max} \cdot \vec{1}_{1 \times 25} \quad (3.56)$$

$$-P_{BS,r} \cdot \vec{1}_{1 \times 24} \leq \overrightarrow{P_{BS}}(t) \leq P_{BS,r} \cdot \vec{1}_{1 \times 24} \quad (3.57)$$

$$DPSP \leq DPSP_{max} \quad (3.58)$$

$$\sum_{i=1}^{i=4} w_i = 1 \quad (3.59)$$

$$\mathbb{1}\{P_{DG}(t) > 0\} = \begin{cases} 1 & \text{if } P_{DG}(t) > 0 \text{ i.e. } DG_{ON}(t) = 1 \\ 0 & \text{otherwise} \end{cases}$$

where $\overrightarrow{P_{DG}}$ and $\overrightarrow{P_{BS}}$ are 1×24 row vectors representing hourly DG and BS power flows while \overrightarrow{SOC} is a 1×25 row vector¹⁵. The value of $DPSP_{max}$ is set according to the desired reliability of the system and specifies the maximum proportion of daily capacity shortage allowed. Thus, the value of both the sizing and dispatch objective functions always lie between 0 and 1. Initially both problems are run using equal weights on all objectives. Thus, $w_i = 0.2 \forall i$ in the sizing optimization and $w_i = 0.25 \forall i$ in the dispatch optimization.

3.2.5 Mathematical properties of the model

A convex optimization problem is one with a convex objective as well as all convex constraints. In the case of both the sizing and dispatch optimization problems, although all the constraints are linear and thus also convex, the objective functions themselves are non-convex and non-smooth¹⁶ primarily due to the use of discrete variables like DG_{ON} and BS_{cycled} tracking the operational state of the DG and cycling of the battery in each time step. There are also sub-models included within the objective function program in MATLAB that are non-linear. Furthermore, the inputs n_s and n_w in the sizing problem are restricted to being integers, and such mixed integer program (MIP) have been demonstrated to be NP-hard [32].

Furthermore, it can be clearly seen from above that the number of constraints rapidly increases if a longer study period (T) is chosen or smaller time steps are used since the dimensions of the vector input variables would also increase accordingly. Complexity and runtime scale relatively poorly with problem size and thus, it was decided to perform only day-ahead dispatch with 1 h steps as a starting point. Future work could look into more efficient ways of formulating this problem.

3.2.6 Solvers available in MATLAB

Since the formulated minimization problem in its current form is non-smooth and non-convex, popular solver packages like CVX cannot be used. However, there are a plethora of free alternatives available such as GUROBI¹⁷ and YALMIP¹⁸ that are dedicated to solving such problems and can be integrated with the MATLAB application interface. However, after

¹⁵the SOC vector has an extra element, $SOC(25)$ to ensure that the SOC of the BS remains within limits at the end of the last hour of the day as well

¹⁶i.e. discontinuous and non-differentiable at certain points

¹⁷<https://www.gurobi.com>

¹⁸<https://yalmip.github.io/>

exploring a few of these options, it was finally decided to use MATLAB's inbuilt solvers due to their straightforward setup and intuitive implementation. In order to do so, the optimization¹⁹ and global optimization²⁰ toolboxes were installed as add-ons. Another benefit to using these in-house solvers was that a large amount of detailed documentation and exhaustive resources were made available directly by Mathworks along with help, troubleshooting and advice from the extensive online community of MATLAB users, unlike some of the other solver packages.

¹⁹<https://www.mathworks.com/products/optimization.html>

²⁰<https://www.mathworks.com/products/global-optimization.html>

Chapter 4

Results and discussion

All of the following results were obtained using a Dell XPS 15 9560 system with a 2.8GHz Intel Core i7-7700HQ (3.8GHz boost) having 4 cores and 8 threads, alongside an Nvidia GTX 1050 GPU with 4GB RAM.

4.1 MG planning and design optimization results

Due to the problem formulated in section 3.2 being non-convex and non-smooth, the objective function has several local minima. Thus, it may output different local optima, depending on the initial value chosen by the solver. This necessitates the use of solvers that fully search the space of feasible solutions to find global, rather than local optima.

4.1.1 Comparison of solution algorithms

Various solvers from MATLAB's global optimization toolbox were experimented with to find globally optimal solutions, as summarized in table 4.1. Although the model was initially formulated as an MIP, the integer constraints on n_s and n_w were relaxed for ease of computation and also because most of MATLAB's global solvers cannot handle such integer constraints (except for GA). The optimal n_s and n_w can simply be rounded up to the nearest integer in order to obtain the number of PV modules and wind turbines needed.

This testing was done for a base case LI+DE system i.e. using a DE as the backup DG and LI as the BS, with the DE rated at 16 kW, slightly higher than the peak daily load. All of the solvers were run using parallel processing to speed up computation, except for SA where this is not an option. Most of these global solvers are stochastic in the sense that they use a population of multiple randomized local solvers with different initial values (start points) in order to find a global optimum. Thus, a random number seed was fixed in order to ensure reproducibility of results. Furthermore, equal weights were placed on all five objectives ($w_i = 0.2 \forall i = 1, 2, \dots, 5$) indicating that all five goals are prioritized equally by the MG designer.

The maximum number of function evaluations and iterations were both set to 2000 in order to prevent the solver from stopping prematurely due to hitting either of these limits. This ensured that all solvers terminated only upon reaching a global solution indicated by the stopping criteria. For most solvers, this occurs when the relative change in the objective function value during a step is less than the specified tolerance or lower limit. For direct (pattern) search, this happens when the mesh size becomes less than the mesh tolerance. In general, all these

tolerances and thresholds were kept at their default values supplied by MATLAB. In addition to the function tolerance, these include lower bounds on the step size, mesh size and first-order optimality measure as well as upper bounds on the magnitude of constraint functions¹. Finally, for SO, there is no set stop criterion - the solver finishes based on the computational budget assigned by the user².

For algorithms that required an initial guess³, $n_s = 50$, $n_w = 3$ and $E_{b, init} = 50 \text{ kWh}$ was used as the start value. The lower and upper bounds were set to [0, 0, 0] and [100, 30, 200] respectively. The pattern search solver was repeatedly run using 89 different start points randomly initialized within the finite bounds. The global and multiple starting point search solvers were run using the `active-set` algorithm for minimizing constrained nonlinear multivariable functions, since this allows them to take large steps which adds speed.

Solver	t [s]	Min obj.	Overall	Optimal soln
Particle swarm optimization (PSO)	63.27	0.1460	9.24	[10.9494 4.2058 70.3934]
Genetic algorithm (GA)	289.75	0.1471	42.62	[19.6719 4.1324 70.1466]
Multiple start search (MS)	724.07	0.1489	107.81	[24.9473 3.8415 61.6290]
Simulated annealing (SA)	856.82	0.1489	127.62	[5.2351 4.4121 83.8992]
Global search (GS)	868.86	0.1487	129.20	[12.8042 4.2481 81.6499]
Direct pattern search (DPS)	1875.93	0.1460	273.89	[11.1260 4.1987 70.2943]
Surrogate optimization (SO)	2228.32	0.1480	329.79	[20.7363 4.0413 66.6715]

Table 4.1: Optimization results and performance of MATLAB's global solvers. Both LCOE and emissions are reported as normalized values.

The optimal solution in table 4.1 lists the values of [n_s, n_w and $E_{b, init}$] along with the runtime and minimum value of the objective function attained by the solver. The lower the value of the objective, the greater the optimality of corresponding solutions and the lower the time taken, the faster is the solver's computational performance. Thus, an overall performance metric can be devised as the product of runtime and minimum objective value $Overall = Min\ obj \cdot t$ and the solvers in table 4.1 are listed in ascending order of this measure, with lower performance metric values indicating a 'better' solver. All of the above solvers converged with 'positive exit flags' in MATLAB indicating successful outcomes⁴. The results are also depicted graphically in fig. 4.1.

¹to detect any possible violations

²i.e. an upper limit on either function evaluations or iterations

³i.e. GS, MS, and SA

⁴i.e. the solver did not halt by exceeding an iteration or function evaluation limit

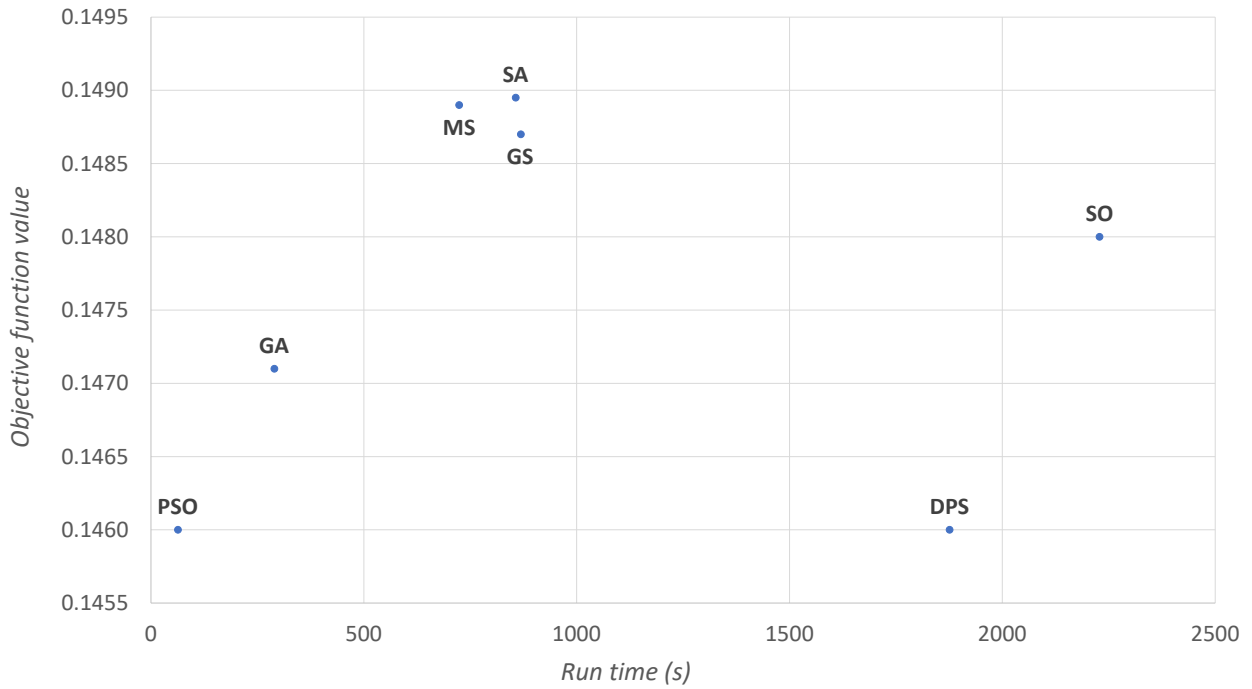
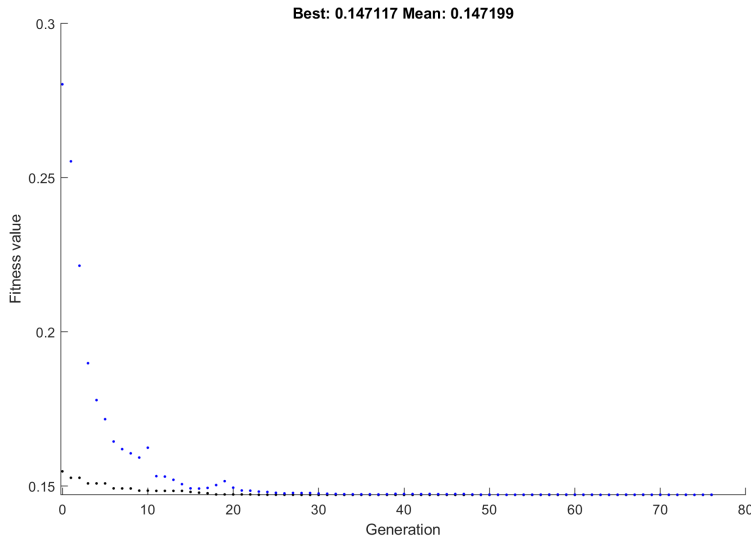
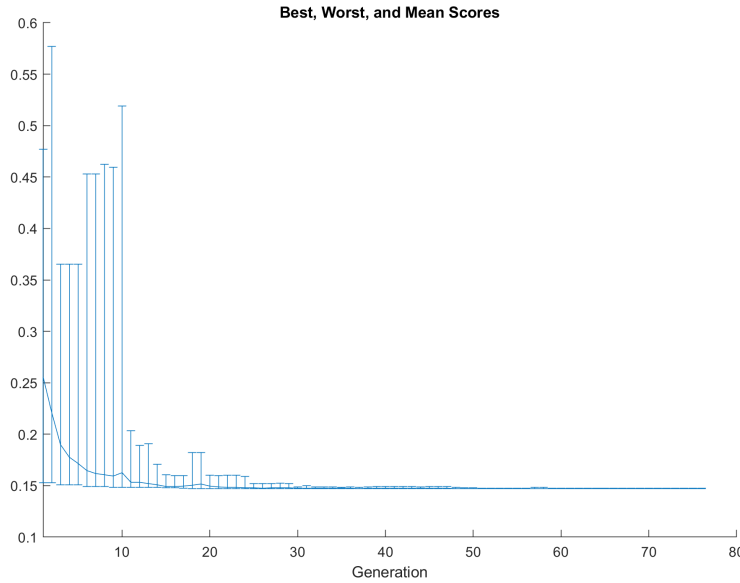


Figure 4.1: Plot of minimum objective value vs run time.

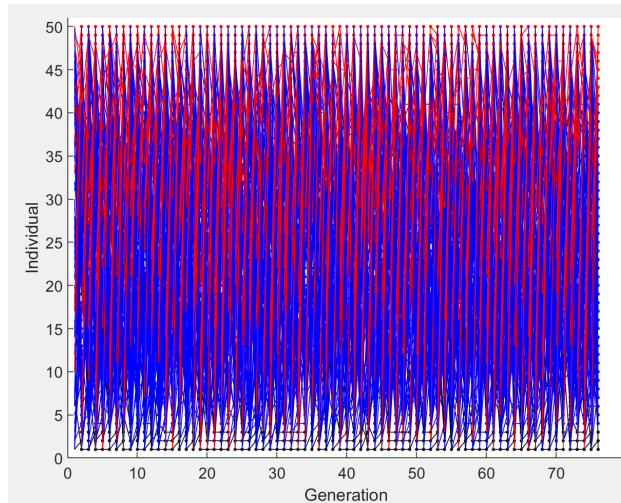
As can be seen from table 4.1 and fig. 4.1, GA and PSO give the best overall performance when considering a balance of both speed (efficiency) and accuracy (optimality). However, such genetic or evolutionary programming methods and swarm intelligence algorithms have little supporting theory and don't guarantee globally optimal solutions. Solver parameters (like population size and initial population range in case of GA) need to be carefully tuned to thoroughly search the hyperspace of possible minima. Despite the lack of proven global convergence, these solvers are usually found to work quite efficiently in practice. Vectorization of the objective can make these methods run even faster. The working of GA can be seen through plots in fig. 4.2. In the genealogy plot (c), lines from one generation to the next are color-coded as follows: Red lines from one generation to the next indicate mutation children while blue lines indicate crossover children and black lines indicate elite individuals.



(a) Convergence plot for GA showing best score value in blue (lowest value of objective function) and mean score value in black, versus generations.



(b) Plot showing range of scores i.e. minimum, maximum, and mean fitness values in each generation.



(c) Plot showing the genealogy of individuals.

Figure 4.2: Plots describing GA optimization.

Pattern search is also able to find the most optimal solution (minimum value of weighted cost function) but takes a much longer time than GA or PSO to converge. Some of the data points like SO, MS, GS and SA in fig. 4.1 contradict intuition since one would expect increased running time to result in improved objectives, but this is not always the case. This implies that biologically-inspired methods like GA and PSO are just better suited to the optimization problem studied here. Also, MS and GS both gradient-based solvers which could explain why they're much faster than DPS and SO.

Although surrogate optimization has good supporting theory and has been proven to converge to a global minimum, it was found to be extremely slow in practice when used to solve the sizing optimization problem. SO took the longest to converge while using the same upper limit on the maximum allowed number of function evaluations (= 2000). Even then, the minimum objective obtained by it is sub-optimal and higher than those obtained by other methods like PSO, DPS and GA, as seen in fig. 4.3.

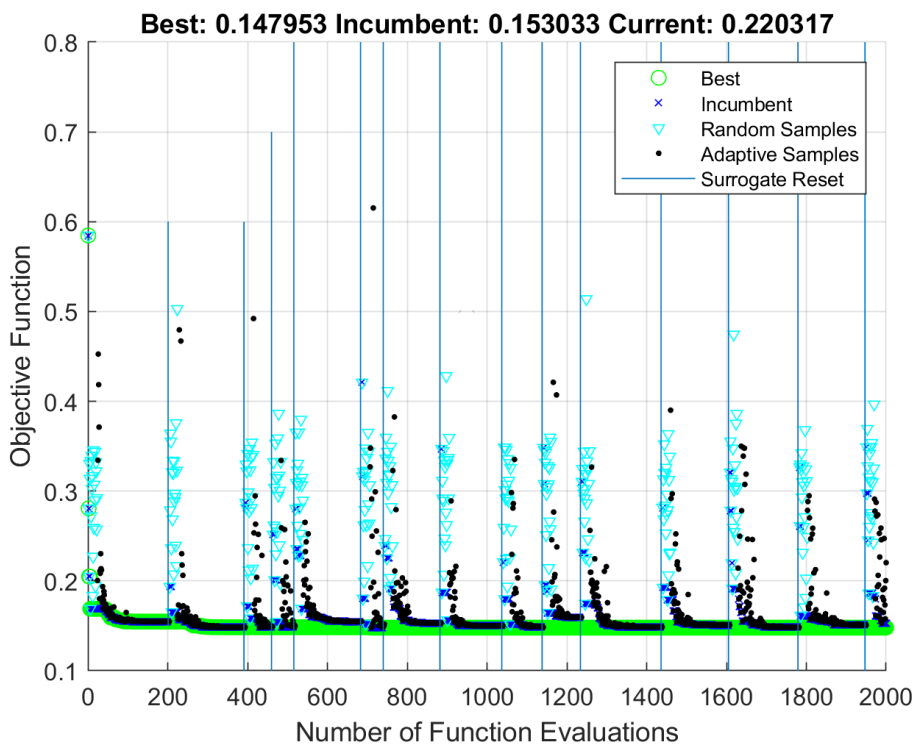
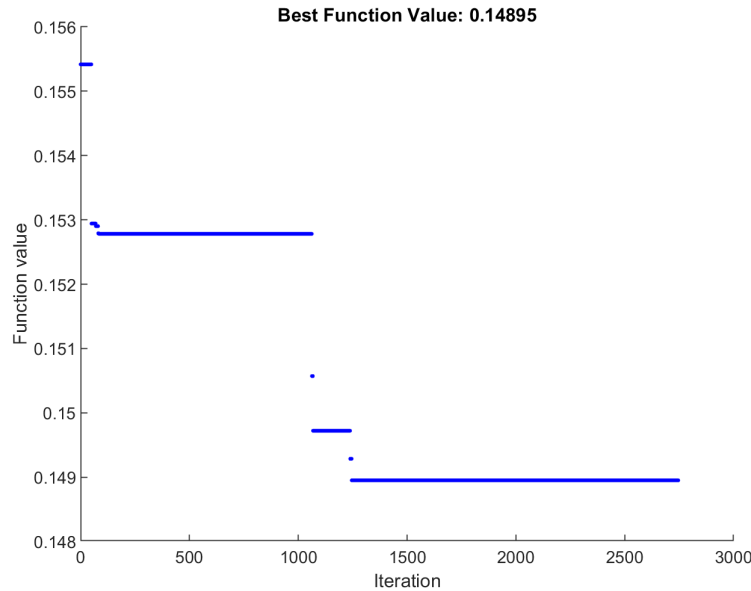
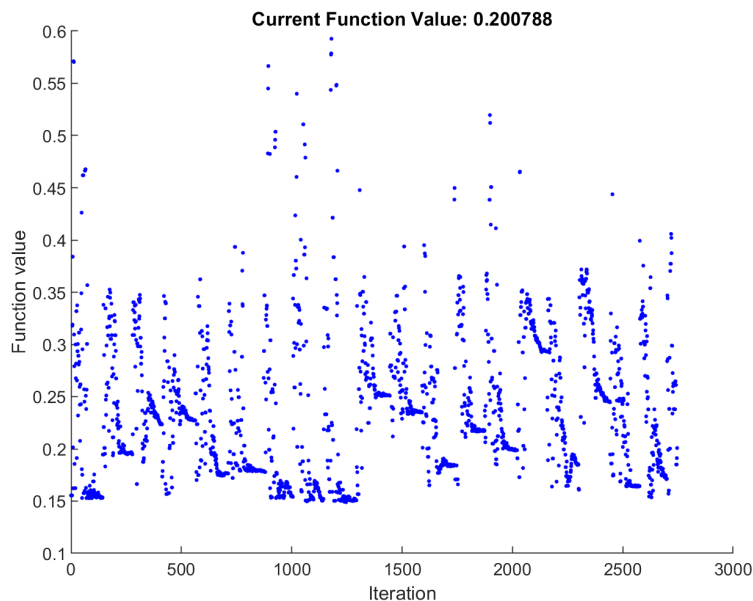


Figure 4.3: Convergence plot for SO.

Similarly, SA is guaranteed to converge to global optima but only with a logarithmic cooling schedule which turns out to be extremely slow in practice. The performance of SA is summarized through fig. 4.4. These examples show how theoretical expectations may not always match actual computational performance. Thus, there is a need to test and tune solvers on the specific problem structure being considered and understand their behavior.



(a) Convergence plot for SA.



(b) Current value of objective function varying with number of iterations.

Figure 4.4: Plots describing SA optimization.

Since PSO has the lowest performance metric value, it was concluded as the best solver for this optimization problem and was used to produce all subsequent sizing results. The convergence behavior of the PSO algorithm is shown in fig. 4.5, which depicts the change in objective function value with increasing number of iterations.

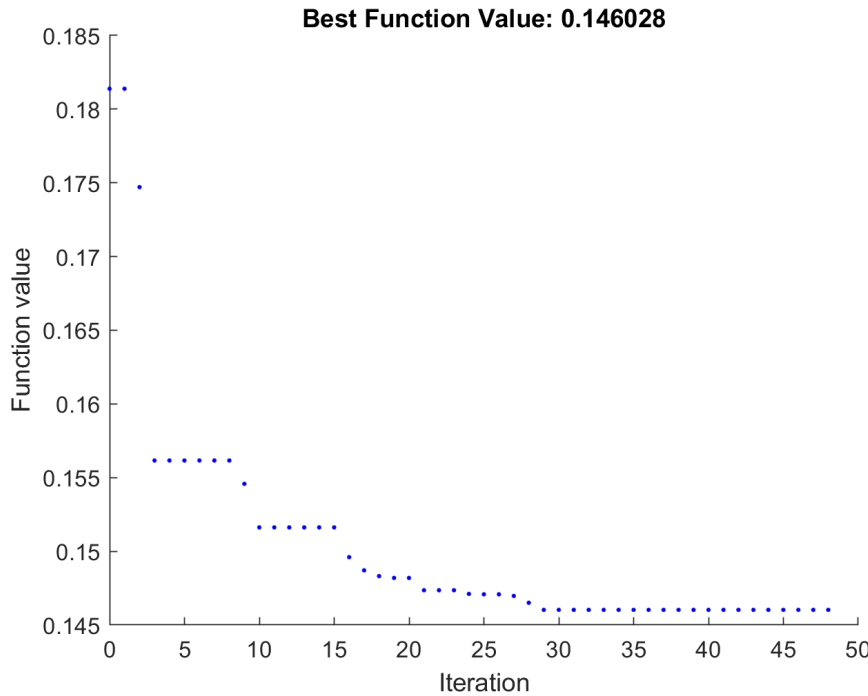


Figure 4.5: Convergence plot for PSO.

4.1.2 Sizing results

Strategy selection

Before optimizing the capacities of the PV, WT and BS components, two important strategy decisions had to be made, relating to (1) the frequency of replacement of the BS and (2) whether or not excess power output from the DG would be allowed to charge the BS.

- The MG operator can choose to replace the battery either at fixed, pre-determined intervals i.e. after a certain number of years specified by the warranty or expected lifetime of the product. Thus, in this case, the LI system would be replaced every 10-15 years while the LA would be replaced every 5 years. Alternatively, the battery replacement decision can be made in real-time during the MG operation based on tracking the actual number of charge-discharge cycles. Thus, for example, the LI system would be replaced after completing 5475 cycles while the LA would be replaced every 1400 cycles. This second approach is likely to be more accurate and realistic.
- Since there is a lower limit to the power output of the DG, any power produced above the minimum level needed to satisfy excess demand can be used to charge the BS by sending the rectified output to the DC bus. Alternatively, the system could be configured so that the backup DG is only used to directly meet excess load during peak conditions and thus any extra power output cannot go towards battery charging.

This results in the following four possible combinations of strategies regarding the DG operation and BS replacement listed in table 4.2.

Strategy	Description
1	DE can charge LI and LI replaced every 15 y
2	DE cannot charge LI and LI replaced every 15 y
3	DE can charge LI and LI replaced every 5475 cycles
4	DE cannot charge LI and LI replaced every 5475 cycles

Table 4.2: Strategy selection for the LI+DE microgrid.

The earlier results in table 4.1 used to select the best solver were obtained with strategy 1.

Case	Soln.	Min obj.	LCOE	Emissions	DPSP	Dump	1-REF
1.	[11.13 4.20 70.29]	0.1460	0.5025	0.0694	0	0.1056	0.053
2.	[6.87 4.43 77.49]	0.1607	0.5267	0.0860	0	0.1279	0.0627
3.	[15.12 4.31 106.53]	0.1367	0.4645	0.0537	0	0.1252	0.0399
4.	[0 4.85 120.98]	0.1468	0.4752	0.0589	0	0.1585	0.0412

Table 4.3: Results of sizing optimization using all four strategies.

The sizing optimization was conducted with all of the above strategies and it was found that strategy 3 is most optimal since it minimizes the objective to the greatest extent giving lower costs, reduced emissions and higher renewable penetration, as seen in table 4.3. Thus, this technique was implemented in all subsequent simulations.

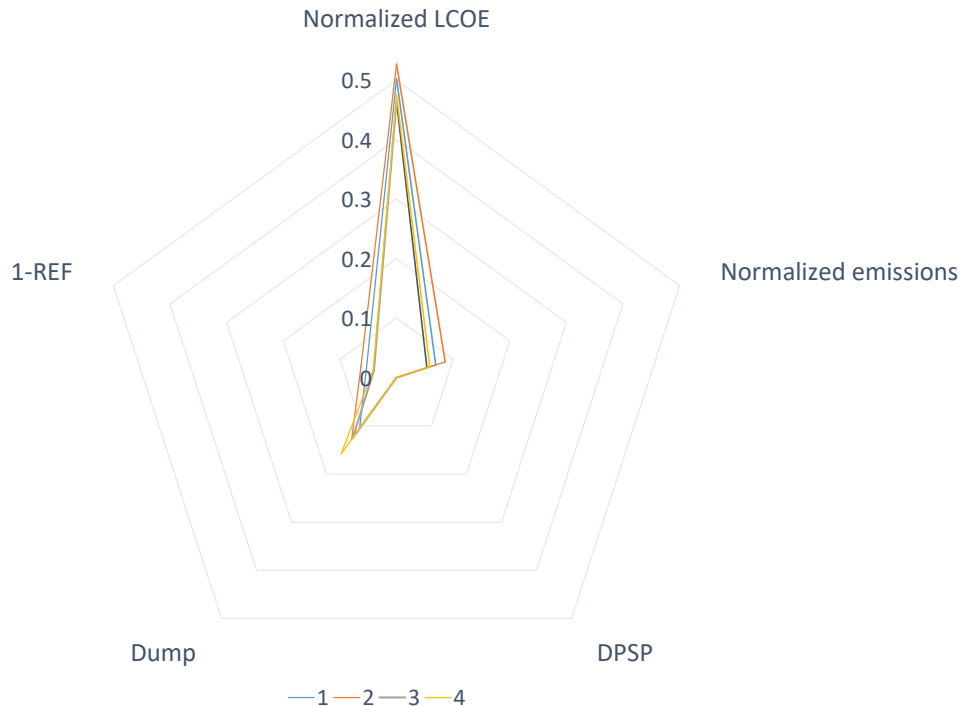


Figure 4.6: Radar plot showing the values of all five objectives, when each of the four strategies is used.

As seen from fig. 4.6, the four strategies produce quite similar results. Real-time replacement of the BS by tracking its cycles is much more cost effective since the BS replacement costs (with

discounting considered) can also be taken into account while making charging or discharging decisions for the MG. This introduces additional tradeoffs that otherwise wouldn't have come into play if the replacement period was kept constant and decided beforehand. Furthermore, allowing the DG to also charge the BS diverts less power to dump loads. This reduces emissions as well since the BS can now be used to meet more of future load in place of the fossil-fuel DG.

Technology selection

Similar to section 4.1.2, the MG designer also needs to choose the optimal technologies for both battery energy storage as well as the standby, distributed generator. Based on the technology options presented in section 3.1.3 and section 3.1.4, the following four combinations were tested in the sizing optimization model as summarized in table 4.4.

System	Soln.	Min obj.	LCOE	Emissions	DPSP	Dump	1-REF
LI+DE	[15.12 4.31 106.53]	0.1367	0.4645	0.0537	0	0.1252	0.0399
LI+MT	[1.27 4.33 4.59]	0.1979	0.5094	0.2051	0	0.1327	0.1429
LA+DE	[14.54 3.92 12.16]	0.1633	0.4406	0.0844	0	0.2246	0.0667
LA+MT	[3.22 4.28 9.50]	0.1711	0.4496	0.0931	0	0.2425	0.0705

Table 4.4: Results of sizing optimization using all four technology combinations.

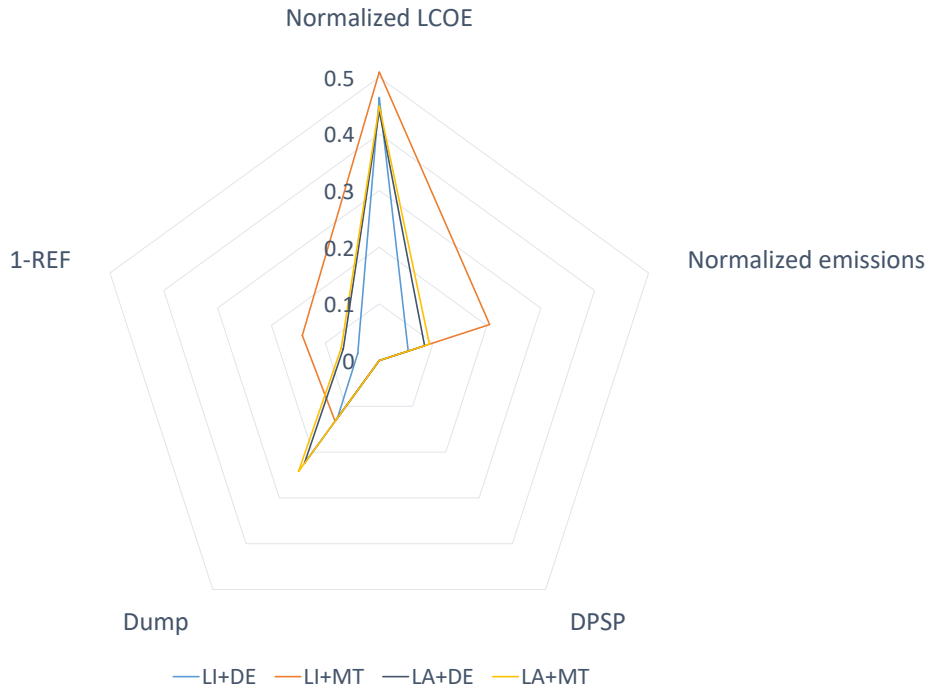


Figure 4.7: Radar plot showing the values of all five objectives for each of the four possible technology combinations.

It can clearly be inferred from table 4.4 and the radar plot in fig. 4.7 that the combination using a DE as the backup DG and LI as the BS results in the most optimal system and the lowest values across all five objectives. As described in section 3.2.2, both the LCOE and emissions values are normalized with respect to a base case using either only the DE or the MT alone to power the MG. The baseline values for LCOE and emissions are listed in table 4.5.

Parameter	DE system	MT system
LCOE [\$/kWh]	0.4968	0.3321
Emissions [kg of pollutants/y]	50,189	48,562
Emissions [kg of pollutants/kWh]	0.6774	0.6555

Table 4.5: Baseline LCOE and emissions for the MG running solely on a single fossil-fueled DG rated at 16 kW, calculated using the current model.

Microturbines running on natural gas have lower overall emissions than generators using diesel (a relatively dirtier fuel), for the same amount of output energy. However, they are more expensive to install compared to diesel engines which are also the more commonly used, widely available and mature technology across Africa. From table 4.5, it is interesting to note that although microturbines by themselves are a superior technology to diesel engines (having lower baseline LCOE and emissions), the MG using renewables and a DE backup has lower emissions and costs than one running on MT as the backup generator. This is most likely due to the higher capital costs of the MT compared to the DE and also because the DG is not actually dispatched that often during the MG operation. The system relies largely on wind and solar (coupled with battery storage) under normal conditions to meet most of its load, with the DG only being called upon as backup under special conditions of excess demand or insufficient RES generation. In fact, minimizing total emissions is equivalent to minimizing fuel costs and the number of DG operational hours. Thus, the DE or MT remains offline for most of the time, increasing the payback time on more capital-intensive MTs. A similar reasoning can be applied to understand why LI is preferred over LA, despite the lower capital costs and lower self-discharge of the latter.

Optimal capacities for baseline LI+DE system

Having decided upon the best technologies and strategy, the optimal capacities of the WT, PV and BS were determined. For comparison purposes, the sizing optimization was done using both (i) $[n_s, n_w, E_b, init]$ and (ii) $[P_{PV, r, total}, P_{WT, r, total}, E_b, init]$ as input variables, where $P_{PV, r, total} = n_s \cdot P_{PV, r}$ and $P_{WT, r, total} = n_w \cdot P_{WT, r}$.

Parameter	(i)	(ii)
$LCOE_{normalized}$	0.4645	0.4585
LCOE [\$/kWh]	0.2308	0.2278
$Emissions_{normalized}$	0.0537	0.0613
Annual emissions [kg/y]	2695	3077
DPSP	0	0
Dump	0.1252	0.1171
1-REF	0.0399	0.0460
No. of online DE hours [h/y]	585	665
No. of LI BS cycles [/y]	69	85
Optimal soln.	$[n_s, n_w, E_b, init] = [15.12 \ 4.31 \ 106.53]$	$[P_{PV, r, total}, P_{WT, r, total}, E_b, init] = [2.51 \ 15.16 \ 85.29]$
Minimum objective	0.1367	0.1366

Table 4.6: Sizing optimization results for baseline LI+DE system using two approaches.

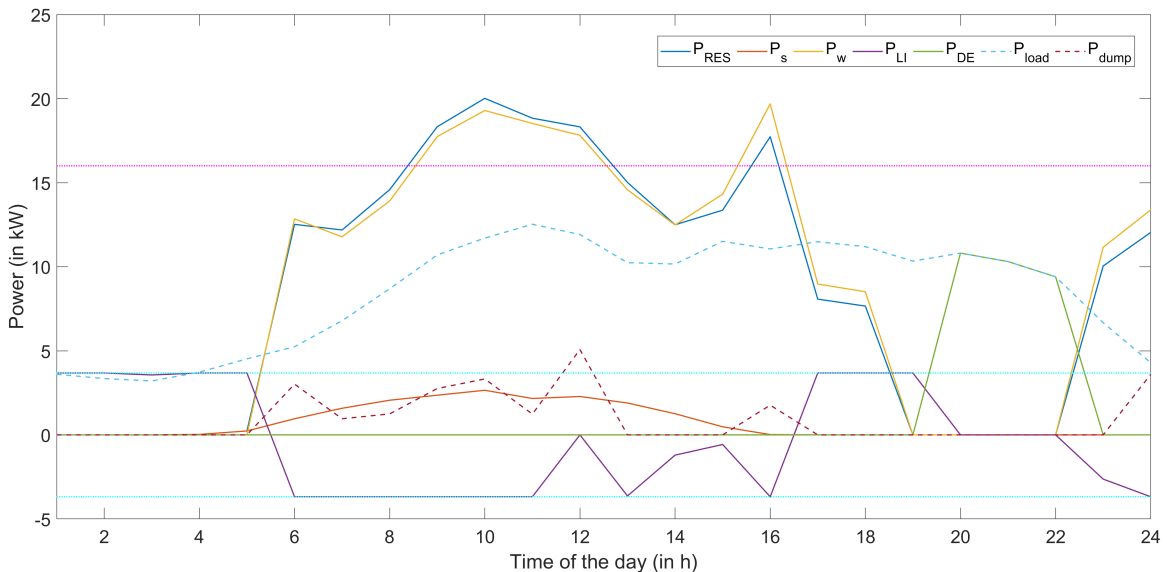
The solutions obtained using both optimization approaches are relatively similar, with the result from (i) being [3.86 15.07 106.53] when converted to total rated capacities. Although the WT capacities are nearly identical in the two cases, the differences PV and BS capacities are more significant, with both being higher in (i). When optimizing using total power ratings as control variables, (ii) is found to produce a slightly more optimal solution, with lower costs and excess power but higher emissions and lower renewable energy contribution. However, in practical applications, there are restrictions on the rated powers of PV and WT systems that may be used in the MG. The specific power ratings available depend on the manufacturer and these usually vary only in certain fixed increments. Thus, it is more realistic to optimize relative to the numbers of PV and WT components rather than their total capacities since such results are likely to be more useful to a MG designer having access to only specific PV and WT models.

Regardless of the approach assumed, the hybrid RES microgrid using LI and DE is a significant improvement over the baseline alternative using just a DE. Levelized costs are reduced by more than 50% and emissions by more than 93% in both cases, compared to the baseline, with > 95% RES penetration in the new system.

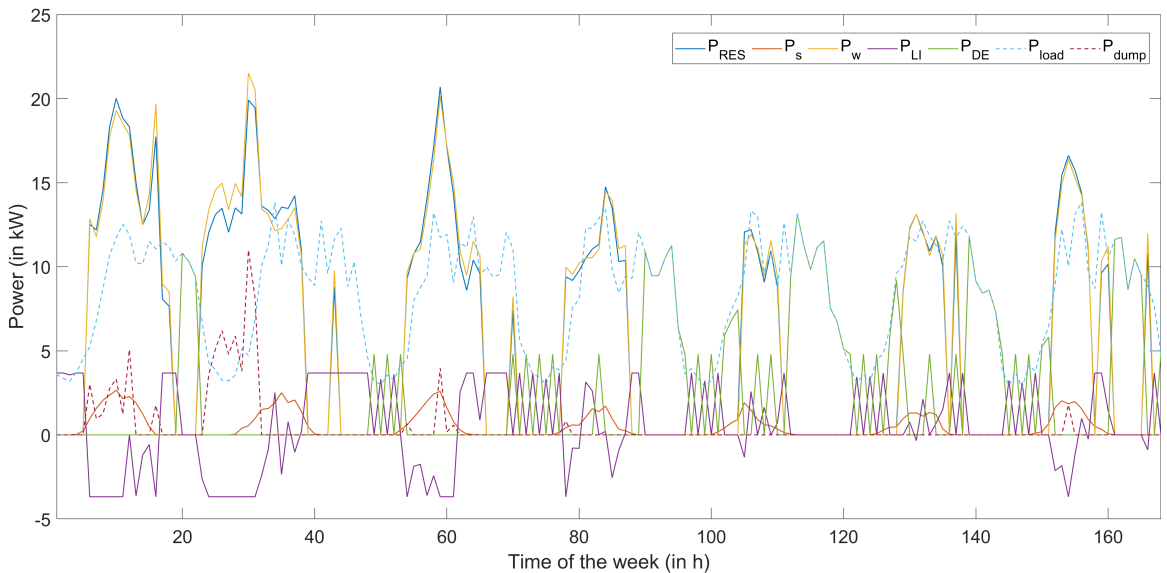
Another interesting result observed from table 4.6 is the relatively low cycling and dispatch rates of the BS and DE under optimal conditions. This can also be seen from the dispatch of P_{DE} in fig. 4.8 and the SOC plots in fig. 4.9. The BS is cycled only $\approx 69\text{-}85$ times per year implying an ideal replacement period of $\approx 64\text{-}80$ years, if it is assumed that the BS is cycled with similar frequency in all subsequent years of MG operation. This means that the LI BS will never have to be replaced during the MG lifetime of 25 years. Similarly, the DG is brought online only for $\approx 585\text{-}665$ hours per year, indicating a replacement period of 22-25 years meaning that it will have to be replaced only once over the system's lifecycle.

In terms of oversizing for system (i), the total optimal rated power of the RES is found to be oversized by $\approx 105.4\%$ relative to the average daily load of 8.48 kW and by $\approx 39.1\%$ relative to the daily peak load of 12.52 kW. The optimal BS capacity is sized to be $\approx 52.5\%$ of the total daily energy consumption of 203 kWh, as mentioned in table 3.6.

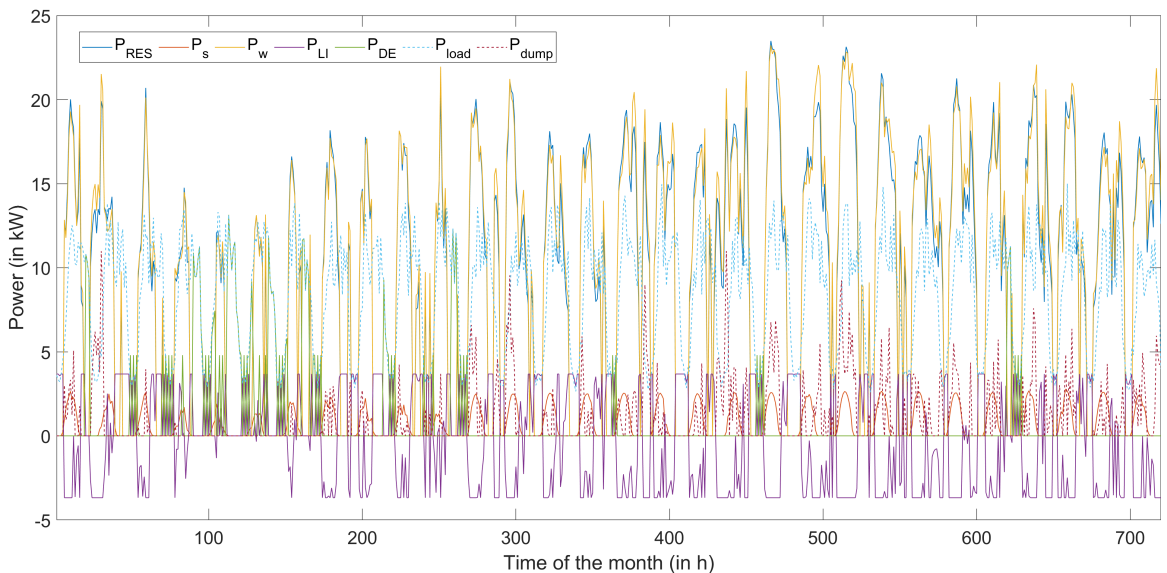
The curves in fig. 4.8 show the power dispatched from each source at the end of every hour, over periods of a day, week and month. These were obtained by implementing the encoded dispatch strategy discussed in section 3.2.3.



(a) Hourly power dispatch over January 1, 2018. The dotted horizontal cyan lines show the charging and discharging limits of the BS while the dotted pink line indicates the maximum DG power rating.

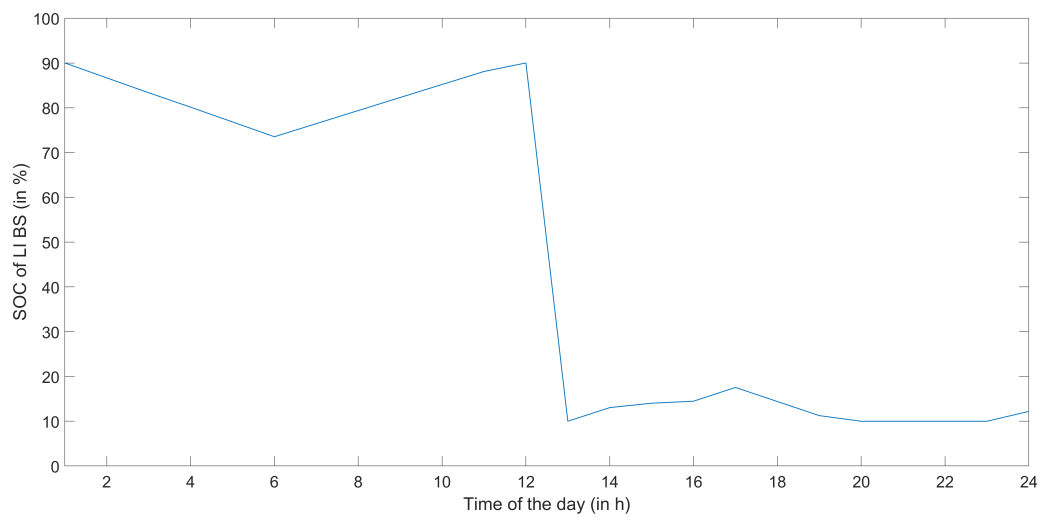


(b) Hourly power dispatch over one week (168 h).

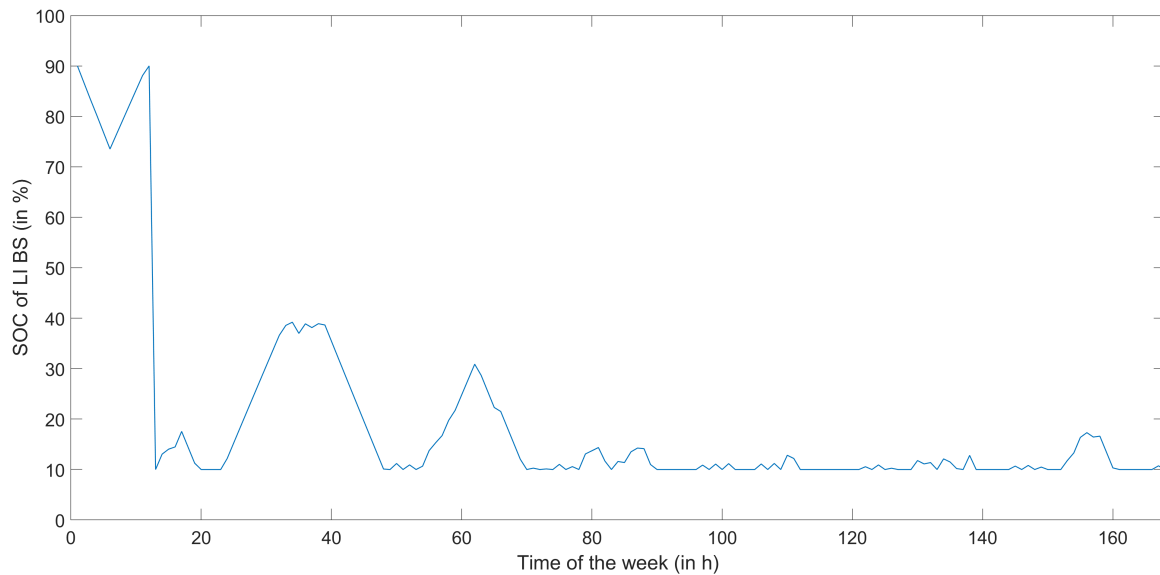


(c) Hourly power dispatch over one month (720 h).

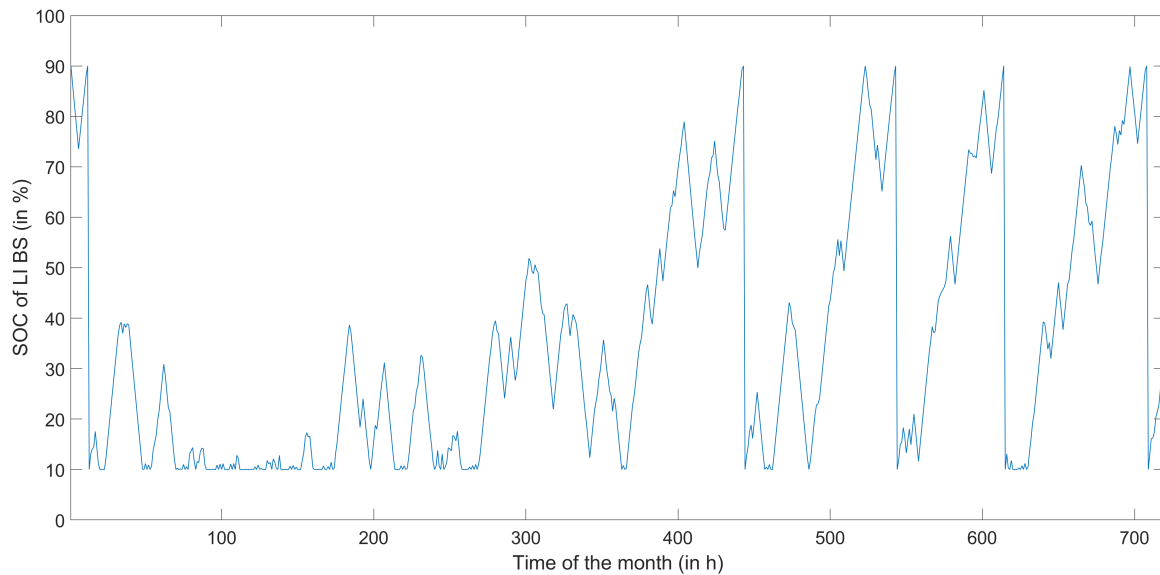
Figure 4.8: Actual dispatch during MG system operation using encoded strategy and optimal capacities for baseline LI+DE MG.



(a) Hourly SOC variation of LI BS on January 1, 2018.



(b) Hourly SOC variation of LI BS over a period of one week.



(c) Hourly SOC variation of LI BS over a period of one month.

Figure 4.9: Variation in state-of-charge of LI BS during MG system operation using encoded strategy and optimal capacities.

It can be seen from table 4.6 and fig. 4.8 that wind power dominates relative to solar PV in terms of both total installed capacity ($P_{r, total}$) and power dispatched during operation. This may be because wind turbines generally have higher capacity factors than solar arrays, which may make them more cost-effective on a $\$/kW$ basis. Wind speeds also tend to be more predictable than solar radiation, with WT forecasts being prone to less error and uncertainty on average.

Another factor is that global averages of installed costs were used for both PV and WT. However, in hindsight, it would have probably been more realistic to instead use module or turbine-specific prices for the PV and WT systems respectively. This is because while small-scale PV has experienced significant cost declines in recent years due to uptake by the residential sector, the same cannot be said for small-scale wind turbines where installation costs have largely stagnated. This is because the wind power sector has mainly been focused its efforts on expanding large, utility-scale onshore and offshore projects to achieve grid parity, while smaller installations are still very rare compared to rooftop residential and commercial PV. Thus, using updated cost values is likely to make small-scale solar a more economical option than wind for the MG communities considered here. It would also make practical sense for solar PV to contribute a greater share to total RES generation than under either approaches (i) or (ii) in table 4.6, given the high levels of solar insolation received in sub-Saharan Africa.

4.1.3 Pareto optimality

Variation of Pareto-optimal combinations of input variables

Although a global optimum does exist in the sense that there is a single lowest possible value that can be attained by the objective function, the combination of inputs n_s , n_w and $E_{b, init}$ (or $P_{PV, r, total}$, $P_{WT, r, total}$ and $E_{b, init}$) that achieves this is not unique. There is actually a whole set of feasible solutions that are all equally optimal and non-dominated, forming a Pareto front. This shows the full array of options available to the MG designer.

The pareto-optimal sets can be obtained using multiobjective optimization solvers in MATLAB's global optimization toolbox, based on either genetic (`gamultiobj`) or direct pattern search algorithms (`paretosearch`). The 3D surface plots in fig. 4.10 were generated using `gamultiobj` and show the variations of the three inputs variables n_s , n_w and $E_{b, init}$ with respect to each other. The black dots represent the actual points in the Pareto set found by the solver and the surface was then created by interpolating between these points. All points on these surfaces correspond to the same value of the objective function, which is the global minimum obtained by GA. The colors simply indicate the value of the z-axis variable i.e. the BS capacity.

For comparison purposes, Pareto fronts were also generated using the total rated powers of PV and WT as inputs, instead of the number of solar modules or wind turbines. These are shown in fig. 4.11 .

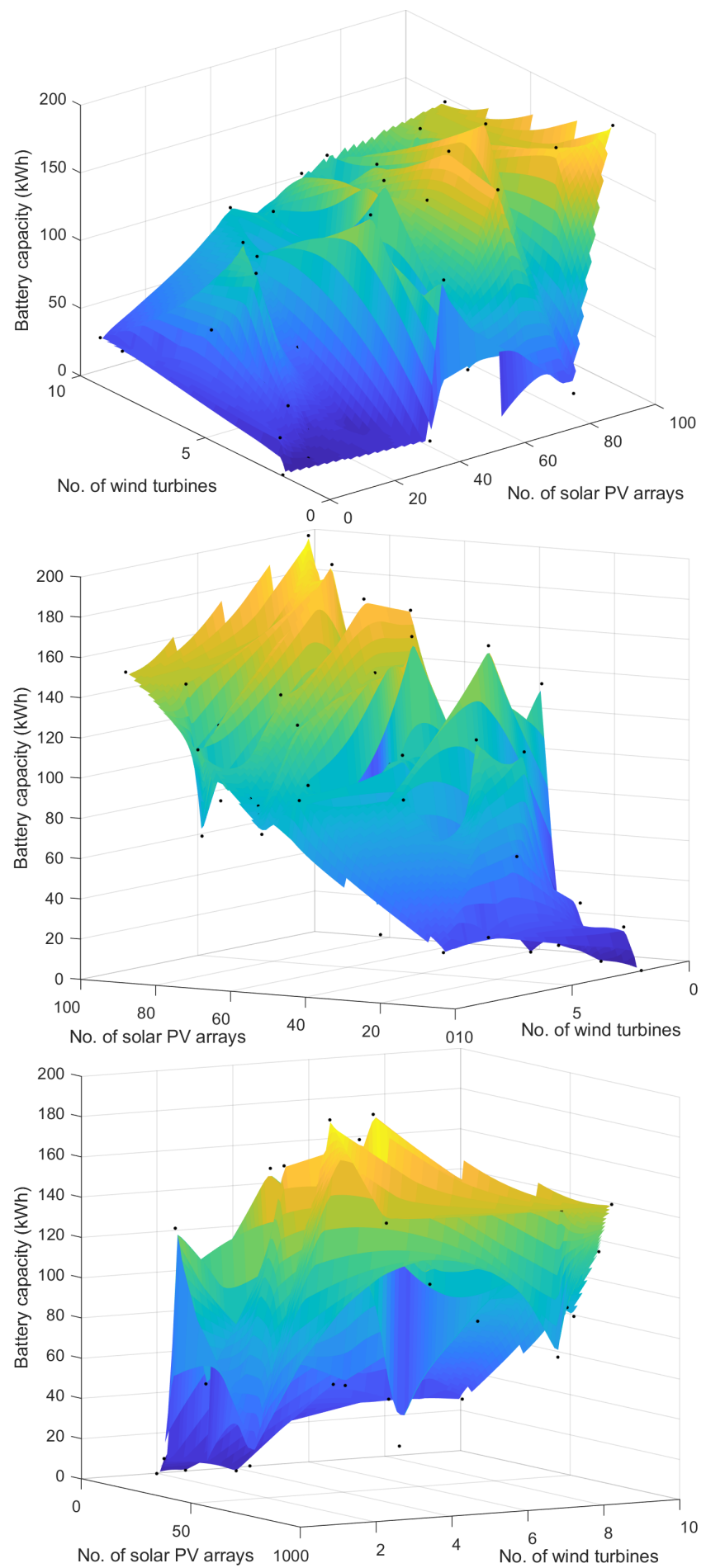


Figure 4.10: Three rotated views of the Pareto set obtained using `gamultiobj` and optimizing with respect to n_s , n_w and $E_b, init$ as inputs.

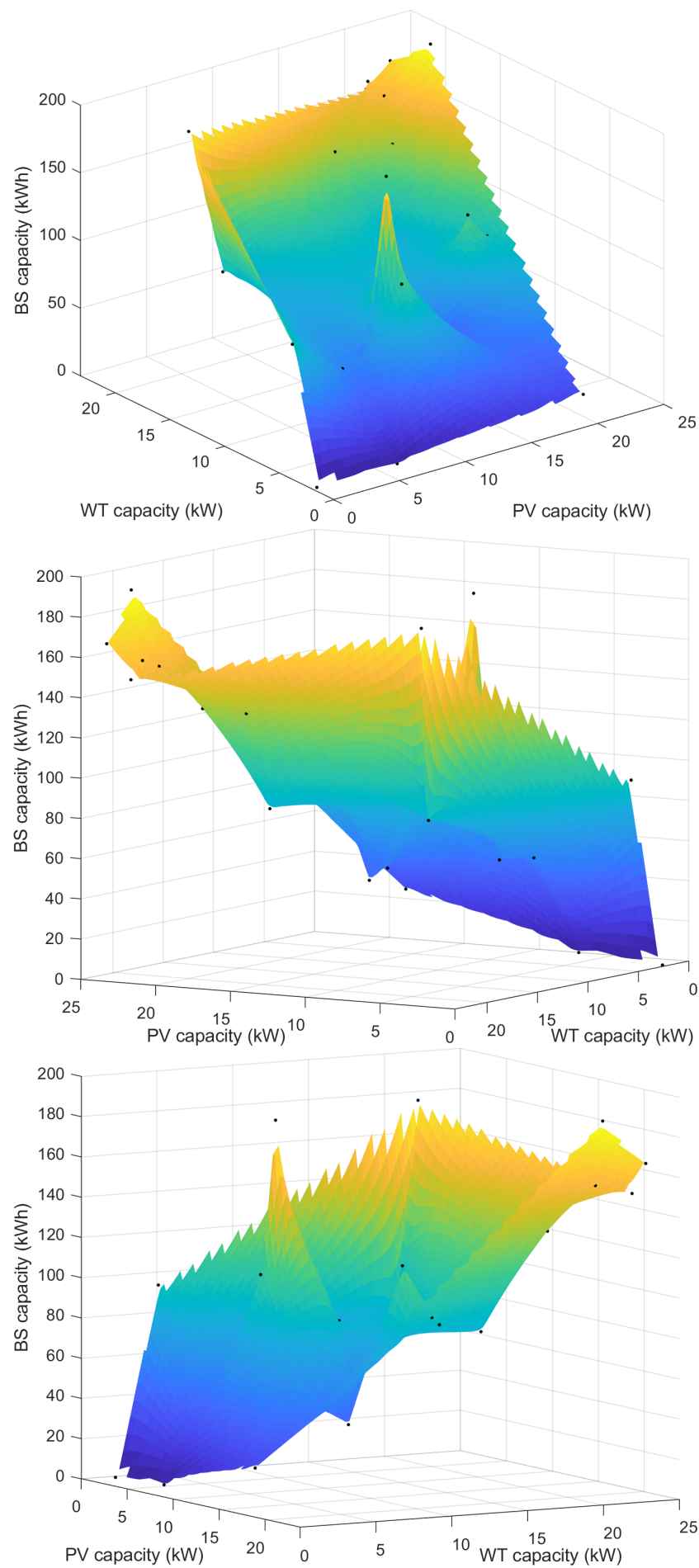
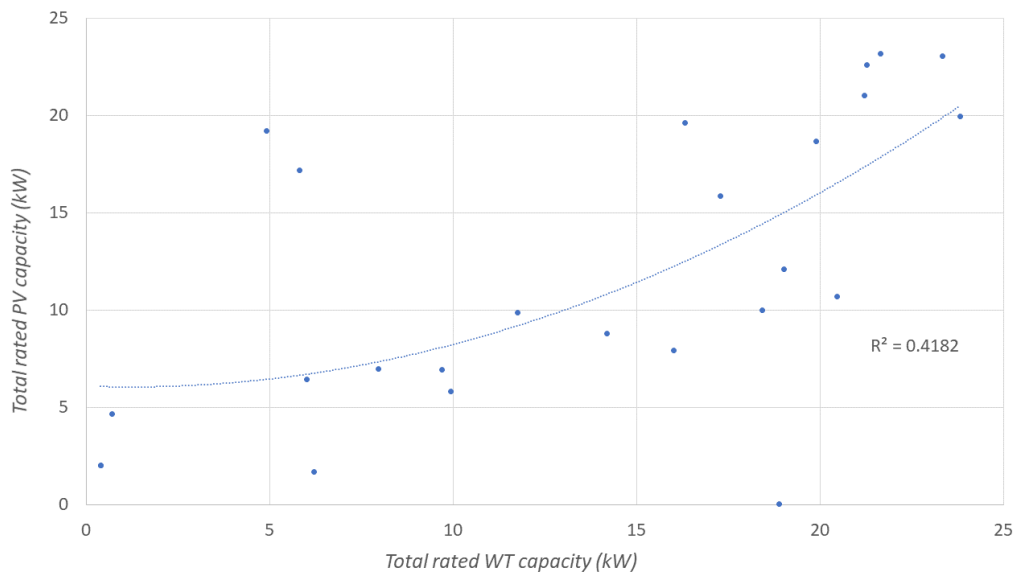


Figure 4.11: Three rotated views of the Pareto set obtained using `gamultiobj` and optimizing with respect to $P_{PV, r, total}$, $P_{WT, r, total}$ and $E_{b, init}$ as inputs.

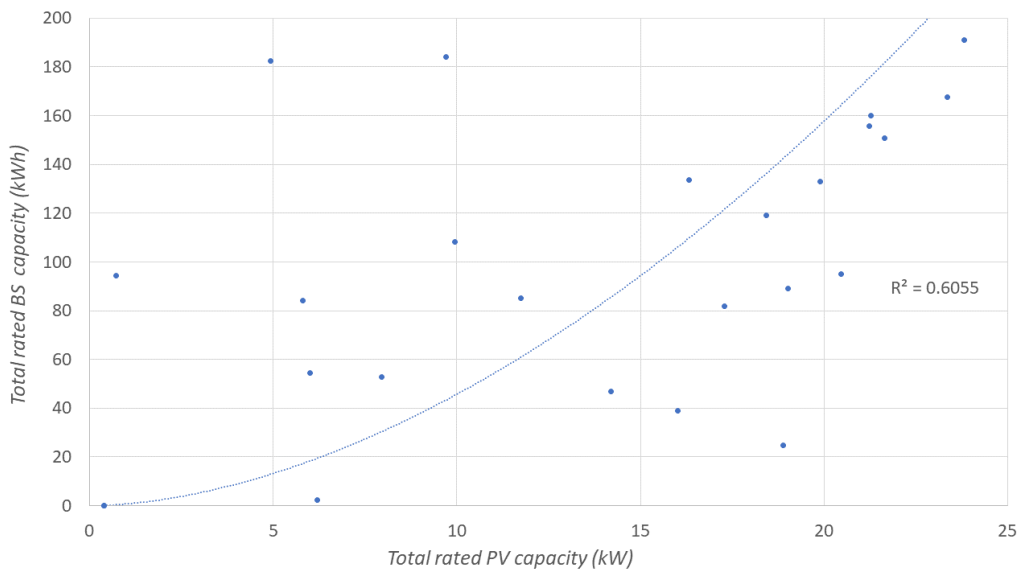
It is a little challenging to discern relationships among the Pareto-optimal input variables from the 3D surfaces shown in fig. 4.10 and fig. 4.11. Thus, 2D graphs were also plotted in fig. 4.12 to show the variations of the inputs with each other, when all three inputs belong to the Pareto set. These were obtained from the Pareto fronts generated in fig. 4.11.

It can be seen from fig. 4.12 that, in general, there is a positive relationship between all three pairs of inputs, although the correlation is often not very strong or clear. Figure 4.12a shows that when installed PV capacity increases, WT capacity also increases weakly. However, when the increase in either quantity is very large, this can lead to a decrease in the other. This results in the relatively low value of $R^2 = 0.4182$, when fitted with a 2nd order polynomial curve. This makes sense physically since if the system is already heavily reliant on a large installed capacity of either PV or WT, then less additional capacity of WT or PV respectively, needs to be installed to satisfy load. Although all these combinations of input variables are equally optimal in the Pareto sense, a designer would still prefer a solution offering a more diversified and balanced portfolio of generation sources, as opposed to one that's too heavily skewed towards either PV or WT.

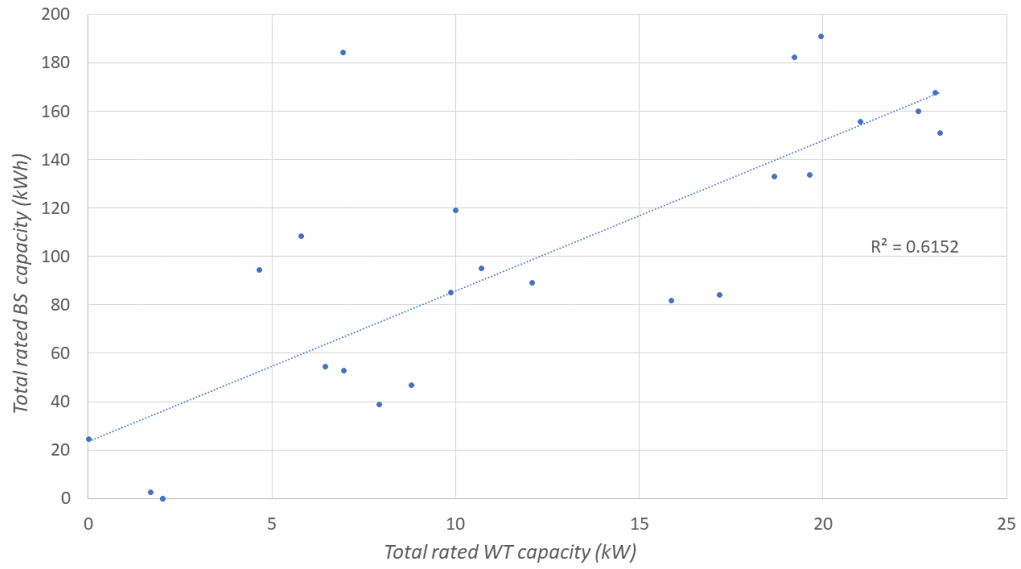
Similarly as seen in fig. 4.12b and fig. 4.12c, the installed BS capacity increases both with an increase in PV capacity as well as an increase in WT capacity. This positive relationship is stronger than in fig. 4.12a, with $R^2 = 0.6055$ for the BS vs PV capacity curve (fitted with a power curve) and $R^2 = 0.6152$ for the BS vs WT capacity (fitted with a linear trendline). These results follow from the fact that renewables like wind and solar power are both intermittent, unpredictable and their time of availability does not necessarily match up well with the actual time of use of electricity by customers in the MG. Thus, as RES capacity increases, BS capacity will also likely need to increase on account of this uncertainty and mismatch between supply and demand, in order to ensure MG operation with the same level of reliability.



(a) Variation of installed WT and PV capacity.



(b) Variation of installed PV and BS capacity



(c) Variation of installed WT and BS capacity

Figure 4.12: 2D plots showing the variations of Pareto-optimal values of the inputs $P_{PV, r, total}$, $P_{WT, r, total}$ and $E_{b, init}$ relative to one another.

Variation of different objectives on the Pareto front

Similar to the analysis conducted for the inputs, the Pareto front can also be used to visualize how the optimal, minimum attainable values of the objectives vary with respect to each other. This helps identify tradeoffs as well as co-benefits that arise while pursuing different goals during MG design and sizing. In order to obtain some non-zero values for DPSP, this Pareto set was produced using a smaller DG rated at 7 kW. Furthermore, it was found that the *REF* is strongly negatively correlated with the normalized *Emissions* term in a nearly linear fashion. This makes intuitive sense since raising penetration of clean renewables leads to lower emissions. Thus, the Pareto-set generation was simplified by excluding the $(1 - \text{REF})$ objective for simplicity, since its trends would follow those of emissions.

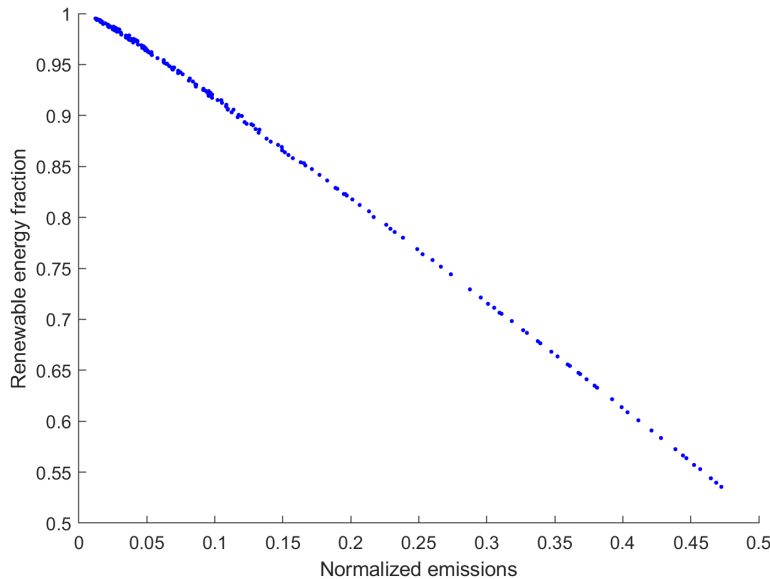


Figure 4.13: Almost linear relationship obtained between renewable energy fraction and normalized emissions,

The Pareto front was then calculated using pattern search on the remaining four objective with 200 points so as to obtain a dense set. 2D plots in fig. 4.14 show the relationships between different pairs of objectives. Reducing emissions and load deficiency both raise system costs as shown in fig. 4.14a and fig. 4.14b. Minimizing the amount of energy wasted⁵ requires increasing BS capacity and/or operating the DE more frequently (with reduction in installed RES capacity), which generally result in higher costs as in fig. 4.14c. Thus, some non-zero dump energy ratio is usually necessary for optimal operation, the value being $\approx 10\text{-}25\%$ of total generation in this case. However, beyond a certain point, further increase in dumped energy also increases LCOE since the system is likely oversized implying higher capital and operational costs.

Interestingly, emissions rise with DPSP because load is lost most often when even the backup DE operated at its full rated power is insufficient to meet demand. Thus, higher DPSP values generally indicate excess demand situations caused by peaky, sub-optimal load profiles that require the DE to run for longer periods and increase diesel consumption. Finally, normalized emissions in fig. 4.14e as well as DPSP in fig. 4.14f fall with rise in dumped energy ratio, both of which make intuitive sense. Increase in dumped energy implies more extensive use of cleaner renewables leading to more curtailment. Keeping the lost load (DPSP) at low levels

⁵i.e. grounded or sent to dump loads

also often requires meeting excess demand by bringing the backup generator online, which can result in excess power production⁶.

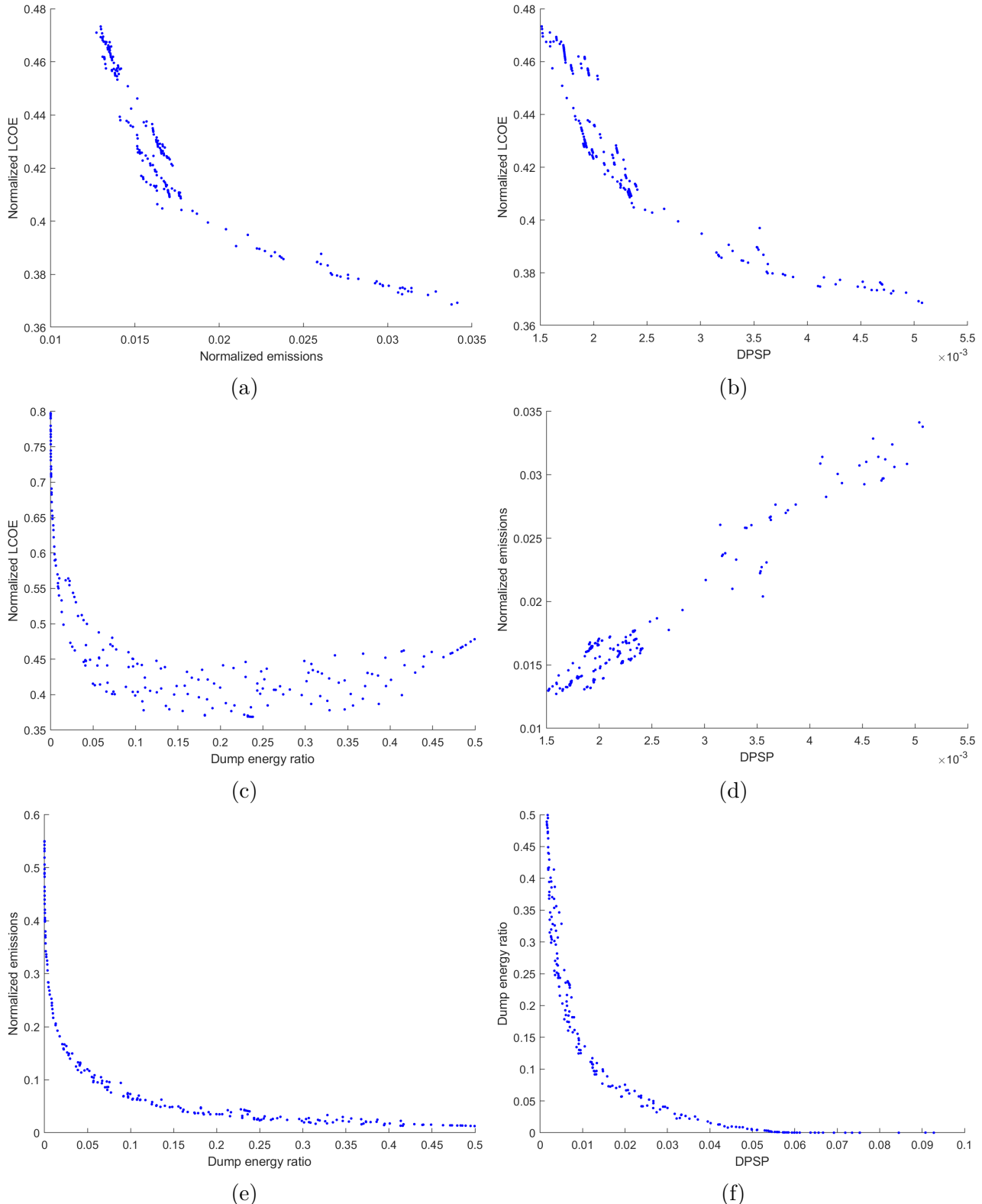


Figure 4.14: Two-way correlations between objectives derived from Pareto-set obtained via `paretosearch`.

⁶particularly if the excess demand remaining to be met is below the DG's rated power

4.1.4 Break-even distance analysis

This determines the how far the location of the stand-alone, islanded hybrid RES-based MG should be from the existing macrogrid and any utility T&D lines, in order to be cost-effective (i.e. break even) when compared to using power from the conventional power network through grid extension. This is an important metric for off-grid systems since the economic feasibility of such decentralized systems is strongly affected by the distance of grid connection, and can be calculated using [19]:

$$BED \text{ [km]} = \frac{[TAC - (LCOE_{grid} \cdot \sum_{t=1}^{t=8760} E_{load}(t))]}{C_{ext} \cdot CRF} \quad (4.1)$$

$$= \frac{[TAC - (LCOE_{grid} \cdot \sum_{t=1}^{t=8760} P_{load}(t) \cdot \Delta t)]}{C_{ext} \cdot CRF} \quad (4.2)$$

where $LCOE_{grid}$ is the leveledized electricity cost of the conventional utility and C_{ext} is the average cost of line extension from the main grid, while $TAC = \$17,097$ and $CRF = 0.0582$ are calculated from the model for the baseline MG with a 16 kW DG and optimal RES and BS capacities. Using a value of $LCOE_{grid} = \$0.125/kWh$ [92] and $C_{ext} = \$157,470/km$ [93] for electric utilities in Kenya, the break-even distance is estimated to be 0.855 km. The MG site in Timbila, Taveta is situated $\approx 111 \text{ km}$ away from Voi, the nearest large town and $\approx 305 \text{ km}$, away Nairobi, the capital and largest city in Kenya. Thus, the islanded MG is deemed to be a much cheaper alternative to grid extension.

4.2 Sensitivity analysis of sizing

The sensitivity of microgrid design, operation and performance is assessed by varying several parameters and observing the impacts of these changes on the objectives as well as sizes of the components. Unless mentioned otherwise, the default values used for all parameters are listed in table 4.7.

Parameter	Default value
DG power rating [kW]	16
Diesel fuel price \$/gal	3.20
Nominal interest rate (%)	9
Inflation rate (%)	5.70
Price of BS (\$/kWh)	300
$[w_1 \ w_2 \ w_3 \ w_4 \ w_5]$	[0.2 0.2 0.2 0.2 0.2]

Table 4.7: Default parameter values used for sensitivity analysis.

4.2.1 Varying DG power rating

In all the results presented so far, DPSP has always been zero for all cases, strategy and technology choices considered. This is because the rated power of the backup DG (at 16 kW) was sized to be larger than the community's peak load. Even in the event of unusually high demand or less than expected supply from RES and BS, the DG can be brought online to meet any leftover load. Thus, there will never be any situation with unmet load if the standby DG's

power rating is set high enough. In order to understand the impact of the DG size on system performance and reliability, its rated power was varied from 0 to 20 kW.

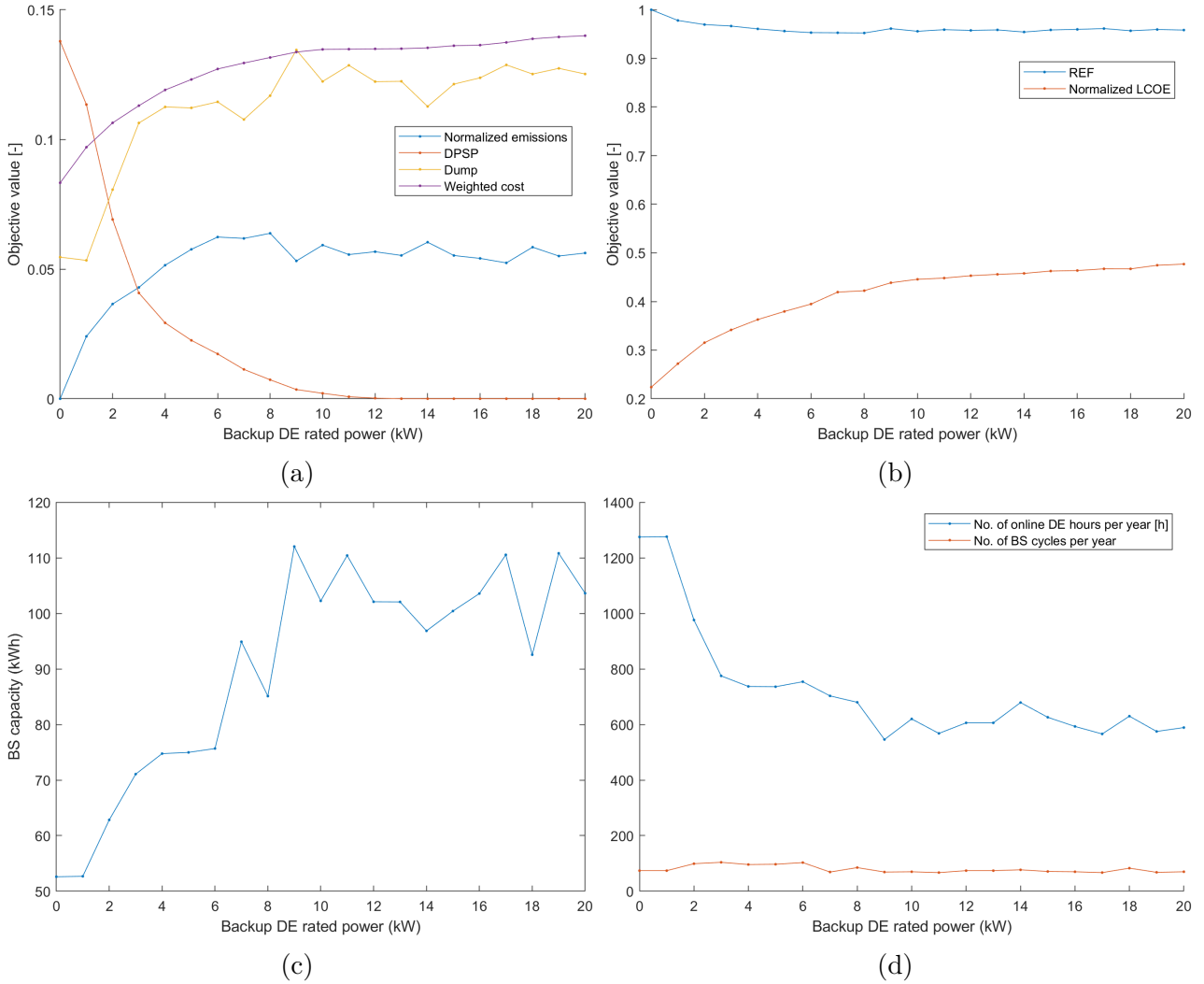


Figure 4.15: Effects of varying the rated power of the backup DG.

As expected, increasing the size of the DE increases emissions, leveled costs and dump energy ratio (REPG) while reducing REF and DPSP. It can also be seen that a DG rating of at least $\approx 11 \text{ kW}$ is needed to ensure 100% reliability and meet all load. This means that as long as $P_{DE,r} \geq 11 \text{ kW}$, the encoded load-following dispatch and scheduling strategy ensures that the value of DPSP will uniformly be zero in the sensitivity analysis for all possible values taken by the other parameters listed in table 4.7. Another result that's not surprising is that the number of annual operational hours of the DE falls as its capacity rises while the BS cycling frequency remains mostly unaffected.

Contrary to intuition, installed BS capacity increases with the DE size. This is because the dispatch strategy allows for excess DE output to charge the battery. Thus a larger battery is needed alongside a higher rated DE to minimize the excess energy sent to dump loads. Another interesting observation is that the increase in normalized emissions, LCOE and REP古 is steep at first, as $P_{DE,rated}$ rises above zero. However, the values of these variables eventually level off for higher DG ratings as does the value of the weighted multiobjective cost function, following which their increase with DE rating is relatively low. This indicates that a sensible design rule would be to oversize the DE by a sizeable amount in order to provide high reliability and security of supply, at the cost of only a small, initial decline in overall performance.

If the requirement for 100% reliability⁷ is relaxed and the designer instead allows for a small, positive DPSP value, then the DG rating can be reduced quite significantly. For instance, if the maximum allowed DPSP is 0.01⁸, then a DG rated at 8 kW would satisfy this as seen in fig. 4.15a. While optimizing dispatch later in section 4.3, the MG will also be simulated using this smaller DG size to obtain more interesting results involving some non-zero DPSP points.

4.2.2 Varying fuel price

The price of diesel was allowed to vary between \$0.2-\$12 per gallon, reflecting the current range in global diesel prices [88]⁹.

As seen in fig. 4.16 below, higher diesel fuel prices actually cause the MG to operate more optimally since the weighted cost (i.e. value of overall multiobjective function) and emissions decrease in fig. 4.16a. This makes DE operation more expensive, reduces DE online hours as in fig. 4.16d and instead favours boosting BS capacity as in fig. 4.16c. Lower fuel consumption also reduces running costs and this is likely why LCOE falls with increasing diesel price in fig. 4.16b, which is opposite to what one would expect.

⁷i.e. DPSP always equals zero

⁸i.e. 1% of annual load is permitted to not be met

⁹The lower limit corresponds to observed prices in Iran and Venezuela while the upper limit is for Zimbabwe which is currently experiencing a fuel crisis [88], and Nordic countries like Iceland

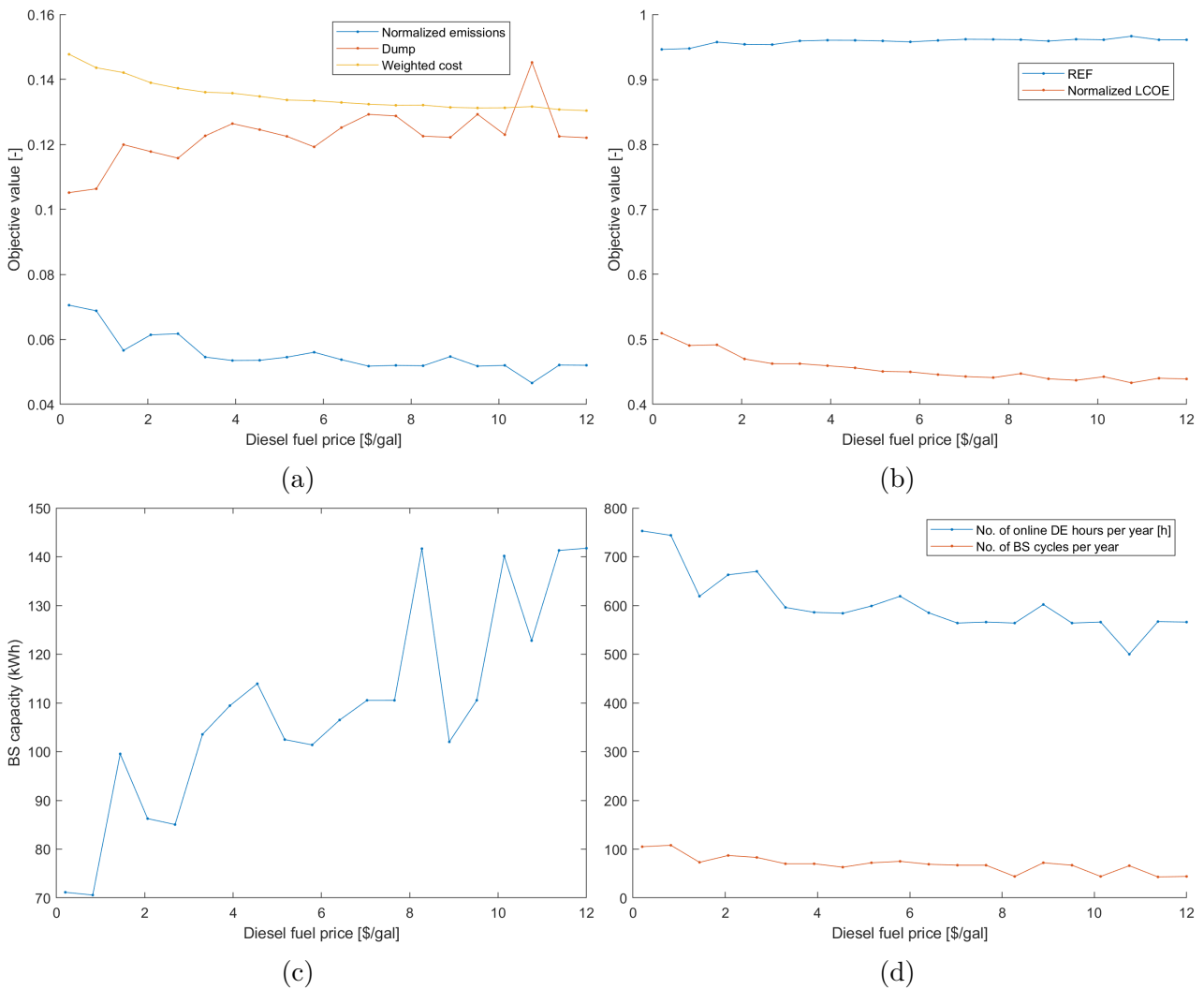


Figure 4.16: Effects of varying the fuel price of diesel used in the backup engine generator.

4.2.3 Varying financial factors

Nominal interest or discount rate

This affects an investment's risk and expected return, which determines the opportunity cost of spending more upfront on RES and BS¹⁰ versus conventional fossil fuel generators which require lower initial capital but incur higher operational costs over their lifetime¹¹.

The nominal interest rate is set by each country's central bank. This determines the cost at which other banks can borrow from it, shaping monetary policy. This value was varied between 0 and 20%, similar to the current global spread seen in central bank rates [89].

¹⁰along with supporting infrastructure like converters and controllers

¹¹for fuel, maintenance, startup and shutdown etc.

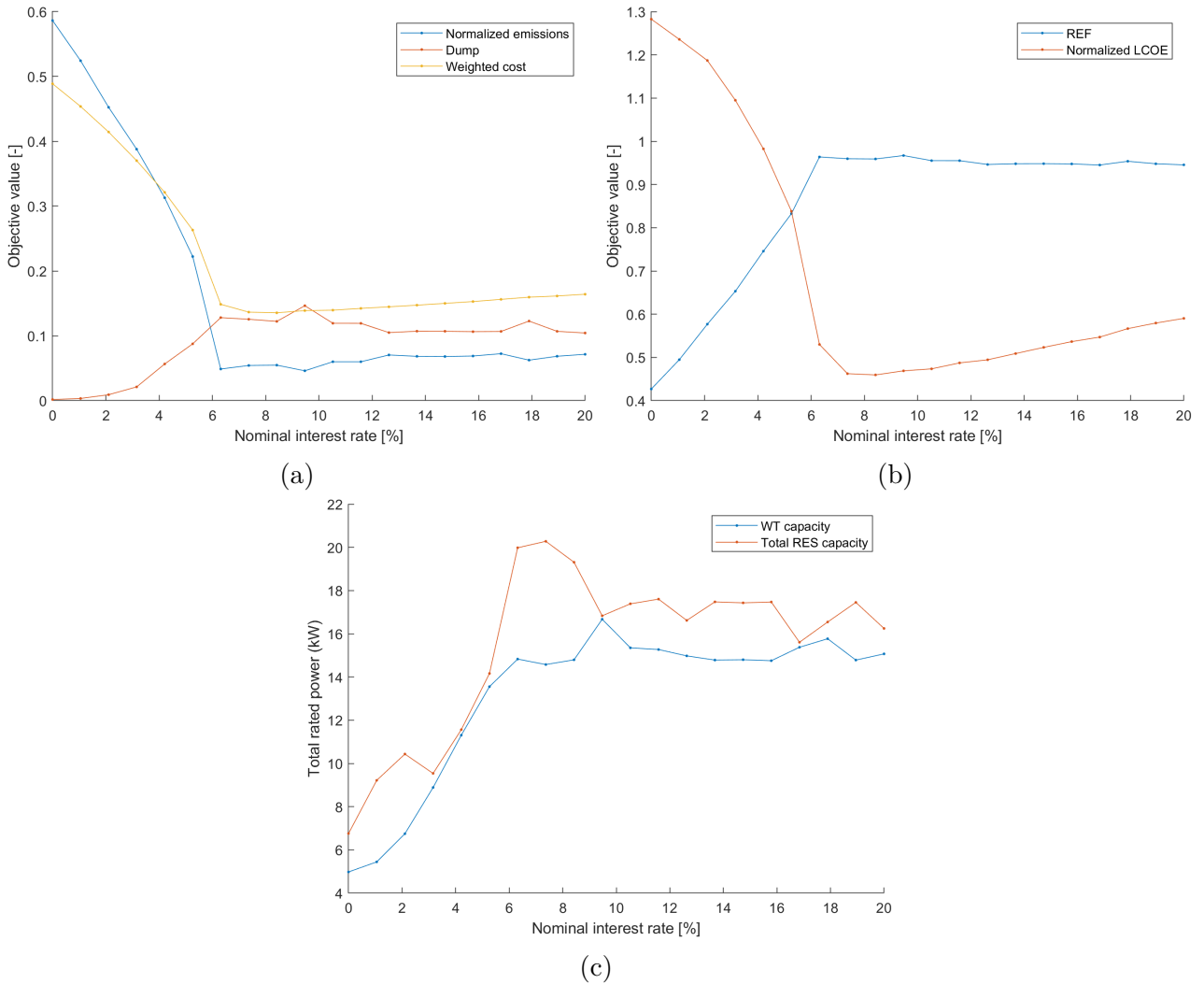


Figure 4.17: Effects of varying the nominal interest rate.

The trend shown by the above curves is due to the real discount rate (calculated using eq. (3.36)) being negative for nominal interest rates below the default inflation rate (5.7%). Negative interest means that capital is much more readily available i.e. investors are essentially paid to borrow funds. This incentivizes them to invest more upfront on renewables and storage as opposed to paying more in the future for DE fuel costs. This effect causes the rise of WT and RES capacity in fig. 4.17c and resulting REF rise in fig. 4.17b until $i \approx 6\%$. The expansion of renewables also causes emissions and overall weighted cost to fall in fig. 4.17a, while lower borrowing costs cause LCOE to decline sharply up to this 6% point. After this, real interest rates become positive and most variables only vary slightly with further increase in i . Emissions, LCOE and weighted cost all grow slightly because higher interest payments make capital intensive projects like renewables and battery storage less profitable.

Inflation rate

The inflation or escalation rate describes the annual increase of the average price level in a country, as measured by the consumer price index (CPI). It determines the purchasing power of money in terms of real goods and services and affects investment as well as operational decisions. This was allowed to vary between 0-15%, in accordance with the range of inflation values presently experienced across the world [90].

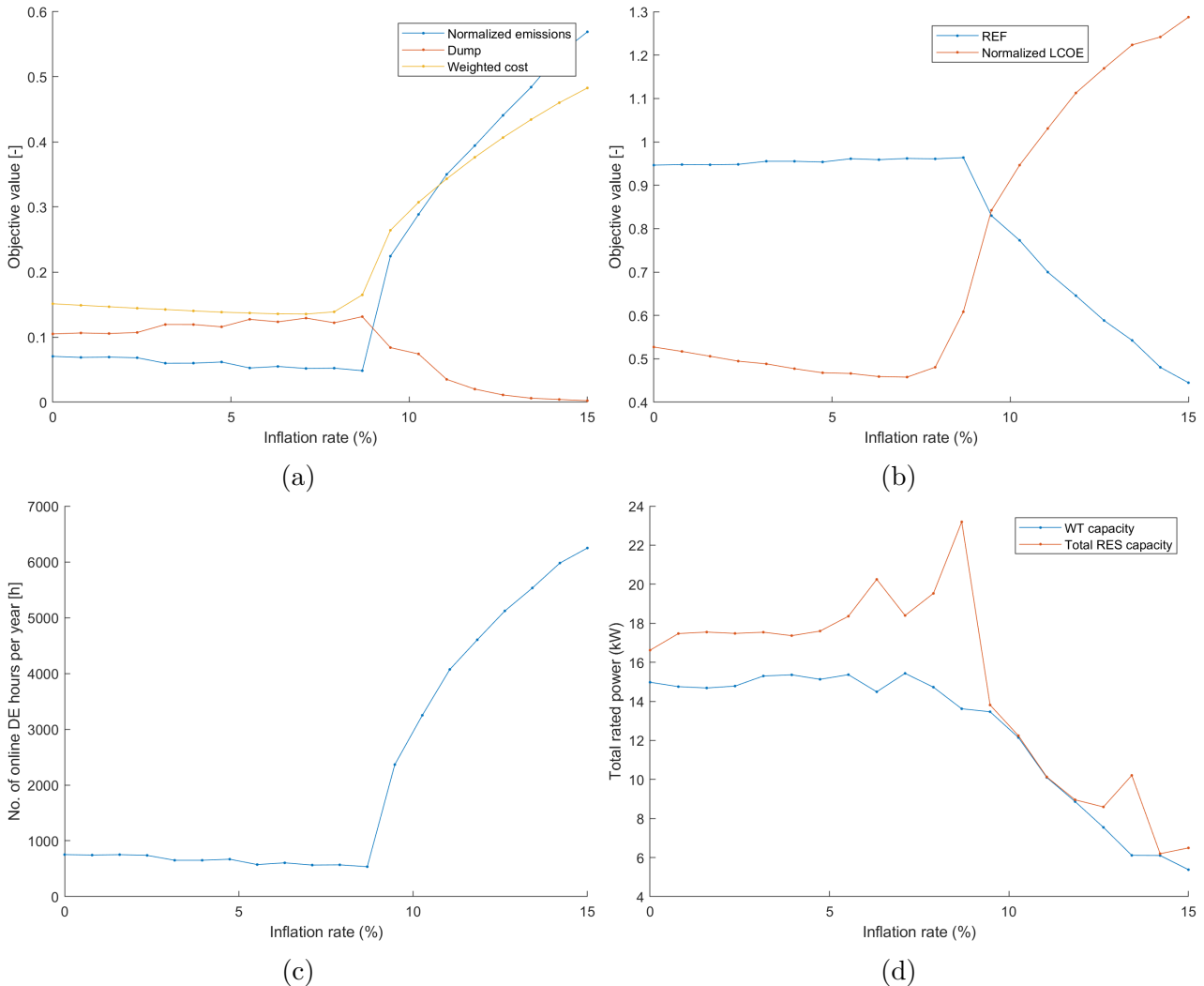


Figure 4.18: Effects of varying inflation rate.

Similar to section 4.2.3, the results in fig. 4.18 above also result largely from the interplay between the nominal interest and inflation rates to set the real discount rate using eq. (3.36), which causes the real interest rate to be negative for inflation values above 9%.

4.2.4 Varying price of battery energy storage (BS)

The price of electrical energy storage in the form of batteries is expected to decline significantly over the next few years and decades, owing to intensive R&D, exploding demand and increased focus from various stakeholders in this area, particularly automobile manufacturers. It has been estimated that the average price of Li-ion BS will fall to $\approx \$94/kWh$ by 2024 and $\approx \$62/kWh$ by 2030 as shown in fig. 4.19 below. Thus, the cost of BS was allowed to vary between $\$50/kWh$ to $\$300/kWh$ in this analysis.

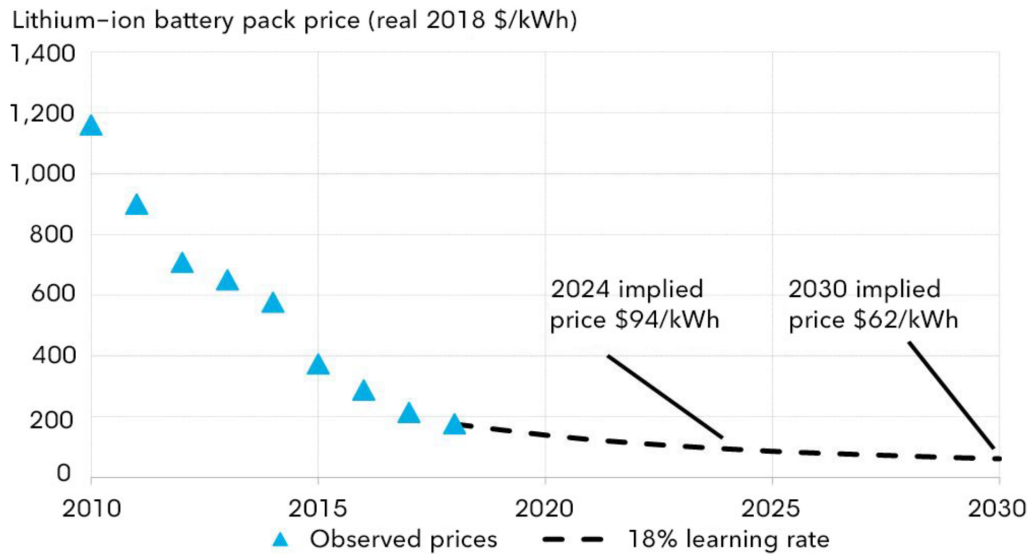


Figure 4.19: Price outlook for Lithium-ion battery packs [87].

Agreeing with intuition, installed energy storage capacity falls in fig. 4.20c as battery costs increase and cycling frequency of the remaining BS consequently rises in fig. 4.20d, along with LCOE in fig. 4.20b. A smaller battery system also raises emissions and weighted costs in fig. 4.20d (i.e. MG operation becomes less optimal) since the backup DE now needs to be run more often shutdown and at higher powers when RES availability is not enough to meet demand, causing DE online hours to rise in fig. 4.20d along with fuel usage¹².

¹²This also results in higher startup, shutdown and variable O&M costs for the DG.

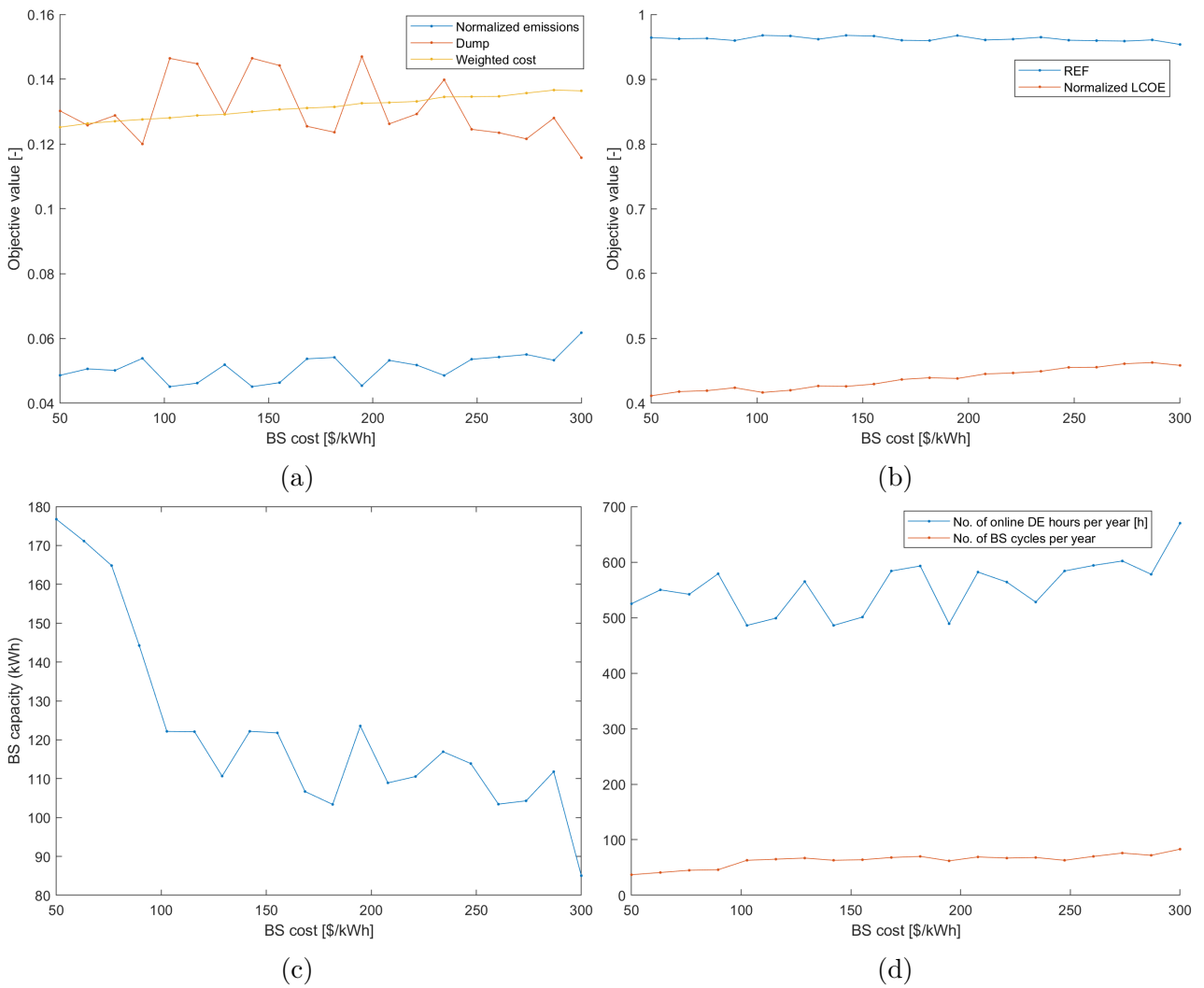


Figure 4.20: Effects of varying the costs of BS.

4.2.5 Varying relative weights

Here, the weights w_i on each of the five objectives in the multiobjective function were individually varied while keeping the values of the other four equal to each other i.e. $\frac{1-w_i}{4}$. This allows the designer to understand the impacts of prioritizing different objectives on the three input variables and also how these objectives might be correlated with one another.

Varying weight w_1 on normalized LCOE

Increasing w_1 prioritizes minimization of leveled electricity costs in the optimization. From fig. 4.21a there seems to be a minimum threshold to which MG costs can be reduced (relative to the baseline system running solely on the DE). The LCOE only falls initially as w_1 rises above zero but then remains more or less stagnant. In other words, the cheapest MG configuration possible costs slightly less than half of the baseline alternative and further cost-minimization beyond this point may worsen other objectives.

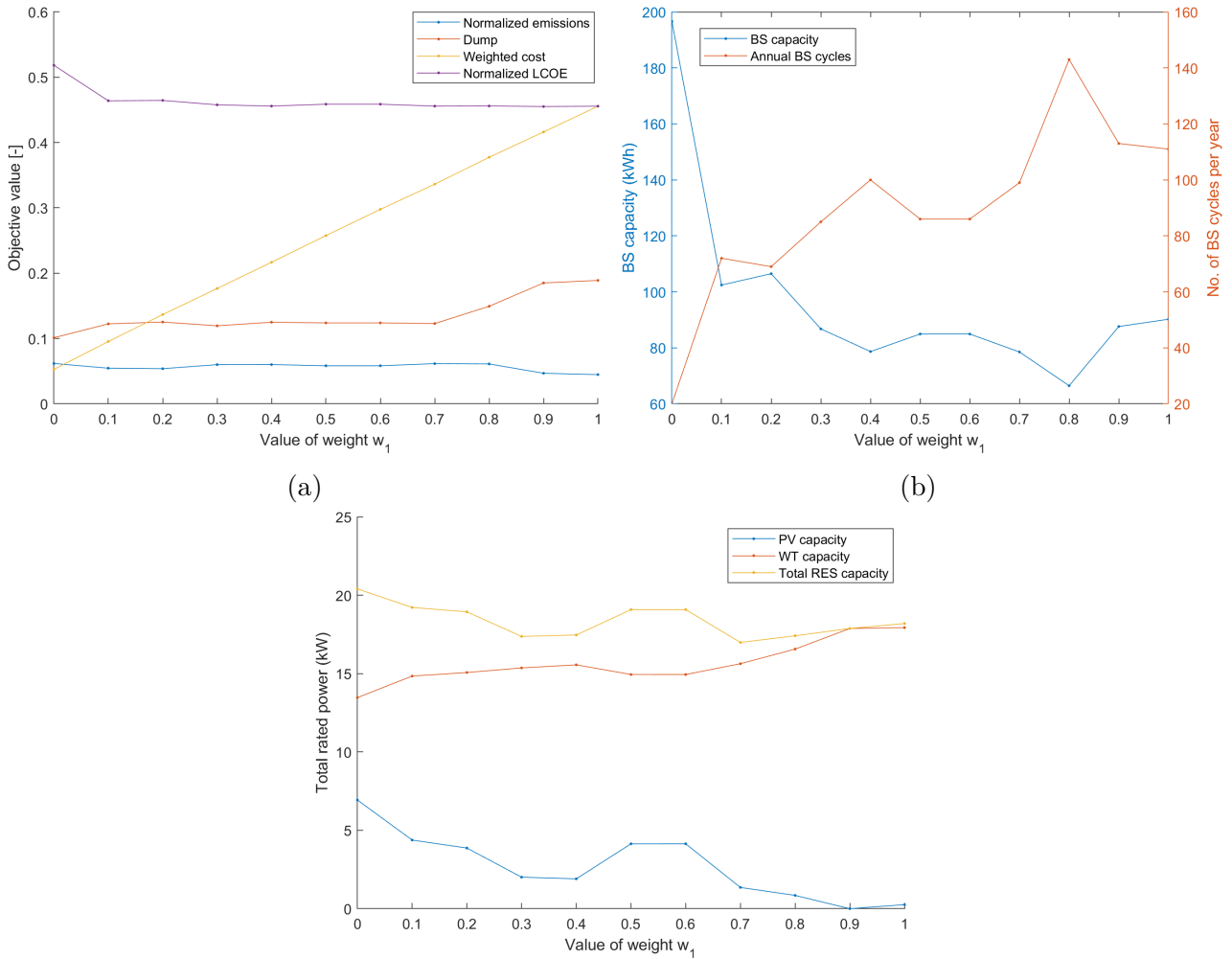


Figure 4.21: Effects of varying the weight placed on the LCOE term in the multiobjective optimization.

Thus, prioritizing LCOE minimization actually leads to a linear increase in the overall weighted cost function. As w_1 increases, emissions gradually fall signalling increased use of RES sources over fossil-fueled backup generators. This also causes dumped energy ratio to rise, indicating that pursuing cost-effectiveness may lead to solutions that aren't as efficient. To cut down on costs, the BS capacity installed is reduced and to account for this, the remaining battery storage needs to be cycled more often as fig. 4.21b shows. Similarly in section 4.2.5, there is a shift in RES capacity away from solar PV towards WT power, which is relatively cheaper on a levelized cost basis¹³.

¹³primarily due to higher capacity factors

Varying weight w_2 on emissions

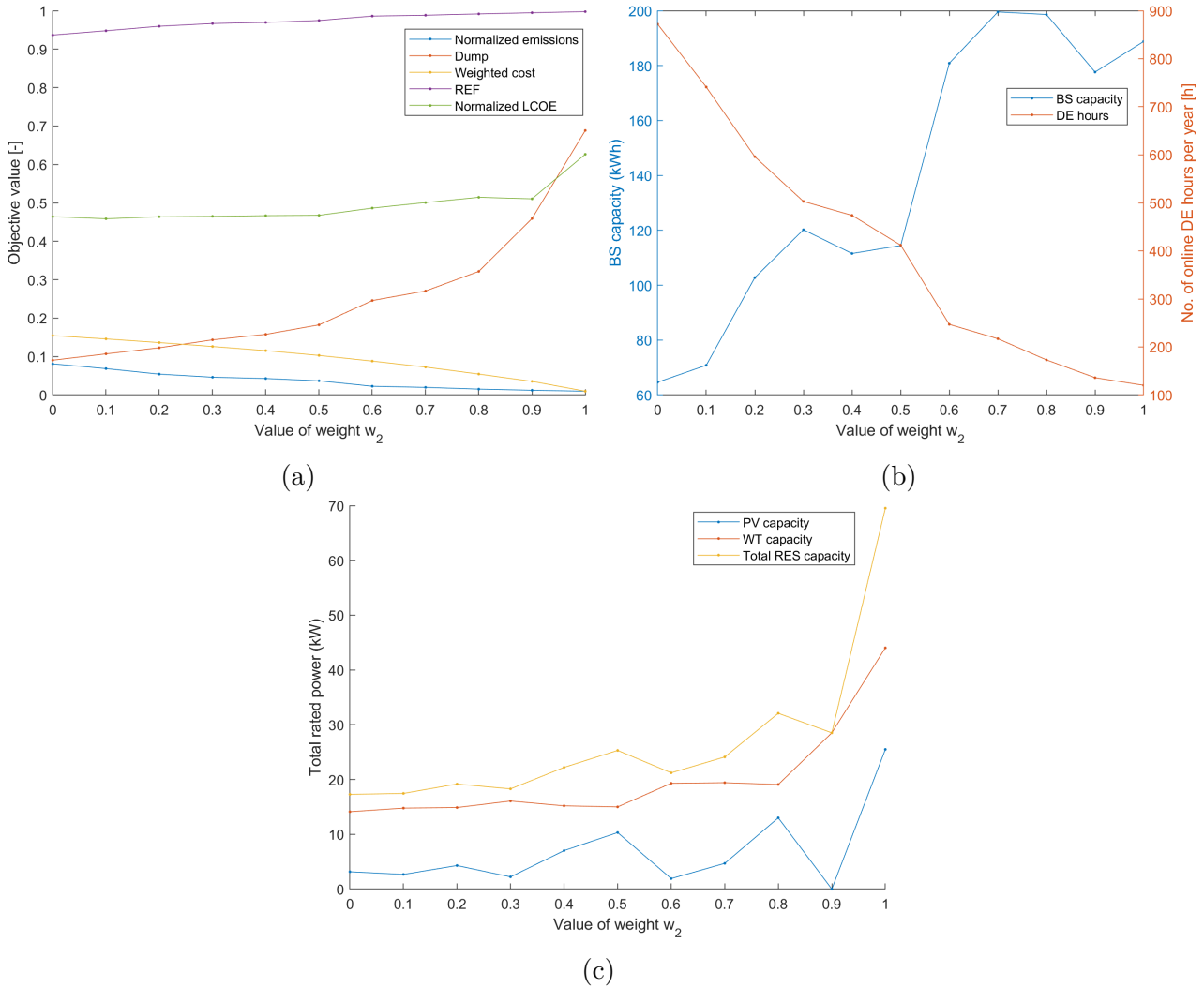


Figure 4.22: Effects of varying the weight placed on the emissions term in the multiobjective optimization.

Unlike the case with LCOE, prioritizing emissions reduction results in co-benefits by increasing the renewable energy penetration to nearly 100%. This brings both annual emissions and weighted cost to almost zero in fig. 4.22a, with an increase of both PV and WT capacity in fig. 4.22c. However, this causes LCOE and dump energy to rise especially as w_2 gets close to 1, implying that the last few kg of emissions are the most expensive to eradicate and usually entail high RES curtailment. Higher reliance on RES reduces DE online time and requires larger BS to compensate, as in fig. 4.22b.

Varying weight w_3 on DPSP

Since the DPSP is always zero for the default DG power rating of 16 kW, the sensitivity analysis on w_3 was performed on a system with a smaller DG rated at 7 kW.

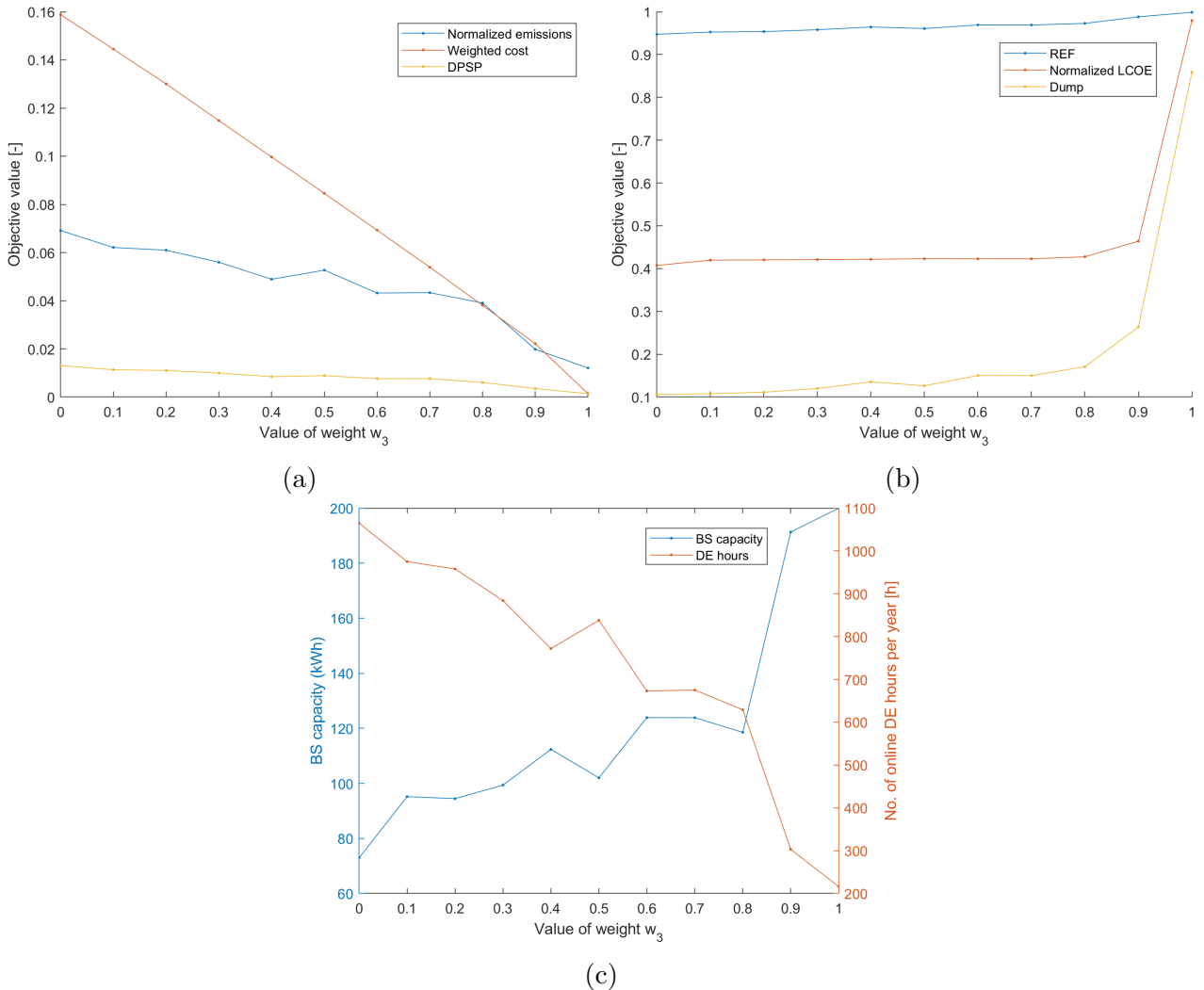


Figure 4.23: Effects of varying the weight placed on the DPSP term in the multiobjective optimization.

Placing greater emphasis on minimizing load deficiency also reduces emissions in fig. 4.23a and increases REF, but leads to an increase in LCOE and excess energy ratio in fig. 4.23b. Surprisingly, it also causes a decline in DE operational hours in fig. 4.23c which suggests that oversizing RES coupled with larger BS may actually be the more optimal design choice to meet a greater portion of load, rather than depending on the backup DE more heavily during peak load periods.

Varying weight w_4 on dump energy ratio

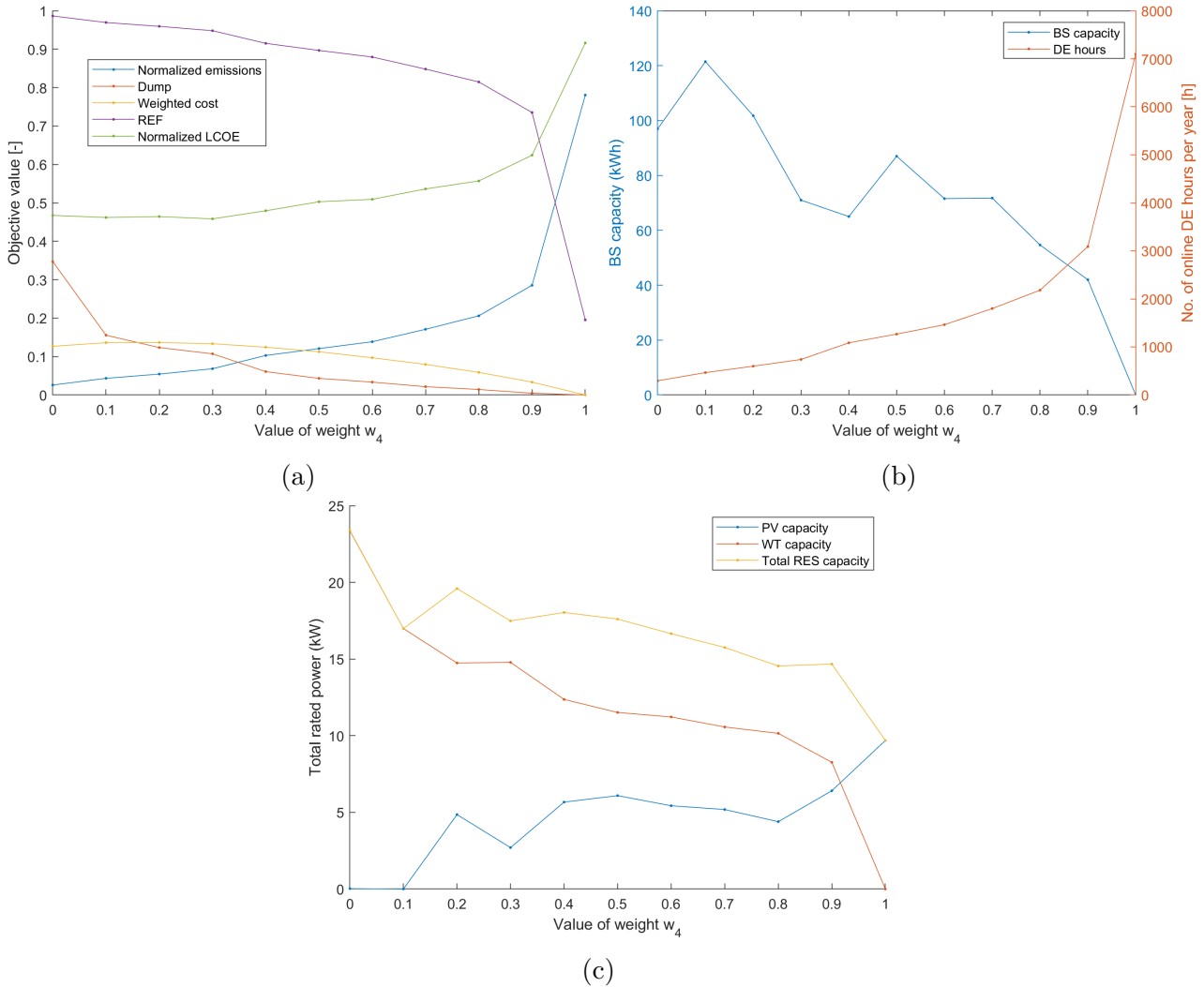


Figure 4.24: Effects of varying the weight placed on the dump or excess energy ratio in the multiobjective optimization.

Excess energy production in the MG occurs mainly due to curtailment of wind and solar output. In order to mitigate this wasted energy that's earthed or sent to dump loads, RES capacity needs to be reduced as seen in fig. 4.24c, which also leads to contraction of BS size in fig. 4.24b. Thus, the DE needs to be used to meet a greater extent of the load and is online for longer in fig. 4.24b. This increased fossil-fuel dependence raises emissions and LCOE making the system less optimal, which is why the weighted cost initially increases slightly with w_4 in fig. 4.24a, before decreasing to zero as w_4 approaches 1.

Varying weight w_5 on (1-REF)

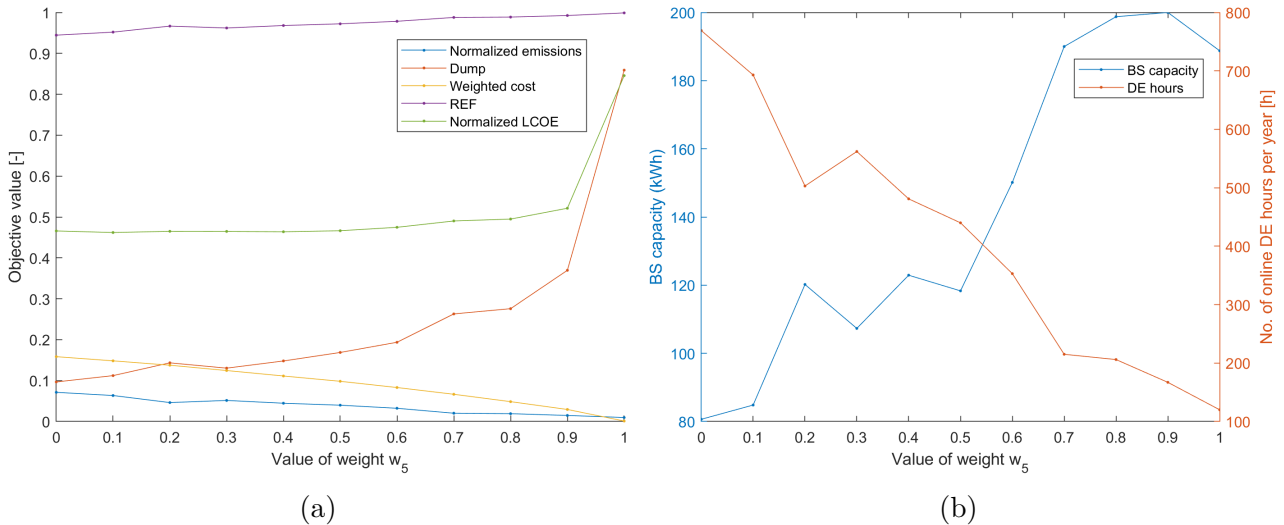


Figure 4.25: Effects of varying the weight placed on the (1-REF) term in the multiobjective optimization.

The results in fig. 4.25 which focus on maximizing renewables penetration show similar trends and patterns to those for emissions reduction in fig. 4.22. This follows from the strong correlation between these two objectives found earlier in fig. 4.13.

4.3 Optimal economic and environmental dispatch results

The dispatch optimization was performed using the `fmincon` solver using initial guesses of $P_{LI}(t) = 1 \text{ kW}$ and $P_{DE}(t) = 7 \text{ kW} \forall t = 1 : 24$. The MG controller optimizes over the entire next day (time horizon = 24 h) using vector-valued variables $\overrightarrow{P_{DE}}$ and $\overrightarrow{P_{BS}}$, hourly time steps and assuming perfect foresight over load and weather. Although the `active-set` algorithm was used with `fmincon` earlier for sizing optimization, it can violate bound constraints at intermediate iterations. This caused the solver to sometimes converge to infeasible points while solving the dispatch problem. Thus, the `sqp` algorithm was implemented here instead since it satisfies bounds during all iterations and is faster than the `interior-point` method. The maximum allowable load shortage was set to 1% i.e. $DPSP_{max} = 0.01$. To start, the simulation was run using optimal PV, WT and BS capacities found in table 4.6 for the LI+DE system with a 16 kW DG (ensures 100% reliability).

System	Min obj.	COE	Emissions	DPSP	Dump	REF
(i) 16 kW DE	0.4717	1.0291	0.6202	0.004	0.3559	0.6506
(ii) 8 kW DE (old sizing)	0.2695	0.6948	0.2469	0.007	0.2228	0.8239
(iii) 8 kW DE (new sizing)	0.2669	0.6895	0.2350	0.010	0.2346	0.8346

Table 4.8: Summary of the dispatch results and performance with a few different possible DG and RES sizes considered. Both COE and emissions are reported as normalized values. The minimum objective value reported here was calculated as an equally weighted linear combination of *COE*, *emissions*, *DPSP*, *Dump* and $(1 - \text{REF})$.

From table 4.8, it can be seen that the MG using a 16 kW DE actually costs more daily than the baseline system running only on diesel. The main reason for poor performance is that there is a lower limit of 4.8 kW on the DE's power output set by eq. (3.9) and it needs to be run at this level even if the actual demand may be much lower. This unnecessarily increases fuel consumption, emissions and dumped energy. To improve this, a smaller DG size of 8 kW was also tested since this was found in fig. 4.15a to be the lowest backup power rating that minimized weighted cost while still satisfying 99% reliability. The 8 kW DG was 1st simulated using RES capacities equal to that for the 16 kW case and then with updated values found by rerunning the sizing optimization to account for the smaller DG size. According to table 4.8, both cases (ii) and (iii) produce quite similar results (as seen in fig. 4.26) and are a major improvement over the 16 kW option. As expected, the updated sizing values in (ii) produce slightly more optimal outcomes. However, the difference is very small and system (iii) was eventually chosen for further analysis since it's more diversified and well-balanced among PV, WT and BS dependence.

Comparing the actual dispatch obtained during sizing optimization in fig. 4.8 with fig. 4.26, it is clear that the optimal strategy found here for day-ahead dispatch differs in several ways from the load-following strategy prescribed in section 3.2.3 used for sizing purposes. The load-following strategy enforced a clear, fixed priority order in which generation units are dispatched. For instance, the DG is never brought online in fig. 4.8 unless both the RES and BS have been exhausted¹⁴ or are unavailable. However, this is not the case in fig. 4.26 as there are several time intervals where both the BS and DG are dispatched simultaneously, sometimes even during periods of high RES output. Thus, the unit commitment decision here is made according to the current (and future) supply-demand situation(s) rather than sticking to a preset scheduling strategy.

¹⁴i.e. either fully discharged or already discharging at maximum power

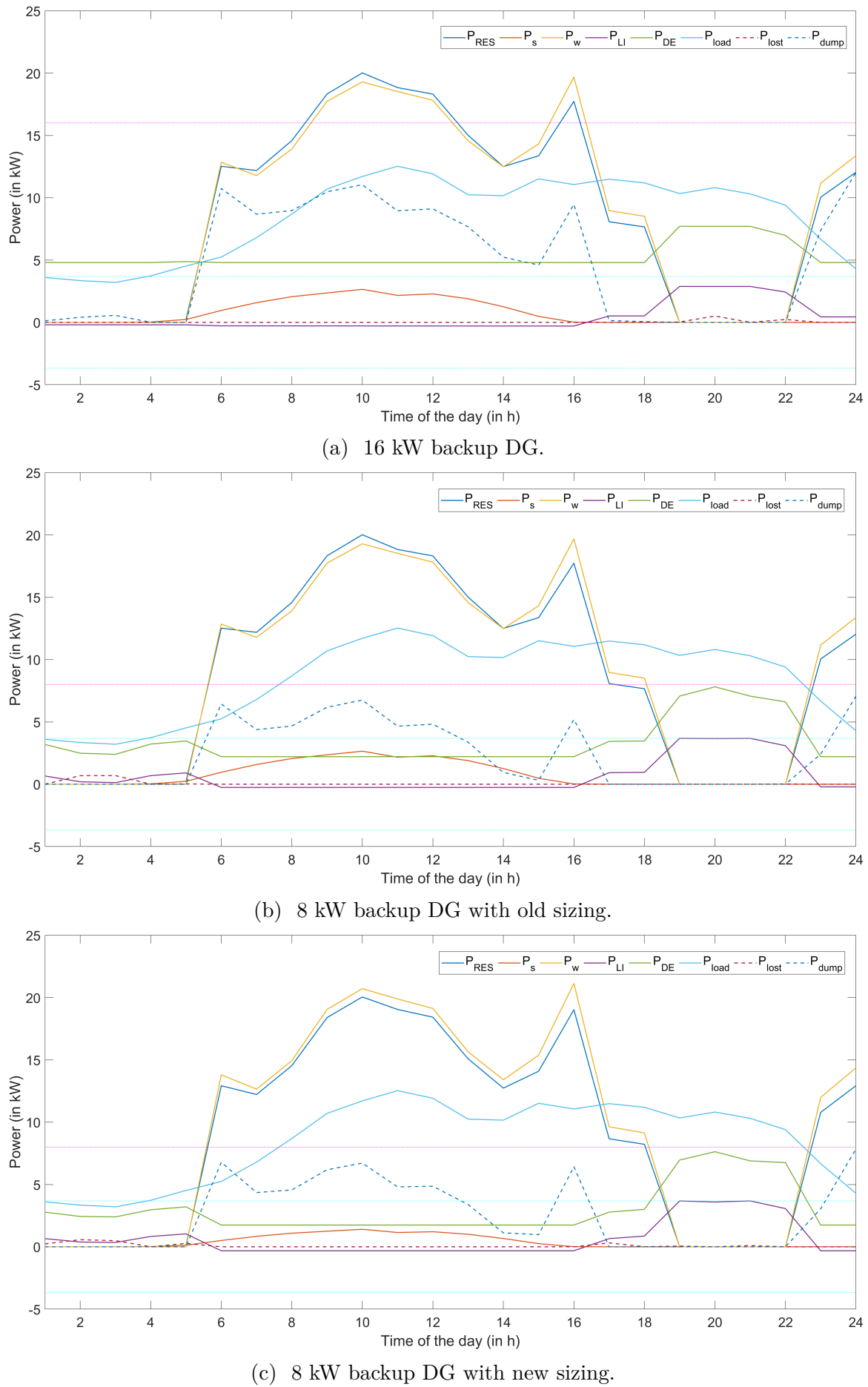


Figure 4.26: Hourly power dispatch curves over one day (24 h) period on January 1, 2018.

4.4 Robustness of dispatch to uncertainty and disturbances

Here, the robustness of the system's daily operation to uncertainties and disturbances such as sudden demand peaks and shocks to RES generation, is assessed. All the subsequent analysis was done using an 8 kW DG as opposed to the initially set default value of 16 kW, for reasons specified in section 4.3 and also because meeting the DPSP requirement would be too trivial in the latter case.

4.4.1 Intermittency and unpredictability of RES generation

The system was tested under conditions of low solar irradiance as well as low wind speeds, in order to see how it responds to the variability of renewable sources. Both the low irradiance and low wind-speed days were set to be 10% of the values for the baseline day used for the simulations in section 4.3, as shown in fig. 4.27 and fig. 4.28.

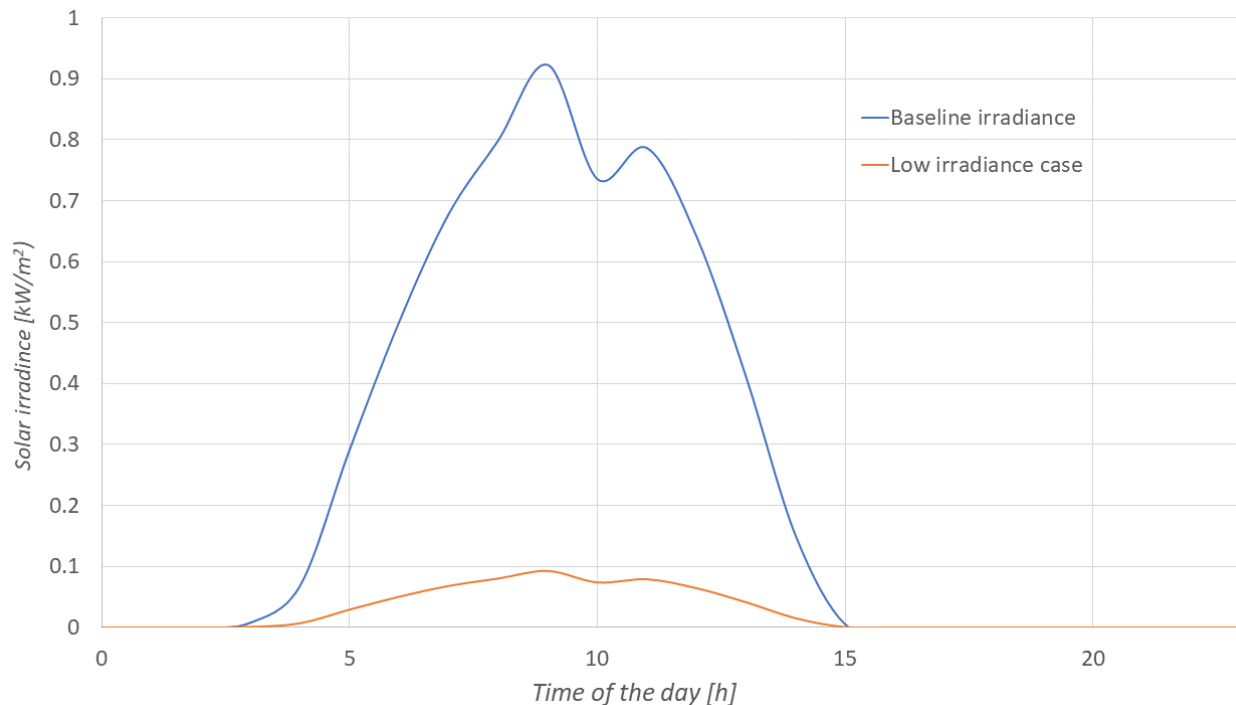


Figure 4.27: Comparison of days with normal (baseline) and extremely low solar radiation levels.

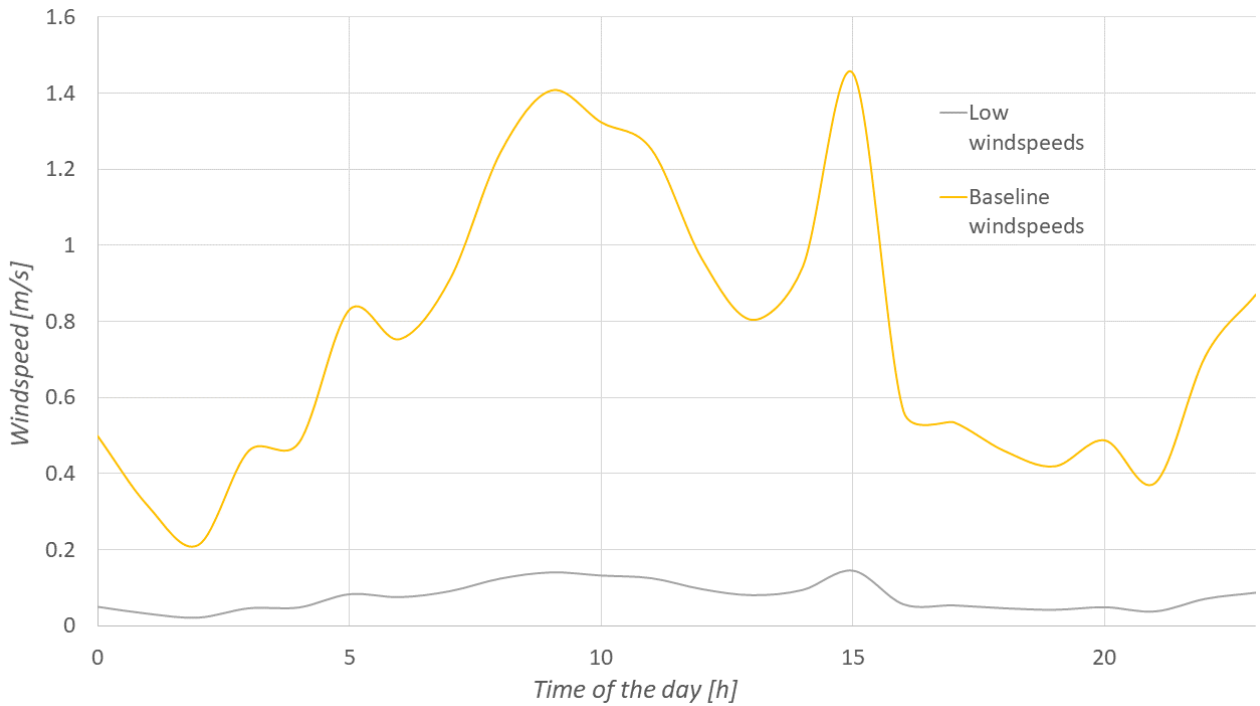


Figure 4.28: Comparison of days with normal (baseline) and extremely low wind speeds.

Scenario	Min obj.	COE	Emissions	DPSP	Dump	REF
Low solar radiation	0.2507	0.6793	0.2242	0.007	0.1699	0.8264
Low wind speeds	0.5119	1.047	0.6374	0.009	0	0.1335
Both low solar irradiance and low wind speeds	0.5331	0.9156	0.7	0.010	0.0546	0.0151

Table 4.9: Summary of dispatch results and performance under several scenarios representing RES uncertainty.

From table 4.9, it can be seen that the islanded MG is very sensitive to sudden drops in renewable generation owing to unfavorable weather conditions. Since the system is largely dominated by wind power, it is particularly vulnerable to wind speed changes. In cases of extremely low winds, the MG resorts to running the backup DE almost continuously and close to its rated power, leading to sub-optimal performance by raising costs (even above the baseline diesel system) and emissions. Furthermore, the results presented here are only for one day and the performance may be even more negatively affected if such weather persists for longer periods. For e.g. extended will lulls lasting several consecutive days may drain all the BS and force the MG to rely purely on diesel. Surprisingly, the low solar irradiance situation marginally improves MG performance compared to case (ii) in table 4.8. The main reason for this is the reduction in dump energy ratio since both peak PV and WT outputs tend to coincide near mid-day and thus less solar curtailment is needed with low PV output.

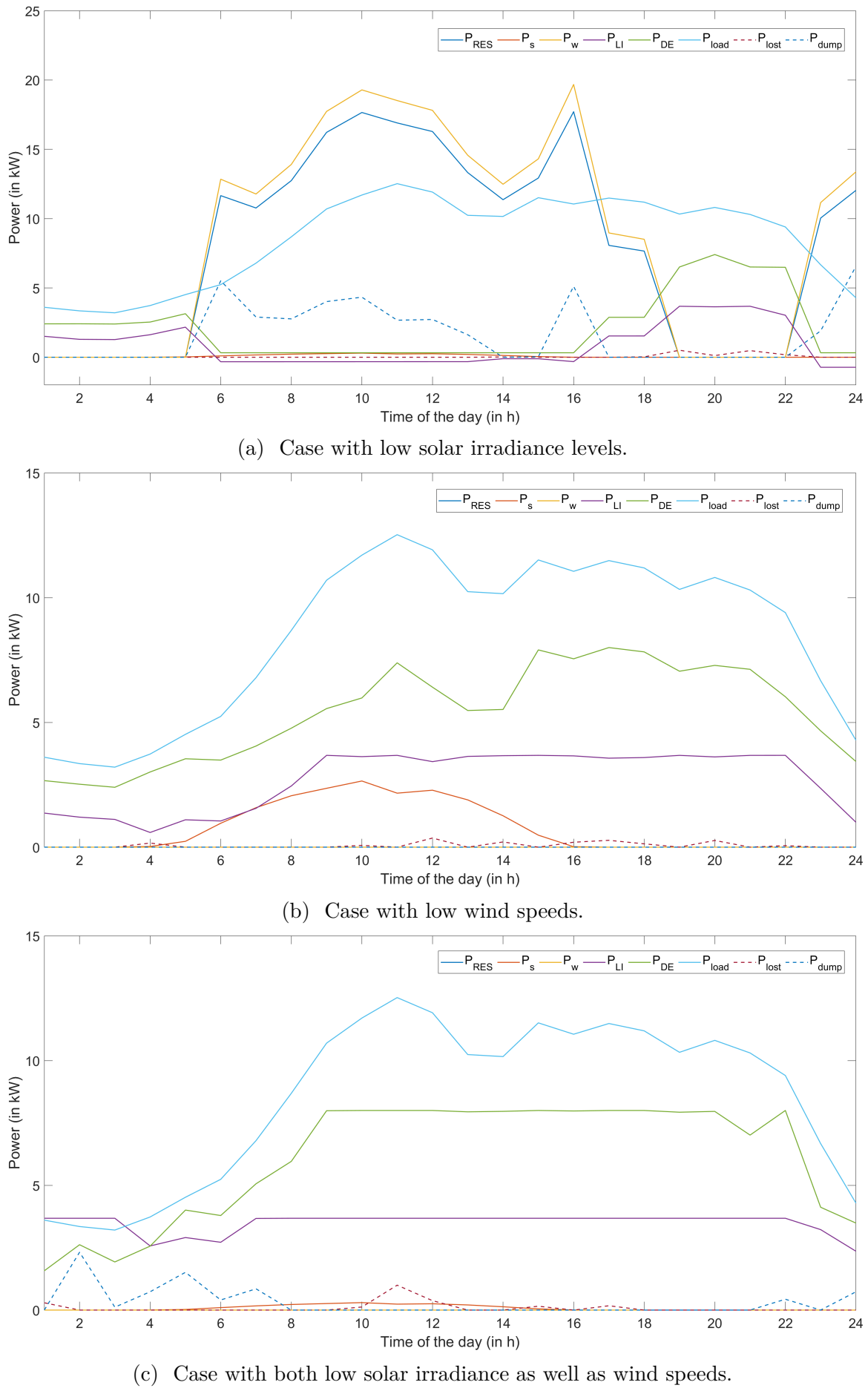


Figure 4.29: Hourly power dispatch curves over one day (24 h) period under different RES output scenarios.

4.4.2 Stochastic demand

The day-ahead dispatch optimization was repeated using several different characteristic load profiles to understand the MG performance under various demand patterns. Three different load profiles were used and compared to the baseline NREL ReOpt profile [27] used earlier in section 4.3, as shown in fig. 4.30.

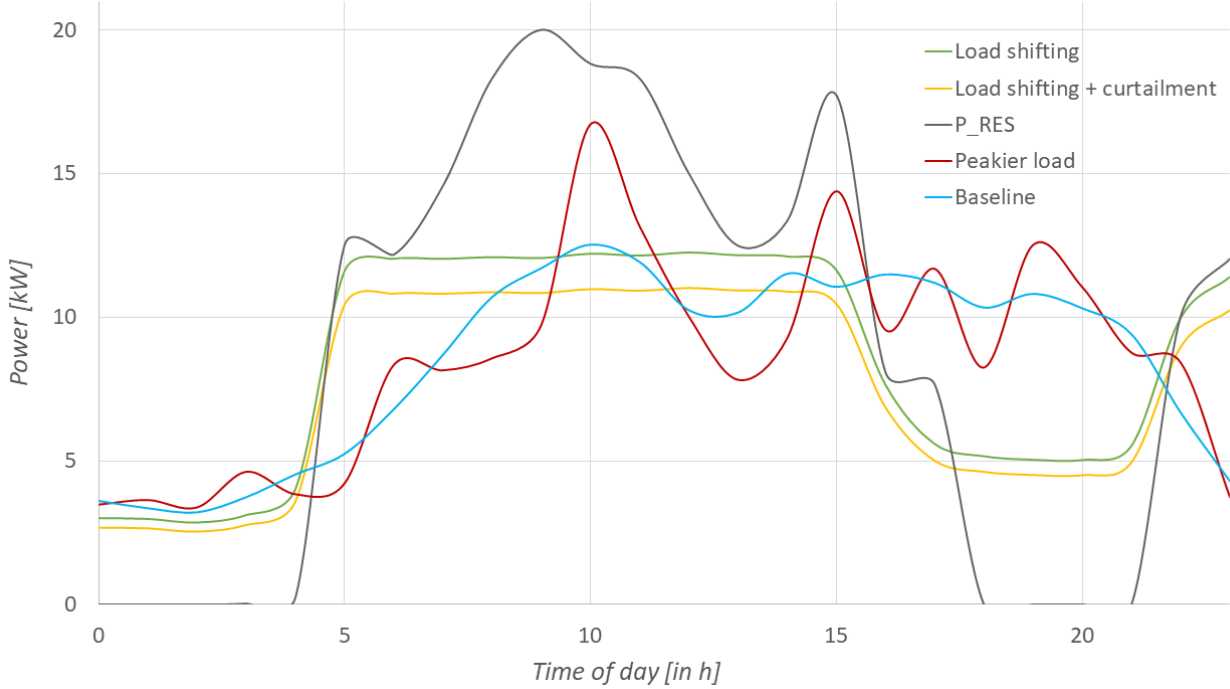


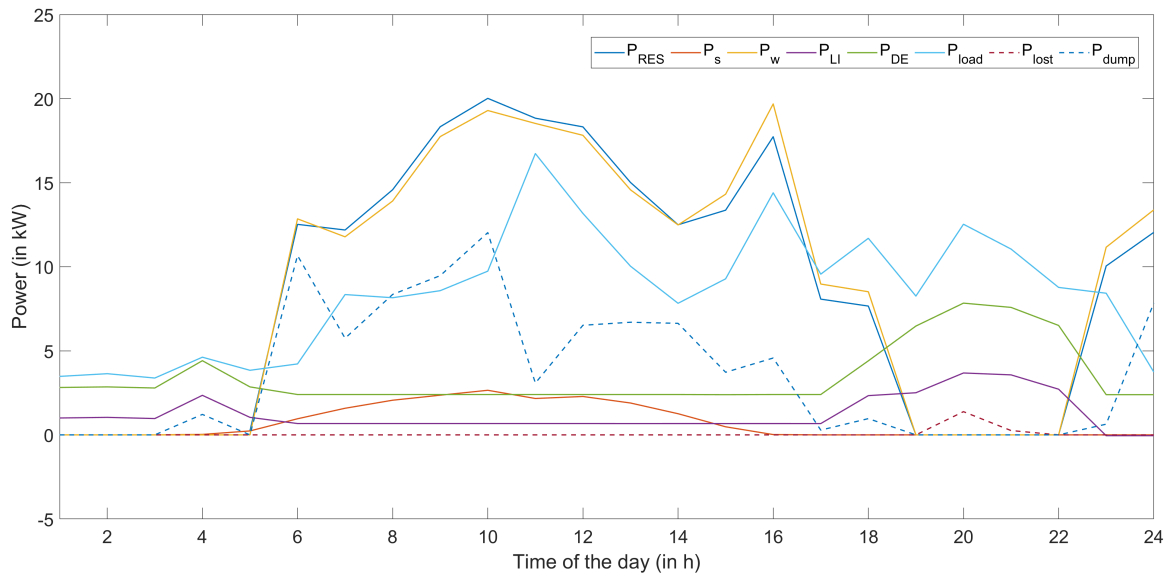
Figure 4.30: Different load profiles used in the simulation. The peakier profile was artificially generated by allowing hourly loads to vary by $\pm 30\%$ from the baseline value. The flatter profile was created by shifting hourly load values to better align with the P_{RES} curve shown, along with some additional flattening using moving averages and exponential smoothing.

Scenario	Min obj.	COE	Emissions	DPSP	Dump	REF
Peakier load profile	0.3529	0.8443	0.3565	0.008	0.3196	0.7641
Flatter profile: Load shifting only	0.2055	0.6165	0.1539	0.004	0.1355	0.8824
Flatter profile: Load shifting and curtailment	0.1527	0.3573	0.0524	0.010	0.3042	0.9607

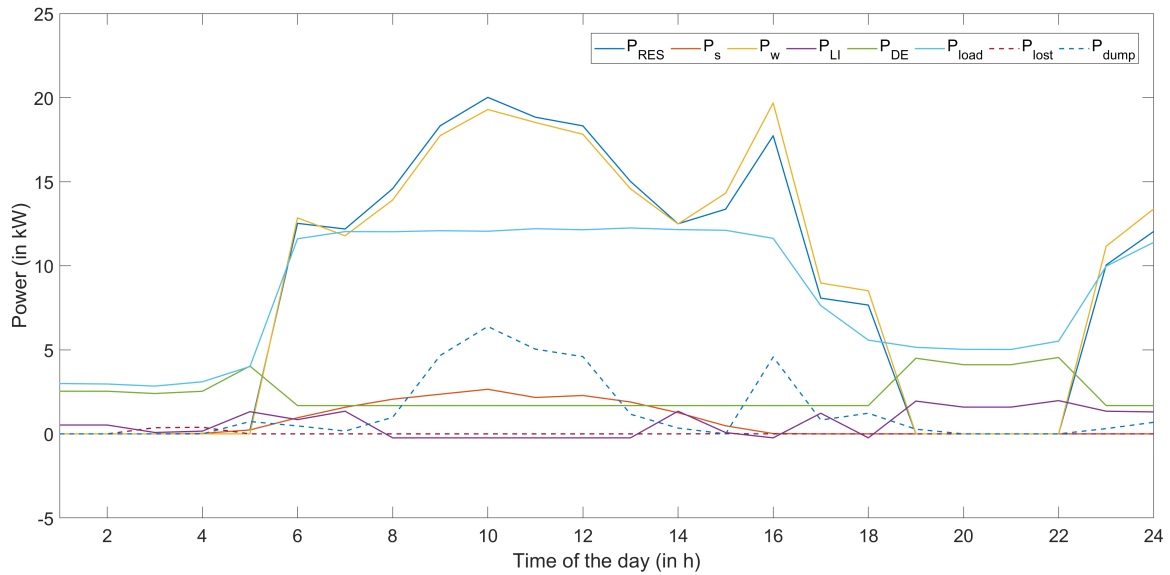
Table 4.10: Summary of dispatch results and performance under different possible demand profiles of the MG community.

From table 4.10, it can be seen that the shape of the load curve has a strong influence on the operation of the MG. Peakier profiles with greater temporal variation over the course of the day result in a greater number of demand spikes that degrade the performance of the system and reduces optimality. As seen from fig. 4.31a, the DE needs to be ramped up quickly to meet sudden increases in load and the uneven pattern also causes more RES output to be curtailed. The increased mismatch between supply and demand worsens all five objectives.

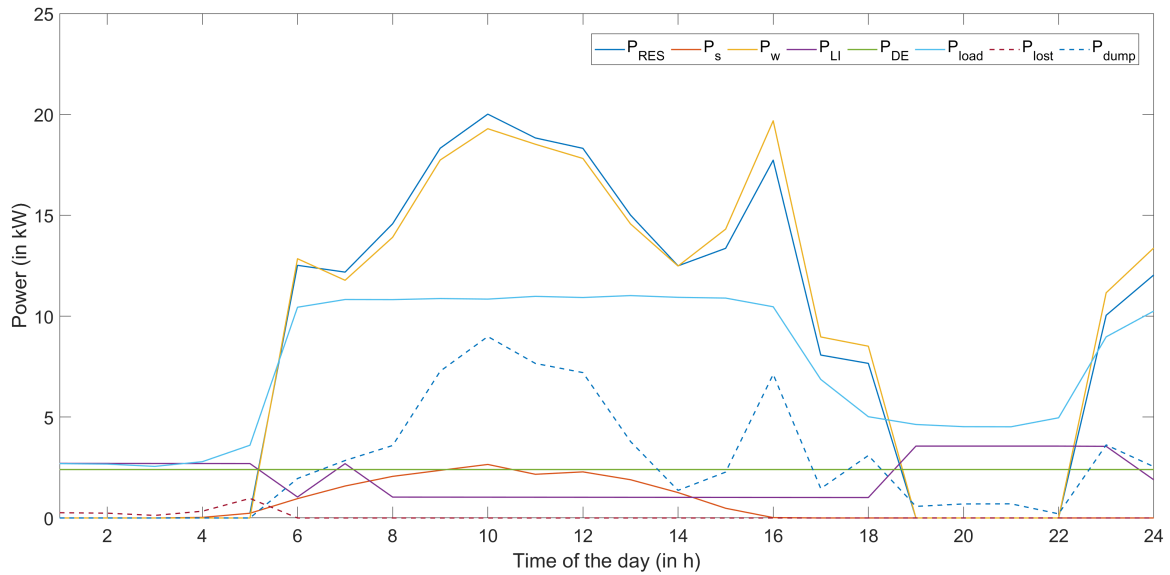
On the other hand, flatter load profiles are more optimal and result in improved performance across the board, improving all objectives relative to the baseline profile. In fig. 4.31b, significant improvements are achieved simply by shifting power demands so that their time of use matches up better with the availability of solar PV and wind resources during the day. This enables fuller and more efficient utilization of renewable power while minimizing curtailment and dumped power. In this case, load shifting is done in a way that also results in peak-shaving and a more uniform, averaged load curve. Furthermore, load shifting when combined with even small amounts of curtailment (for e.g. 10%) can improve results further, as seen in table 4.10 and fig. 4.31c, where the use of the DE is minimized. It remains online throughout the day but operates only at its minimum possible output level (2.4 kW), essentially functioning as a baseload while most of the demand is met by renewables. This results in even lower costs, emissions and higher REF than with just load shifting, although the dump energy ratio also rises quite a bit. These results motivate the need for demand response programs to shape load curves into being flatter and more optimal. Here, MG users shift and/or reduce their power consumption at specific times either voluntarily, or are incentivized to do so by the operator. Energy efficiency programs could also produce a similar, desirable effect. Finally, comparing table 4.9 and table 4.10, it may be concluded that the system is more sensitive to supply-side variations than demand changes, since the former causes larger changes in the value of the weighted objective cost function.



(a) Peakier load profile with higher variability, more peaks and valleys than baseline.



(b) Flatter load profile using only demand shifting i.e. the total amount of daily load served (area under the curve) is conserved.



(c) Flatter profile with load shifting along with 10% daily curtailment.

Figure 4.31: Hourly power dispatch curves over one day period under different demand scenarios.

Chapter 5

Caveats of model and potential refinements

5.1 Alternative dispatch strategies

The current strategy assumed for sizing optimization results in DGs being used during peak demand conditions. However, it may be more optimal to instead use DGs under off-peak situations and use BS or RES during higher demand. This would entail a different priority order for unit commitment and dispatch since all the RES would not just be used to meet as much of load as possible at the instant when solar or wind power are available. Some portion of this would also be directed towards charging the BS during off-peak times. Similarly, there may be other innovative methods which could improve objectives even more. Thus, it is necessary to explore the full space of possible strategies more comprehensively even at the design and planning stage.

5.2 Improve computational efficiency

Non-convex formulations generally entail greater computational complexity and are more challenging to solve, requiring further processing time. Future work could look into relaxations, variable transformations and/or linearizations that would make the problem easier to solve. For e.g. trying to remove the currently used discrete decision variables and making all variables continuous could be one way to convexify the problem and increase the speed of optimization. This could potentially also allow incorporation of more complex, realistic, non-linear models describing MG components, which improve accuracy but would not be tractable with problems that are not convex. Another potential method to increase speed would be vectorization of the objective functions.

5.3 More comprehensive multiyear modelling

The multi-period optimization could also be refined to simulate the system more accurately over its entire lifetime. Currently, the sizing optimization only simulates the MG for one year and then assumes that all remaining years in its lifecycle are similar to the 1st, accounting for discounting and interest. While this is a reasonable approach, it has some deficiencies due to which it doesn't reflect the actual operation of the MG perfectly. For instance, this doesn't

account for the average annual increase in electricity load of 10-15% expected in Kenya and Tanzania due to population growth, economic development, rising incomes and living standards [86]. Similarly, variations are possible in several other model parameters as well (e.g. volatile fuel prices) and the current model doesn't fully account for this, even though a sensitivity analysis was performed. Finally, the dispatch optimization was only performed for a time horizon of one day due to computational constraints. Optimizing the dispatch over longer periods could help explore the system's performance and response to disturbances in the longer term.

5.4 Simulation using smaller time steps

Discretizing into finer time steps in the order of minutes or even seconds (for e.g. $\Delta t = 5 \text{ min}$) instead of the currently used hourly time step ($\Delta t = 1 \text{ h}$) is likely to produce more realistic results since it simulates the time-marching battery dynamics and evolution of its SOC more accurately. The modelling of the DG dispatch would also be enhanced since ramp rate constraints can now be enforced, which limit how fast the unit can either be brought online (startup) or taken offline (shutdown). Furthermore, it offers more detailed resolution for all variables across the board. Currently, there are discontinuities in the dispatch and *SOC* plots produced by the model which are not physically feasible and are likely caused by the time step being too large. Reducing Δt will help obtain more continuous, smooth dispatch curves that are closer to those expected during actual operation.

However, it is challenging to achieve this in reality due to the additional complexity, extra computational burden and longer runtimes that result. It's also extremely difficult to obtain reliable and accurate sub-hourly climate and load data, particularly for locations and settlements in Africa.

5.5 Demand response (DR) and Demand-side management (DSM)

The system's robustness to stochasticity of demand and load fluctuations can be improved by implementing a demand-side management program in the MG. Several possible approaches have been suggested in the past to mathematically model DR programs and interpret their results using concepts like game theory, mechanism design and auction theory. One such intuitive model is described in [35] where the net expected benefit to the MG operator is maximized:

$$\max_{x,y} V_2(\theta, \lambda) \quad (5.1)$$

where V_2 is the benefit function of the operator:

$$V_2(\theta, \lambda) = \lambda x - y \quad (5.2)$$

where x is the amount of power consumption that's shifted or curbed by a customer of type $0 \leq \theta \leq 1$. The customer type indicates their readiness to shift or curb their power demand, with $\theta = 1$ for the most willing and for the least willing. λ is the 'value of power interruptibility', a measure of how beneficial it is for the grid operator to modify a specific load, and is determined from optimal power flow (OPF). y is the amount of monetary compensation given to a customer for a particular amount of load shifted or curbed. The customer's benefit function is then given

by:

$$V_1(\theta, x, y) = y - c(\theta, x) \quad (5.3)$$

where $c(\theta, x)$ is the cost incurred by a customer of type θ for shifting or reducing their load by x kW, which is increasing in x and decreasing in θ . Finally, there are constraints on the operator's total budget (for compensating customers) and daily limits on each customer's interruptible power.

Such agent-based formulations can be useful for simulating behavior in small networks like microgrids with relatively few market participants. However, their computational complexity scales poorly with the number of agents, resulting in larger networks, more nodes and increasingly complex interlinks between these. Another technical barrier is that such programs would require two-way communication channels for all agents involving bidirectional flows. This would entail extensive upgrades to existing network infrastructure. Furthermore, smart meters and home energy monitors integrated with the Internet of Things (IoT) also bring up concerns regarding the privacy of individual users. However, there are techniques available that can help preserve privacy while still providing enough useful information and resolution to perform load management, such as non-intrusive load monitoring (NILM) and disaggregation.

The results of such models are also non-deterministic since they involve decision making by consumers, producers and prosumers, who can often be irrational as well. There is a need to determine response functions for each agent involved and approximate their individual preferences and private costs. For instance, in the example model given above, it is challenging to actually determine the types θ_i and cost functions $c_i(\theta_i, x)$ of all the consumers and prosumers in the MG. Finally, these results can often only be presented in a probabilistic sense, which presents another barrier to practical implementation.

5.6 Load and RES forecasting

Another approach to mitigate the MG's sensitivity and effects of uncertainty is to build forecasting models that generate more accurate predictions for load as well as solar and wind output. These could also be combined with predictive control and online optimization methods to dynamically update forecasts at each time step, rather than using static forecasts or relying on historical weather (temperature, wind speed, irradiance) and consumption data.

It would also be worthwhile to test both the sizing and dispatch optimization with community load profiles calculated using methods and sources other than NREL ReOpt. For instance, past studies have determined empirical relationships to approximate the power demand of typical isolated, off-grid rural African villages as a function of time, such as [99]:

$$P [kW] = e^{[\sin(0.3409 - \sin(0.68039t) - 0.16801t)]} \quad (5.4)$$

5.7 Improved control techniques

The current model assumes perfect foresight and no errors in forecasts. The scheduler knows all the actual values of both demand and RES output over the full prediction or planning horizon, by using precalculated annual (or daily) load profiles and known historical climate data. This method is useful for initially sizing the system and devising nominal dispatch strategies, as well as an idealized benchmark to evaluate other strategies against [31]. However, it is often very challenging to achieve this in reality due to lack of availability such data with high reliability.

As described in more detail in section 2.5.2, the MG's performance can be improved by applying control strategies like model predictive or receding horizon control. Since this problem involves a non-convex, non-smooth, 'black box' objective function (i.e. having no closed form solution or gradient), it may prove to be more challenging to reformulate it into standard MPC form. Nevertheless, commercial solvers like GUROBI and YALMIP have been shown to efficiently solve such mixed-integer linear and quadratic programs without requiring complicated heuristics or decomposition methods [31].

Chapter 6

Conclusions

6.1 Key takeaways

This study considered the optimal design and energy management of islanded microgrids serving remote rural areas lacking grid connection and external power transfers. The hybrid MG combines renewable sources with battery storage and backup fossil-fuel generators. By simulating a system located in Timbila, Kenya over a one year period using hourly time-steps while assuming perfect foresight over climate and loads, optimal capacities for the PV, WT and BS components were obtained. This was done for a DG size based on the community's peak daily power demand, to ensure reliability. A multiobjective optimization was performed that considered several goals including economic cost and emissions minimization as well as reliability and efficiency maximization.

In order to solve the sizing and dispatch optimization problems, several different solution algorithms in MATLAB's optimization and global optimization toolboxes were tested. Particle swarm optimization was found to perform best in terms of both runtime and optimality of the resulting solution. More broadly, biologically inspired techniques like GA and PSO seem to be well-suited to this class of problems, in agreement with literature.

For the location chosen, the combination using LI as the BS and DE as the backup DG was found to be more optimal than configurations including LA and/or MT. There exists a whole Pareto-set of input variables, all of which achieve the same global optimum. These were used to extract relationships between different input variables as well as output objectives. For instance, PV and WT act as substitutes relative to each other while increases in RES capacity will likely need to be accompanied by increased investment into BS, to account for intermittency and associated uncertainty in renewables. Similarly, there are tradeoffs between pursuing different objectives in the MG. For example, more aggressive emissions reductions or reliability improvements raise system costs.

The results show that RES can provide reliable and secure power for an islanded microgrid without external grid support but require either dispatchable, fossil fuel-based DGs as backup or sufficiently large battery storage, preferably both. In order to ensure high reliability, RES systems often need to be oversized in relation to the community's power demand. This can greatly increase the initial capital investment needed and high upfront costs may discourage the community from setting up the MG. However, the break-even distance analysis confirms that the optimized microgrid is still the most well-suited design choice for the chosen location, being much cheaper than grid extension. Decentralized RES is indeed cheaper than grid extension for areas with low demand and high connection costs, a finding that agrees with literature.

Furthermore, the optimal system has high renewable penetration and much lower emissions and costs than a system relying solely on fossil-fuels, while still being efficient and meeting load shortage constraints.

According to the sensitivity analysis, MG design is affected significantly by variations in external parameters like fuel prices and financial factors, and the sizing of the RES and BS components depend heavily on the rated power of the corresponding backup DG used. The dispatch optimization produced scheduling strategies that differ slightly from the load following strategy used for the sizing stage. It was found that the MG is relatively robust to uncertainty and disturbances in load and RES output, but only with a sufficiently large DG capacity. Low RES availability (especially for the wind resource) and/or undesirable demand patterns degrade(s) system performance since it resorts to mainly using fossil fuels via the DG. The performance is worsened further if such conditions persist for longer periods like wind lulls lasting several days, during which BS resources could also be completely drained. These weaknesses of the current model also motivate the need to incorporate demand-side management schemes and more sophisticated, predictive control to improve the MG's robustness.

6.2 Future work

There are several model refinements possible that could improve the system's performance under non-ideal or unforeseen situations, including advanced adaptive and predictive control techniques, more accurate forecasting of load and RES availability as well as demand-response programs to shape and/or curtail load. These were discussed further in chapter 5.

The current work looks at microgrids producing only electric power output. However, the modelling approach could be extended to the design and control of Combined Heat & Power (CHP) and Combined Cooling, Heating & Power (CCHP) microgrids as well i.e. those with thermal loads in addition to electric ones.

Finally, future research could also focus on modelling other possible MG designs, particularly those that implement energy storage and backup generation options apart from those considered here. Only electrochemical energy storage in the form of batteries was included in this MG. However, there are several other technologies that could be used including electrical, mechanical, thermal and magnetic storage methods [94]. Another attractive option for rural Africa is small-scale pumped hydro or micro-hydropower schemes. Similarly, there are also non-fossil fuel based backup generators like Hydrogen fuel cells and thermal power using biomass, which is the most abundant renewable resource available in many African countries [86].

Bibliography

- [1] Ritchie., H. & Roser, M. Energy Production & Changing Energy Sources. *Our World in Data*. <https://ourworldindata.org/energy-production-and-changing-energy-sources#access-to-electricity>. Accessed 15 June, 2019.
- [2] Dagnachew, A. G., Lucas, P. L., Hof, A. F., Gernaat, D. E., de Boer, H. S., & van Vuuren, D. P. (2017). The role of decentralized systems in providing universal electricity access in Sub-Saharan Africa–A model-based approach. *Energy*, 139, 184-195.
- [3] Szabó, S., Moner-Girona, M., Kougias, I., Bailis, R., & Bódis, K. (2016). Identification of advantageous electricity generation options in sub-Saharan Africa integrating existing resources. *Nature Energy*, 1(10), 16140.
- [4] World Energy Outlook (2018). *International Energy Agency (IEA)* <https://www.iea.org/weo2018/>. Accessed 17 June, 2019.
- [5] Casillas, C. E., & Kammen, D. M. (2010). The energy-poverty-climate nexus. *Science*, 330(6008), 1181-1182.
- [6] Odarno, L., Sawe, E., Swai, M., Katyega, M. J., & Lee, A. (2017). Accelerating Mini-Grid Deployment in Sub-Saharan Africa. *World Resources Institute and Tatedo*.
- [7] Mentis, D., Howells, M., Rogner, H., Korkovelos, A., Siyal, S., Broad, O., ... & Bazilian, M. (2016, April). Lighting up the World The first global application of the open source, spatial electrification toolkit (ONSSET). In *EGU General Assembly Conference Abstracts* (Vol. 18).
- [8] Baurzhan, S., & Jenkins, G. P. (2016). Off-grid solar PV: Is it an affordable or appropriate solution for rural electrification in Sub-Saharan African countries?. *Renewable and Sustainable Energy Reviews*, 60, 1405-1418.
- [9] Quak, E. J. (2018). The costs and benefits of lighting and electricity services for off-grid populations in sub-Saharan Africa. *Institute of Development Studies (IDS)*.
- [10] Murenzi, J. P., & Ustun, T. S. (2015, March). The case for microgrids in electrifying Sub-Saharan Africa. In *textitIREC2015 The Sixth International Renewable Energy Congress* (pp. 1-6). IEEE.
- [11] Attia, B., Shirley, R. (2018). Distributed Models for Grid Extension Could Save African Utilities Billions of Dollars. *Greentech Media*. <https://www.greentechmedia.com/articles/read/grid-extension-done-right-for-sub-saharan-africas-utilities#gs.q0ytps>. Accessed 16 July, 2019.
- [12] Amin, M. (2008, July). Challenges in reliability, security, efficiency, and resilience of energy infrastructure: Toward smart self-healing electric power grid. In *2008 IEEE Power and energy society general meeting-conversion and delivery of electrical energy in the 21st century* (pp. 1-5). IEEE.
- [13] Salam, A. A., Mohamed, A., & Hannan, M. A. (2008). Technical challenges on microgrids. *ARPN Journal of engineering and applied sciences*, 3(6), 64-69.

- [14] Akinyele, D., Belikov, J., & Levron, Y. (2018). Challenges of microgrids in remote communities: a STEEP model application. *Energies*, 11(2), 432.
- [15] Hirsch, A., Parag, Y., & Guerrero, J. (2018). Microgrids: A review of technologies, key drivers, and outstanding issues. *Renewable and Sustainable Energy Reviews*, 90, 402-411.
- [16] Porsinger, T., Janik, P., Leonowicz, Z., & Gono, R. (2017). Modelling and optimization in microgrids. *Energies*, 10(4), 523.
- [17] Kaabeche, A., & Ibtiouen, R. (2014). Techno-economic optimization of hybrid photovoltaic/wind/diesel/battery generation in a stand-alone power system. *Solar Energy*, 103, 171-182.
- [18] Tazvinga, H., Xia, X., & Zhang, J. (2013). Minimum cost solution of photovoltaic–diesel–battery hybrid power systems for remote consumers. *Solar Energy*, 96, 292-299.
- [19] Kaabeche, A., Belhamel, M., & Ibtiouen, R. (2011). Techno-economic valuation and optimization of integrated photovoltaic/wind energy conversion system. *Solar energy*, 85(10), 2407-2420.
- [20] Bhandari, B., Poudel, S. R., Lee, K. T., & Ahn, S. H. (2014). Mathematical modeling of hybrid renewable energy system: A review on small hydro-solar-wind power generation. *International journal of precision engineering and manufacturing-green technology*, 1(2), 157-173.
- [21] Gu, W., Wu, Z., Bo, R., Liu, W., Zhou, G., Chen, W., & Wu, Z. (2014). Modeling, planning and optimal energy management of combined cooling, heating and power microgrid: A review. *International Journal of Electrical Power & Energy Systems*, 54, 26-37.
- [22] Logenthiran, T., Srinivasan, D., Khambadkone, A. M., & Raj, T. S. (2010, June). Optimal sizing of an islanded microgrid using evolutionary strategy. In *2010 IEEE 11th International Conference on Probabilistic Methods Applied to Power Systems* (pp. 12-17). IEEE.
- [23] Bahramara, S., Moghaddam, M. P., & Haghifam, M. R. (2016). Optimal planning of hybrid renewable energy systems using HOMER: A review. *Renewable and Sustainable Energy Reviews*, 62, 609-620.
- [24] Weng, D. (2016). *Microgrid Techno-Economic Assessment Presentation*. Electric Power Research Institute, Inc.
- [25] Lawrence Berkeley National Lab. *Distributed Energy Resources - Customer Adoption Model (DER-CAM)*. <https://building-microgrid.lbl.gov/projects/der-cam>. Accessed July 18, 2019.
- [26] Jimenez, Antonio, Haase, Scott G., & Mathur, Shivani. *Microgrid Analysis Tools Summary*. United States. doi:10.2172/1425364.
- [27] Li, Xiangkun et al. (2018): *Microgrid Load and LCOE Modelling Results*. National Renewable Energy Laboratory. <https://data.nrel.gov/submissions/79>. Accessed June 12, 2019.
- [28] Saravanan, B., Das, S., Sikri, S., & Kothari, D. P. (2013). A solution to the unit commitment problem—a review. *Frontiers in Energy*, 7(2), 223-236.
- [29] Pathak, A., Pandit, M., & Kumar, Y. (2017). Combined Economic Emission Dispatch in a Micro Grid: A Comprehensive Survey. *International Journal of Applied Engineering Research*, 12(24), 15876-15901.
- [30] Zachar, M., Daoutidis, P. (2016). Economic dispatch for microgrids with constrained external power exchange. *IFAC-PapersOnLine*, 49(7), 833-838.

- [31] Parisio, A., Rikos, E., & Glielmo, L. (2014). A model predictive control approach to microgrid operation optimization. *IEEE Transactions on Control Systems Technology*, 22(5), 1813-1827.
- [32] Parisio, A., Rikos, E., Tzamalis, G., & Glielmo, L. (2014). Use of model predictive control for experimental microgrid optimization. *Applied Energy*, 115, 37-46.
- [33] Baran, P. (1964). On distributed communications networks. *IEEE transactions on Communications Systems*, 12(1), 1-9.
- [34] Nemati, M., Bennimmar, K., Tenbohlen, S., Tao, L., Mueller, H., & Braun, M. (2015, June). Optimization of microgrids short term operation based on an enhanced genetic algorithm. In *2015 IEEE Eindhoven PowerTech* (pp. 1-6). IEEE.
- [35] Nwulu, N. I., & Xia, X. (2017). Optimal dispatch for a microgrid incorporating renewables and demand response. *Renewable Energy*, 101, 16-28.
- [36] De Paola, A., Angeli, D., & Strbac, G. (2017). Price-based schemes for distributed coordination of flexible demand in the electricity market. *IEEE Transactions on Smart Grid*, 8(6), 3104-3116.
- [37] Fadaee, M., & Radzi, M. A. M. (2012). Multi-objective optimization of a stand-alone hybrid renewable energy system by using evolutionary algorithms: A review. *Renewable and sustainable energy reviews*, 16(5), 3364-3369.
- [38] Fathima, A. H., & Palanisamy, K. (2015). Optimization in microgrids with hybrid energy systems—A review. *Renewable and Sustainable Energy Reviews*, 45, 431-446.
- [39] Qu, B. Y., Zhu, Y. S., Jiao, Y. C., Wu, M. Y., Suganthan, P. N., & Liang, J. J. (2018). A survey on multi-objective evolutionary algorithms for the solution of the environmental/economic dispatch problems. *Swarm and Evolutionary Computation*, 38, 1-11.
- [40] Xiao, J., Bai, L., Li, F., Liang, H., & Wang, C. (2014). Sizing of energy storage and diesel generators in an isolated microgrid using discrete Fourier transform (DFT). *IEEE Transactions on Sustainable Energy*, 5(3), 907-916.
- [41] Wu, H., Zhuang, H., Zhang, W., & Ding, M. (2016). Optimal allocation of microgrid considering economic dispatch based on hybrid weighted bilevel planning method and algorithm improvement. *International Journal of Electrical Power & Energy Systems*, 75, 28-37.
- [42] Lu, Y., Zhou, J., Qin, H., Wang, Y., & Zhang, Y. (2011). Environmental/economic dispatch problem of power system by using an enhanced multi-objective differential evolution algorithm. *Energy Conversion and Management*, 52(2), 1175-1183.
- [43] Wu, H., Liu, X., & Ding, M. (2014). Dynamic economic dispatch of a microgrid: Mathematical models and solution algorithm. *International Journal of Electrical Power & Energy Systems*, 63, 336-346.
- [44] Borhanazad, H., Mekhilef, S., Ganapathy, V. G., Modiri-Delshad, M., & Mirtaheri, A. (2014). Optimization of micro-grid system using MOPSO. *Renewable Energy*, 71, 295-306.
- [45] Moshi, G. G., Bovo, C., Berizzi, A., & Taccari, L. (2016, June). Optimization of integrated design and operation of microgrids under uncertainty. In *2016 Power Systems Computation Conference (PSCC)* (pp. 1-7). IEEE.
- [46] AlRashidi, M. R., AlHajri, M. F., & El-Hawary, M. E. (2010). Enhanced particle swarm optimization approach for solving the non-convex optimal power flow. *World Academy of Science, Engineering and Technology*, 62(2), 651-655.

- [47] Gutmann, H. M. (2001). A radial basis function method for global optimization. *Journal of global optimization*, 19(3), 201-227.
- [48] Tazvinga, H., Zhu, B., & Xia, X. (2014). Energy dispatch strategy for a photovoltaic–wind–diesel–battery hybrid power system. *Solar Energy*, 108, 412-420.
- [49] Pourbabak, H., Chen, T., Zhang, B., & Su, W. (2017). Control and energy management system in microgrids. *arXiv preprint arXiv:1705.10196*.
- [50] Katsigiannis, Y. A., Georgilakis, P. S., & Karapidakis, E. S. (2012). Hybrid simulated annealing–tabu search method for optimal sizing of autonomous power systems with renewables. *IEEE Transactions on Sustainable Energy*, 3(3), 330-338.
- [51] Su, W., Wang, J., & Ton, D. (2015). Smart grid impact on operation and planning of electric energy systems. *Handbook of Clean Energy Systems*, 1-13.
- [52] Dragicevic, T., Wu, D., Shafiee, Q., & Meng, L. (2017). Distributed and decentralized control architectures for converter-interfaced microgrids. *Chinese Journal of Electrical Engineering*, 3(2), 41-52.
- [53] Higgs, M. A. (2000). Electrical SCADA systems from the operators perspective.
- [54] Farina, M., & Trecate, G. F. (2012). Decentralized and distributed control. In *ECCI-HYCON2 Graduate School on Control 2012*.
- [55] Gan, L., Topcu, U., & Low, S. H. (2012). Optimal decentralized protocol for electric vehicle charging. *IEEE Transactions on Power Systems*, 28(2), 940-951.
- [56] Senju, T., Kuninaka, R., Urasaki, N., Fujita, H., & Funabashi, T. (2005, December). Power system stabilization based on robust centralized and decentralized controllers. In *2005 International Power Engineering Conference* (pp. 905-910). IEEE.
- [57] Nikkhajoei, H., & Lasseter, R. H. (2007, June). Microgrid protection. In *2007 IEEE Power Engineering Society General Meeting* (pp. 1-6). IEEE.
- [58] Deng, R., Yang, Z., Hou, F., Chow, M. Y., & Chen, J. (2014). Distributed real-time demand response in multiseller–multibuyer smart distribution grid. *IEEE Transactions on Power Systems*, 30(5), 2364-2374.
- [59] Rahbari-Asr, N., Ojha, U., Zhang, Z., & Chow, M. Y. (2014). Incremental welfare consensus algorithm for cooperative distributed generation/demand response in smart grid. *IEEE Transactions on Smart Grid*, 5(6), 2836-2845.
- [60] Mudumbai, R., Dasgupta, S., & Cho, B. B. (2012). Distributed control for optimal economic dispatch of a network of heterogeneous power generators. *IEEE Transactions on Power Systems*, 27(4), 1750-1760.
- [61] Canizes, B., Silva, M., Faria, P., Ramos, S., & Vale, Z. (2015, March). Resource scheduling in residential microgrids considering energy selling to external players. In *2015 Clemson University Power Systems Conference (PSC)* (pp. 1-7). IEEE.
- [62] MLU Series Technical Specifications Sheet. *Mitsubishi Electric Photovoltaic Modules*. https://www.mitsubishielectricsolar.com/images/uploads/documents/specs/MLU_spec_sheet_250W_255W.pdf. Accessed June 23, 2019.
- [63] Kaabeche, A., Belhamel, M., & Ibtiouen, R. (2011). Sizing optimization of grid-independent hybrid photovoltaic/wind power generation system. *Energy*, 36(2), 1214-1222.
- [64] 3.5 kW Wind Turbine System Specification Sheet. *Raum Energy*. https://farm-energy-extension.org/wp-content/uploads/2019/04/3.5kW_Spec_Sheet.pdf. Accessed June 20, 2019.

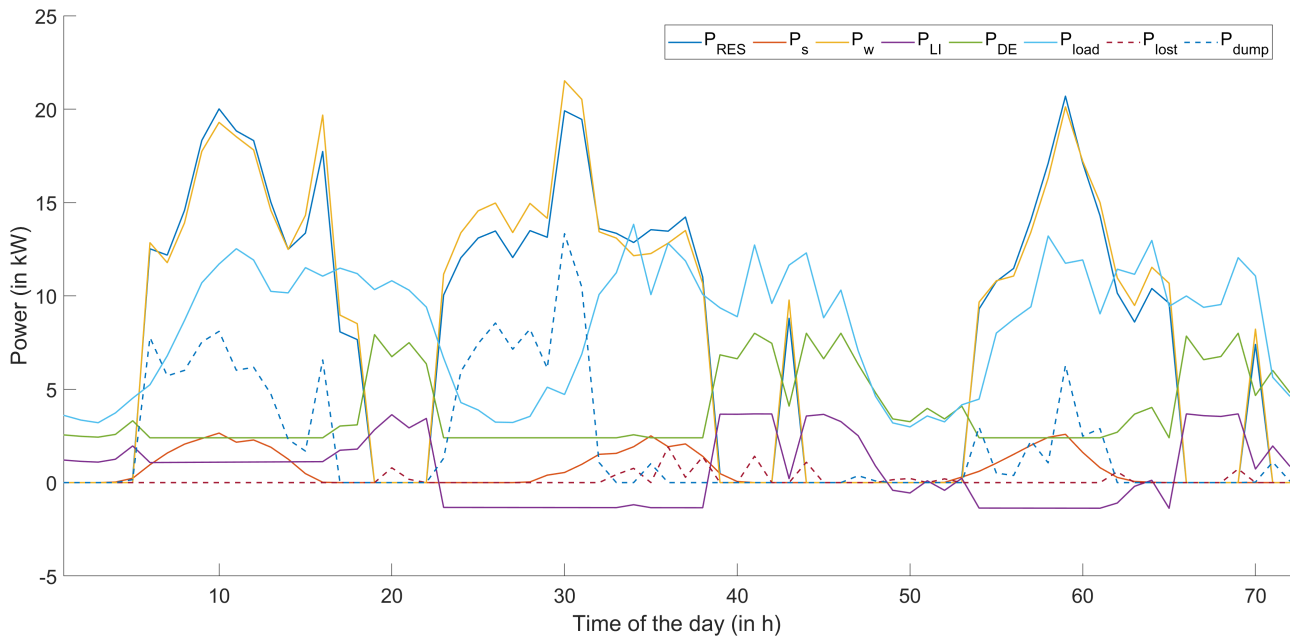
- [65] Seeling-Hochmuth, G. C. (1997). A combined optimisation concept for the design and operation strategy of hybrid-PV energy systems. *Solar energy*, 61(2), 77-87.
- [66] Kaviani, A. K., Riahy, G. H., & Kouhsari, S. M. (2009). Optimal design of a reliable hydrogen-based stand-alone wind/PV generating system, considering component outages. *Renewable energy*, 34(11), 2380-2390.
- [67] Wen, J., Zheng, Y., & Donghan, F. (2009). A review on reliability assessment for wind power. *Renewable and sustainable energy reviews*, 13(9), 2485-2494.
- [68] African Climate Data. *Trans-African HydroMeteoroological Observatory*. <https://tahmo.org/african-climate-data/>. Accessed June 30, 2019.
- [69] Weather forecast for Timbila, Kenya. *AccuWeather*. <https://www.accuweather.com/en/ke/timbila/827492/air-travel-hourly-forecast/827492?hour=34>. Accessed July 1, 2019.
- [70] Wind turbine measuring wind speed. *Energy Saving Trust*. https://www.energysavingtrust.org.uk/sites/default/files/reports/wind%20turbine_measuring%20wind%20speed.pdf. Accessed June 28, 2019.
- [71] Ghasemi, A., Asrari, A., Zarif, M., & Abdelwahed, S. (2013). Techno-economic analysis of stand-alone hybrid photovoltaic–diesel–battery systems for rural electrification in eastern part of Iran—A step toward sustainable rural development. *Renewable and Sustainable Energy Reviews*, 28, 456-462.
- [72] Ismail, M. S., Moghavvemi, M., & Mahlia, T. M. I. (2013). Techno-economic analysis of an optimized photovoltaic and diesel generator hybrid power system for remote houses in a tropical climate. *Energy conversion and management*, 69, 163-173.
- [73] Combined Heat and Power Technology Fact Sheet Series: Microturbines. U.S. Department of Energy. https://www.energy.gov/sites/prod/files/2016/09/f33/CHP-Microturbines_0.pdf. Accessed July 3, 2019.
- [74] DiOrio, N., Dobos, A., & Janzou, S. (2015). Economic analysis case studies of battery energy storage with SAM (No. NREL/TP-6A20-64987). National Renewable Energy Lab. (NREL), Golden, CO (United States).
- [75] Powerwall technical specifications. *Tesla*. https://www.tesla.com/en_GB/powerwall. Accessed June 27, 2019.
- [76] Ogunjuyigbe, A. S. O., Ayodele, T. R., & Akinola, O. A. (2016). Optimal allocation and sizing of PV/Wind/Split-diesel/Battery hybrid energy system for minimizing life cycle cost, carbon emission and dump energy of remote residential building. *Applied Energy*, 171, 153-171.
- [77] Renewable Power Generation Costs in 2018. International Renewable Energy Agency (IRENA). <https://www.irena.org/publications/2019/May/Renewable-power-generation-costs-in-2018>. Accessed June 16, 2019.
- [78] Hu, X., Zou, C., Zhang, C., & Li, Y. (2017). Technological developments in batteries: a survey of principal roles, types, and management needs. *IEEE Power and Energy Magazine*, 15(5), 20-31.
- [79] Brown, R. J., & Yanuck, R. R. (1985). Introduction to life-cycle costing. *Fairmont Press*, Englewood Cliffs, NJ.
- [80] Ajan, C. W., Ahmed, S. S., Ahmad, H. B., Taha, F., & Zin, A. A. B. M. (2003). On the policy of photovoltaic and diesel generation mix for an off-grid site: East Malaysian perspectives. *Solar Energy*, 74(6), 453-467.

- [81] Prasad, A. R., & Natarajan, E. (2006). Optimization of integrated photovoltaic–wind power generation systems with battery storage. *Energy*, 31(12), 1943–1954.
- [82] Potential to Emit Calculator for Stationary Compression Ignition Engines (2016). *U.S. Environmental Protection Agency (EPA)*. https://www.epa.gov/sites/production/files/2016-07/engines_ci_pte_calculator_version_1.0_0.xlsx. Accessed June 16, 2019.
- [83] Natural gas price. *Business Insider*. <https://markets.businessinsider.com/commodities/natural-gas-price>. Accessed July 1, 2019.
- [84] Standard INT-003-0 - Interchange Transaction Implementation. *North American Electric Reliability Corporation*. <https://www.nerc.com/files/INT-003-0.pdf>
- [85] <https://www.solaxpower.com/wp-content/uploads/2017/02/X-Hybrid-SingleThree-Phase.pdf>
- [86] Msyani, C. M. (2013). Current status of energy sector in Tanzania. *Presentation at the United States Energy Association Executive Exchange on Developing an Ancillary Service Market, Washington, DC*.
- [87] Goldie-Scot, L. (2019). A Behind the scenes take on lithium-ion battery prices. *Bloomberg New Energy Finance*.
- [88] Diesel prices. https://www.globalpetrolprices.com/diesel_prices/. Accessed July 20, 2019.
- [89] Central banks - summary of current interest rates. *Global-rates.com*. <https://www.global-rates.com/interest-rates/central-banks/central-banks.aspx>. Accessed July 20, 2019.
- [90] List of inflation rates by country. *Trading Economics*. <https://tradingeconomics.com/country-list/inflation-rate>. Accessed July 20, 2019.
- [91] Kenya interest rate. *Trading Economics*. <https://tradingeconomics.com/kenya/interest-rate>. Accessed June 30, 2019.
- [92] Moksnes, N., Korkovelos, A., Mentis, D., & Howells, M. (2017). Electrification pathways for Kenya—linking spatial electrification analysis and medium to long term energy planning. *Environmental Research Letters*, 12(9), 095008.
- [93] Zeyringer, M., Pachauri, S., Schmid, E., Schmidt, J., Worrell, E., & Morawetz, U. B. (2015). Analyzing grid extension and stand-alone photovoltaic systems for the cost-effective electrification of Kenya. *Energy for Sustainable Development*, 25, 75–86.
- [94] Arani, A. K., Gharehpetian, G. B., & Abedi, M. (2019). Review on energy storage systems control methods in microgrids. *International Journal of Electrical Power & Energy Systems*, 107, 745–757.
- [95] Mayne, D. Q., Rawlings, J. B., Rao, C. V., & Scokaert, P. O. (2000). *Constrained model predictive control: Stability and optimality*. *Automatica*, 36(6), 789–814.
- [96] Pereira, M., de la Peña, D. M., & Limón, D. (2017). Robust economic model predictive control of a community micro-grid. *Renewable Energy*, 100, 3–17.
- [97] Prodan, I., & Zio, E. (2014). A model predictive control framework for reliable microgrid energy management. *International Journal of Electrical Power & Energy Systems*, 61, 399–409.
- [98] Zhu, B., Tazvinga, H., & Xia, X. (2014). Switched model predictive control for energy dispatching of a photovoltaic-diesel-battery hybrid power system. *IEEE Transactions on Control Systems Technology*, 23(3), 1229–1236.
- [99] Prinsloo, G., Dobson, R., & Brent, A. (2016). Scoping exercise to determine load profile archetype reference shapes for solar co-generation models in isolated off-grid rural African villages. *Journal of Energy in Southern Africa*, 27(3), 11–27.

Appendix A

Dispatch over longer periods

As a preliminary foray into optimally scheduling dispatch over longer periods, the dispatch optimization was performed over a period of three days ahead. Both the hourly dispatch and *SOC* plots from this are shown below.



(a) Optimal hourly power dispatch over a 3 day (72 h) period.

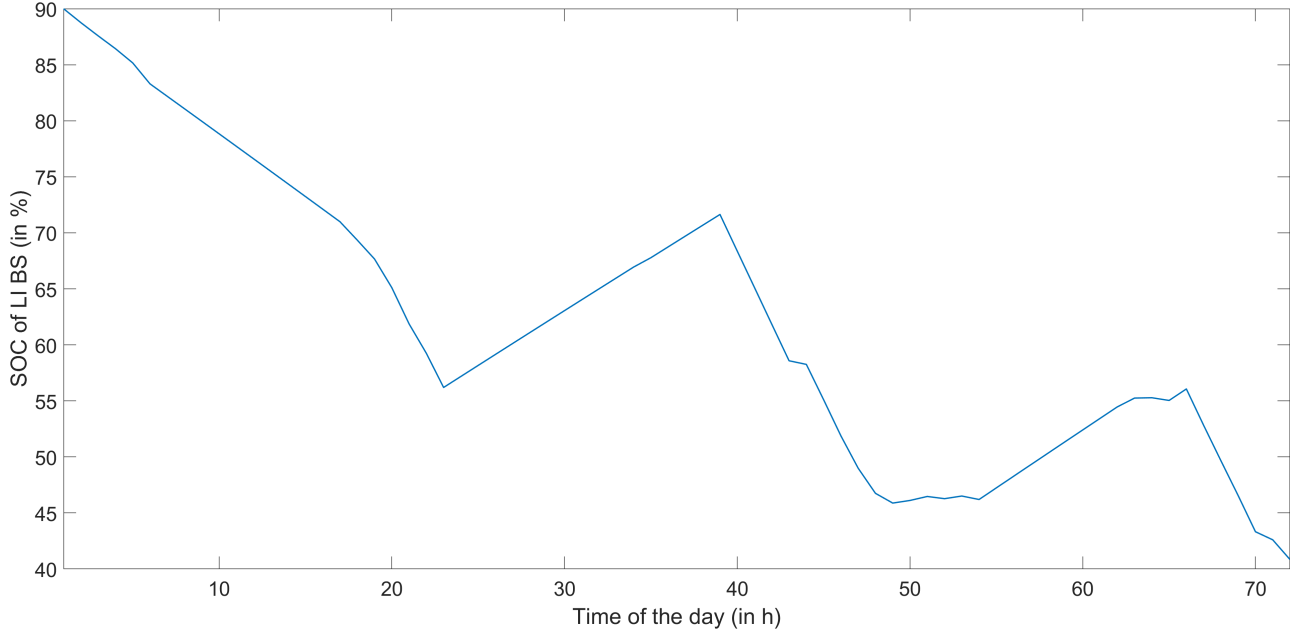
(b) Variation of the *SOC* of the BS over a 3 day (72 h) period.

Figure A.1: Optimized dispatch over a longer time period of three consecutive days.

Appendix B

Code

All of the MATLAB codes used in this dissertation have been uploaded to GitHub. This is publicly available and accessible at this link: <https://github.com/vineetjnair9/ETMphil>.